Synaptic functions of the ubiquitin ligase TRIM3

Schreiber, J.

2016

document version
Publisher's PDF, also known as Version of record

VRIJE UNIVERSITEIT

Synaptic functions of the ubiquitin ligase TRIM3

ACADEMISCH PROEFSCHRIFT

ter verkrijging van de graad Doctor aan
de Vrije Universiteit Amsterdam,
op gezag van de rector magnificus
prof.dr. V. Subramaniam,
in het openbaar te verdedigen
ten overstaan van de promotiecommissie
van de Faculteit der Aard- en Levenswetenschappen
op vrijdag 11 maart 2016 om 11.45 uur
in de aula van de universiteit,
De Boelelaan 1105

door

Joerg Schreiber

geboren te Zossen, Duitsland

promotoren:	prof. dr. A. B. Smit
copromotoren:	dr. R. E. van Kesteren
	prof. dr. C. I. de Zeeuw

All clear, sir.

Leescommissie: prof. dr. M. Kneussel
prof. dr. J. C. Schwamborn
prof. dr. C. C. Hoogenraad
dr. R. F. Toonen
dr. K. W. Li

The research described in this thesis was performed at the department of Molecular and Cellular Neurobiology, Center for Neurogenomics and Cognitive Research, Neuroscience Campus Amsterdam, VU University, Amsterdam, The Netherlands.

Research was funded by Cerebnet, EU-FP7 Initial Training Network

Publication of this thesis was supported by:
Sylics (Synaptologics BV)
Vrije Universiteit Amsterdam
Center for Neurogenomics and Cognitive Research (CNCR)

Printed by Ipskamp Drukkers

Cover: Curious mice, Joerg Schreiber

TABLE OF CONTENTS

List of Abbreviations

ABP280	Actin-Binding Protein 280
aCSF	Artificial Cerebral Spinal Fluid
ACTA	Actin, Alpha
ACTB	Actin, Beta
ACTG1	Actin, Gamma 1
ACTG1-cKO	Actin, Gamma 1 - Conditional Knockout
ACTN4	Actinin, Alpha 4
ADCY1	Adenylate Cyclase 1
AGO2	Argonaute Risc Catalytic Component 2
AMPA	Alpha-Amino-3-Hydroxyl-5-Methyl-4-Isoxazole-Propionate
ANXA5	Annexin A5
AP2A1	Adaptor-Related Protein Complex 2, Alpha 1 Subunit
AP2M1	Adaptor-Related Protein Complex 2, Mu 1 Subunit
APC/C	Anaphase-Promoting Complex/Cyclosome
ARC	Activity-Regulated Cytoskeleton-Associated Protein
ARF	Adp Ribosylation Factor-Like
B-BOX	B-Box-Type Zinc Finger Domain
BBS	Bardet-Biedl Syndrome
BERP	Brain Expressed Ring Finger Protein
BN - PAGE	Blue Native - Polyacrylamide Gel Electrophoresis
BRAT	Brain Tumor Protein
BSA	Bovine Serum Albumin
CA1	CA1 Region of Hippocampus
CA2	CA2 Region of Hippocampus
CA3	CA3 Region of Hippocampus
$CaCl_2$	Calcium Chloride
CamKII	Ca^{2+}/Calmodulin-Dependent Protein Kinase II
CART	Cytoskeleton-Associated Recycling or Transport
CC	Coiled-Coil
cDNA	Complementary Deoxyribonucleic Acid
CNQX	6-Cyano-7-Nitroquinoxaline-2,3-Dione
DNA	Deoxyribonucleic Acid
DDM	N-Dodecyl β-D-Maltoside
DDX3	Dead (Asp-Glu-Ala-Asp) Box Helicase 3, X-Linked
DG	Dentate Gyrus
DMEM	Dulbecco's Modified Eagle Culture Medium
DMSO	Dimethyl Sulfoxide
DNM3	Dynamin 3

DOC	Deoxycholic Acid
DTT	Dithiothreitol
DUBs	Deubiquitinating Enzymes
E1	Ubiquitin-Activating Enzyme
E2	Ubiquitin-Conjugating Enzyme
E3	Ubiquitin Ligase
ECF	Enhanced Chemifluorescence
ECL	Enhanced Chemiluminescent
EEF1A2	Eukaryotic Translation Elongation Factor 1 Alpha 2
EGFR	Epidermal Growth Factor Receptor
EPSC	Excitatory Postsynaptic Current
F-ACTIN	Filamentous-Actin
FBX2	F-Box Protein 2
fEPSP	Field Excitatory Postsynaptic Potential
FIL	Filamin-Type Immunoglobulin
FMRP	Fragile X Mental Retardation Protein 1
FN3	Fibronectin Type 3
GABA	Gamma Amino Butyric Acid
GABAR	GABA Receptor
G-ACTIN	Globular-Actin
GAPDH	Glyceraldehyde-3-Phosphate Dehydrogenase
GFP	Green Fluorescent Protein
GIGYF2	Grb10 Interacting Gyf Protein 2
GKAP	Guanylate Kinase-Associated Protein
GLUK2	Ionotropic Glutamate Receptor Kainate 2
GLUR1	Ionotropic Glutamate Receptor AMPA 1
GLUR2	Ionotropic Glutamate Receptor AMPA 2
HECT	Homologous To The E6-Ap Carboxyl Terminus
HEK293	Human Embryonic Kidney 293 Cells
HEPES	N-2-Hydroxyethylpiperazine-N'-2-Ethanesulfonic Acid
HOMER1	Homer Scaffolding Protein 1
HSP70	Heat Shock 70kDa Protein
HSP90AB1	Heat Shock Protein 90kDa Alpha, Class B Member 1
HSPA2	Heat Shock 70kDa Protein 2
IG-FLMN	Immunoglobulin Filamin-Type
IGFN1	Immunoglobulin-Like And Fibronectin Type I Domain-Containing Protein 1
IPSC	Inhibitory Postsynaptic Current
KALRN	Kalirin, RhoGEF Kinase
KCl	Potassium Chloride
kDa	Kilodalton
kg	Kilogram

KIF21B	Kinesin Family Member 21B
KO	Knockout
LGMD2H	Limb-Girdle Muscular Dystrophy Type 2H
LTD	Long-Term Depression
LTM	Long-Term Memory
LTP	Long-Term Potentiation
MAP2	Microtubule-Associated Protein 2
MATH	Meprin and Tumour-Necrosis Factor Receptor-Associated Factor Homology
MDM2	Mouse Double Minute 2 Homolog
mEPSC	Miniature Excitatory Postsynaptic Current
MG132	Proteasome Inhibitor MG132
mIPSC	Miniature Inhibitory Postsynaptic Current
miRNA	microRNA
ml	Milliliter
mm	Millimeter
mM	Millimolar
mRNA	Messenger Ribonucleic Acid
mRNP	Messenger Ribonucleoprotein
mTOR	Mechanistic Target of Rapamycin (Serine/Threonine Kinase)
mV	Millivolt
NaCl	Sodium Chloride
NaH_2PO_4	Sodium Dihydrogenphosphate
$NaHCO_3$	Sodium Bicarbonate
NF-L	Neurofilament Light Chain
NHL	Ncl-1, Ht2A And Lin-41
NMDA	N-Methyl-D-Aspartic Acid
NME1	Nme/Nm23 Nucleoside Diphosphate Kinase 1
NOT4	E3 Liagse Not4
NPTN	Neuroplastin
NR1	N-Methyl-D-Aspartate Receptor Subunit 1
NR2B	N-Methyl-D-Aspartate Receptor Subunit 2B
P2 + M	Pellet 2 And Microsomes
PARK2	Parkin RBR E3 Ubiquitin Protein Ligase
P-BODIES	Processing Bodies
PBS	Phosphate Buffered Saline
PEI	Polyethylenimine
PEN - STREP	Penicillin-Streptomycin
PHD	Plant Homeodomain
PIASy	Protein Inhibitor Of Activated Stat
PKA	Protein Kinase A
PKC	Protein Kinase C

PSD-95	Postsynaptic Density Protein 95
PTMs	Post-Translational Modifications
PTZ	Pentylenetetrazole
PURA	Purine-Rich Single-Stranded DNA-Binding Protein Alpha
PVDF	Polyvinylidene Fluoride
RBCC	Ring Finger, B-Box, Coiled-Coil
RIM1	Regulating Synaptic Membrane Exocytosis Protein 1
RING	Really Interesting New Gene
RNA	Ribonucleic Acid
RPL3	Ribosomal Protein L3
RT-PCR	Reverse Transcription Polymerase Chain Reaction
SCF COMPLEX	Skp1/Cullin/Fbox Complex
SDS-PAGE	Sodium Dodecyl Sulfate Polyacrylamide Gel Electrophoresis
SEM	Standard Error of the Mean
SHANK	Sh3 And Multiple Ankyrin Repeat Domains
SLC1A3	Solute Carrier Family 1, Member 3
SLC25A4	Solute Carrier Family 25, Member 4
SNAP25	Synaptosomal-Associated Protein, 25kDa
SPRY	Spia Kinase And Ryanodine Receptors Domain
STM	Short-Term Memory
SUMO	Small Ubiquitin-Like Modifier
TBS	Tris Buffered Saline
TBS	Theta Burst Stimulation
TBS-T	Tris Buffered Saline - Tween-20
TFA	Trifluoroacetic Acid
TM	Transmembrane
TMEM57	Transmembrane Protein 57
TPA	12-O-Tetradecanoylphorbol 13-Acetate
TRIM2	Tripartite Motif Containing 2
TRIM3	Tripartite Motif Containing 3
TRIM32	Tripartite Motif Containing 32
TRIM71	Tripartite Motif Containing 71
TRIS	2-Amino-2-(Hydroxymethyl)-1,3-Propanediol
TUBB3	Tubulin, Beta 3
TUBEs	Tandem Ubiquitin Binding Entities
UBE3A	Ubiquitin Protein Ligase E3A
VIM	Vimentin
WB	Western Blot
WT	Wildtype
XIAP	X-Linked Inhibitor Of Apoptosis
ZBP1	Z-DNA Binding Protein 1

CHAPTER 1

General Introduction

Prelude – learning and memory

There are many different definitions of learning and memory, some extensive and complex and others straightforward and easily comprehensible. In its simplest form, learning is a mechanism by which we acquire new information, and memory is the mechanism by which we retain and possibly retrieve that information. As simple as these definitions may appear, they are the basis for any species to survive, adapt, reproduce and finally succeed in even the harshest environment. When Charles Darwin first proposed his theory of natural selection in 1859 it was controversial and highly debated. Nowadays it is largely accepted by its overwhelming evidence and rather intuitive to most. The ability to learn about the environment, store that information and then retrieve and utilize it, presents an invaluable competitive advantage, which can be appreciated when looking at human evolutionary history. First fossils of the human species (genus: *Homo*) date back about two to three million years (Schrenk et al., 2007), which is relatively little compared to most other species living on earth. In those two to three million years humans have undoubtedly changed and adapted to their environment, but they also took control of their environment and shaped it to their needs. Humans have colonized almost all the land masses of the earth regardless of the climate, have created complex social structures, harnessed the power of fire and electricity, and more than anything humans have overcome their own limitations by technological and no less medical advances. Thus, humans have used their ability to learn and memorize to effectively predict the future and accordingly shape their environment to a favorable outcome. By being able to share and pass on acquired knowledge, not genetically but socially, humans have surpassed the learning abilities of any other species, allowing every generation to further the knowledge of the previous. It was therefore almost inevitable that humans would ultimately reach a stage at which they would inquire the very nature of their own abilities. While early human societies often considered the heart being the seat of thought, emotion and no less the soul, recent times revealed that it is the brain that holds our memories and governs our abilities to learn. This organ of about 1.5 kg (Herculano-Houzel, 2009) has become the study object and fascination of many generations of researchers coming from so different fields as biology, philosophy, psychology, chemistry and others.

How is information stored in the brain?

In the beginning of the 20th century Richard Semon brought forward his Mneme or Engram theory of how information is stored in the brain. In short, he postulated that when experiencing an event, certain sub-populations of brain cells would store this information by being excited simultaneously and then undergoing physical and/or chemical changes. Retrieval of that information could then be achieved by reactivation of one or more of the original cells that were active while encoding the memory (Semon, 1904). Most of Semon's work, which goes far beyond the short paragraph above, has gone unnoticed, and although he may have been false in some of his assumptions by following Lamarckian reasoning, one can clearly see foresight on his behalf of what the following century would uncover.

In the middle of the 20th century Donald Hebb elaborated on the engram theory and its underlying mechanisms, taking the current knowledge on synaptic connections into account. As others before him, he postulated that repeated activity of two or more neurons together would cause lasting cellular changes that would increase the efficacy of synapses between them, thereby allowing the storage of information (Hebb, 1949). What set Hebb's postulate apart from that of others, is that he emphasized the causality, arguing that synaptic connections would grow stronger only when presynaptic activity precedes and triggers the activity in postsynaptic neurons. It took about 20 years before the Hebbian rule, as it is now known, was confirmed experimentally when Lomo and Bliss (1973) showed that a strong, repetitive stimulation of neurons in the hippocampus of rabbits, led to long-term potentiation (LTP) of synaptic strength that lasted for up to 10 hours. Another 20 years later several research groups demonstrated that the opposite of what Hebb postulated, non-correlated activity of neurons leading to a decrease of synaptic strength, also holds true (Dudek and Bear, 1992; Fujii et al., 1991; Malenka, 1994). In short, they showed that a prolonged, but weak sub-threshold stimulation of hippocampal neurons leads to decreased synaptic strength, a phenomenon that was named long-term depression (LTD). Both, long-term potentiation and long-term depression are forms of synaptic plasticity and much of what we know today about how we learn, store and retrieve information, comes from studying their underlying molecular mechanisms.

Synaptic plasticity

Synapses undergo changes. Synaptic connections can be weakened or strengthened in an activity-dependent manner. The process of constant synaptic change is considered to be the basis of the brain's ability to store information and is called synaptic plasticity (Holtmaat and Svoboda, 2009). LTP and LTD are the most extensively studied forms of functional synaptic plasticity, but functional plasticity is often accompanied by structural synaptic changes, i.e. changes in spine morphology (size and length increase/decrease) and changes in spine numbers (Caroni et al., 2012; Matsuzaki et al., 2004; Nagerl et al., 2004). These structural synaptic alterations were often viewed as a mere consequence of processes involved in synaptic plasticity, e.g. gene expression and protein synthesis, and most observations to date are indeed correlative and not of causative nature. In recent years, however, numerous studies have pointed to a more pivotal role of morphological synaptic changes in learning and memory. In order to understand how synaptic structure relates to synaptic function and *vice versa*, the following paragraphs will introduce cause and effect in (post-)synaptic plasticity in more detail.

Receptor-mediated plasticity

Synapses are the communication terminals of neurons. They present the bridge between the axon of one neuron (presynaptic) and the dendrite of another neuron (postsynaptic). When an action potential arrives at an axonal terminal, it will trigger the influx of calcium ions through voltage-dependent calcium channels, inducing the exocytosis of neurotransmitters. These bind to specific neurotransmitter receptors allowing the flux of ions, leading to a postsynaptic depolarization or hyperpolarization of the membrane, thereby exerting excitatory or inhibitory effects on the postsynaptic side. In case of an excitatory synapse the neurotransmitter is generally glutamate. Glutamate can bind to three types of receptors: (i) AMPA (α-Amino-3-hydroxy-5-methyl-4-isoxazolepropionic acid), (ii) NMDA (N-methyl-D-aspartate) and (iii) kainate receptors, which all are (transmitter-) ligand-gated ion channels. Under basal conditions glutamate binding will lead to a flux of Na^+ and K^+ ions via AMPA receptors, while NMDA receptors remain impervious due to a Mg^{2+} block. Only when the postsynaptic membrane is sufficiently depolarized, Mg^{2+} dissociates from the receptor and allows an influx of Ca^{2+} ions (Hammond, 2001; Kandel et al., 2000). That Ca^{2+} influx is

assumed to be the initiator of synaptic plasticity. When entering the postsynaptic cell it sets a number of signaling processes in motion, which will finally lead to a LTP state of the synapse. Via binding to the protein calmodulin, Ca^{2+} activates the calcium/calmodulin-dependent protein kinase 2 (CaMKII), protein kinase C (PKC) and protein kinase A (PKA), all of which are able to phosphorylate AMPA receptors (Barria et al., 1997; Boehm et al., 2006; Nayak et al., 1998). AMPA receptor phosphorylation leads to an increase of conductance in two ways: (i) additional AMPA receptors are incorporated in the post-synaptic membrane (Schnell et al., 2002) and (ii) the conductance of individual AMPA receptors is increased (Derkach et al., 1999; Derkach et al., 2007). In addition, activation of the aforementioned kinases causes a downstream effect that induces increased synthesis of synaptic proteins (Miller et al., 2002; Sutton and Schuman, 2006), which further strengthens synapses.

The second most studied form of synaptic plasticity is LTD. As with LTP, LTD induction can also be dependent on NMDA receptors and calcium influx. Whereas LTP requires large amounts of calcium, LTD is triggered by lower calcium levels (Artola and Singer, 1993; Nabavi et al., 2013). In general, LTP increases the number and transmission efficacy of AMPA receptors. LTD in contrast is reported to trigger the opposite: AMPA receptors are dephosphorylated in a NMDA receptor- and calcium-dependent manner and subsequently removed from the synaptic membrane by endocytosis leading to synaptic weakening (Mansuy, 2003; Winder and Sweatt, 2001).

Synaptic structure-related plasticity

In parallel to functional synaptic changes via endo- or exocytosis of receptors on the postsynaptic membrane and direct modulation of their conductance properties, the morphology of spines is also altered. Changes in spine head size have been observed as well as changes in length and thickness of spine necks (Engert and Bonhoeffer, 1999; Fifkova and Anderson, 1981). In addition, the spine density changes after stimulation (Leuner and Gould, 2010). Interestingly, structural and functional processes appear to be interdependently connected. Induction of LTP not only triggers recruitment of AMPA receptors into the postsynaptic membrane, but also causes outgrowth of new spines, growth of spine pairs and triplet spines and an increase in spine size (Harris et al., 2003; Toni et al., 1999). The increase

in spine head size is already visible as quickly as 10 seconds after stimulation and can reach a maximum of more than 200 % within 1 - 5 minutes thereafter. As with LTP, spine enlargement can be inhibited by blocking NMDA receptors or by inhibiting calmodulin (Matsuzaki et al., 2004). Reversely, when blocking spine size enlargement by suppressing actin polymerization, LTP is also suppressed (Fukazawa et al., 2003; Krucker et al., 2000; Matsuzaki et al., 2004). It is thus clear that structural and functional synaptic plasticity are mutually interdependent processes of a plasticity response that share similar inductive mechanisms and are both required for the expression of plasticity.

It is interesting to note that both structural and functional changes associated with LTP require protein synthesis (Tanaka et al., 2008; Yang et al., 2008), and that the Ca^{2+} influx through NMDA channels triggered by LTP induction, not only activates gene transcription, but also mRNA translation (Luscher and Malenka, 2012; West et al., 2002). This protein synthesis not only occurs somatically, but also dendritically from mRNAs that are located in or near spines (Luscher and Malenka, 2012). The concept of local protein synthesis has become crucial in our understanding of synaptic plasticity, and will be further explained in the following paragraphs.

mRNA transport granules

Neurons are highly polarized cells, with dendritic trees and axons often extending far from the cell body. This specialized cellular architecture presents a unique challenge, i.e., how to supply each of the sometimes thousands of synapses with the correct proteins at times of high demand?

In 1982 Steward and Levy showed that polyribosomes are present at the base of spines in hippocampal granule cells (Steward and Levy, 1982). With that finding speculation arose that local translation of mRNAs may be the means to locally and temporally regulate the abundance of specific proteins in neurons. In the following decades more evidence on local protein synthesis was gathered. Many different mRNAs, such as *Map2* (Garner et al., 1988), *CaMKIIα* (Burgin et al., 1990), *Shank* (Bockers et al., 2004) and others were found localized in or near synapses of mouse neurons. Recent studies suggest that the number of different protein coding mRNAs in axons and dendrites is in the thousands (Cajigas et al., 2012; Zivraj et al., 2010). In fact, Lécuyer et al. (2007) showed that in *Drosophila* embryos

71 % of all expressed genes were found to encode mRNAs highly localized in non-nuclear subcellular compartments (Lecuyer et al., 2007), suggesting that local mRNA translation is not an isolated phenomenon in mammalian neurons, but a general mechanism to specifically regulate localization of proteins.

In neurons, localized RNAs are often transported in RNA granules containing mRNAs and a multitude of proteins, many of which are RNA-binding proteins (Kiebler and DesGroseillers, 2000; Knowles et al., 1996; Kohrmann et al., 1999). At least three different kinds of RNA granules can be found in dendrites: (i) stress granules carrying RNAs of stress response proteins such as HSP70, (ii) processing bodies (P-bodies) that regulate RNA degradation and (iii) ribonucleoprotein particles (RNPs) that transport and store mRNAs for local translation (Liu-Yesucevitz et al., 2011). Most common of the three are RNP granules, which are also referred to as mRNA transport granules. They transport the majority of mRNAs. Stress granules and P-bodies on the other hand are rarely observed and appear only after induction of metabolic stress, e.g. heat, oxidative stress, osmotic stress (Anderson and Kedersha, 2009). Most RNP granules in neurons are stationary and only a small percentage is mobile at any given moment (Buchan, 2014). Neuronal activity, however, is able to increase targeted movement of RNP granules into dendrites (Bramham and Wells, 2007). They are able to move in anterograde as well as retrograde directions along microtubules employing different kinesin motor proteins (Kanai et al., 2004; Knowles et al., 1996). The composition of RNP particles varies depending on brain region and developmental stage (Di Liegro et al., 2014). They generally consist of mRNAs, proteins for translation initiation and elongation, regulators of mRNA structure and function, ribosomal subunits, and other RNA-binding proteins many of which are assumed to repress mRNA translation while in transport. The most prominent and most researched RNP proteins are FMRP, PURA, STAUFEN, ZBP1 and TLS, all of which were shown to have an effect on synaptic plasticity and/or spine morphology (Bramham and Wells, 2007; Kanai et al., 2004; Kiebler and Bassell, 2006). Of these proteins FMRP has received special interest. Loss of FMRP, due to a mutation in its gene *FMR1,* leads to a severe form of mental retardation called fragile X syndrome (Bagni and Greenough, 2005). FMRP is assumed to locally control translation of a number of proteins such as CaMKIIα, ARC and MAP1B. On a cellular level, loss of FMRP in neurons results in a reduction of mature spines and an excess of long filopodial like spines (Zalfa et al., 2006; Zalfa et al., 2003). Interestingly, the loss two other aforementioned RNP proteins,

TLS and STAUFEN 2, results in similar spine morphology abnormalities. Loss of TLS leads to an increase in thin spines and a reduction of mushroom spines, whereas loss of STAUFEN 2 increases filopodia and reduces spine number (Fujii et al., 2005; Goetze et al., 2006). As argued above, alterations in spine density, size and shape require structural changes that are mediated by the actin skeleton. Conveniently, messenger ribonucleoprotein (mRNP) complexes are known to transport beta-actin mRNA, bound and translationally inhibited by protein ZBP1 (Zipcode Binding Protein 1) (Eom et al., 2003; Kiebler and DesGroseillers, 2000). Upon stimulation, ZBP1 can be phosphorylated leading to beta-actin mRNA release, which triggers its local translation (Huttelmaier et al., 2005; Zhang et al., 2001), supplying spines with extra building material to increase in size.

Synaptic protein synthesis and breakdown

Many studies have shown that protein synthesis is an essential mechanism regulating protein content of synapses and thereby affecting synaptic strength and learning (Fonseca et al., 2006a; Frey et al., 1988; Huang et al., 1996). However, synaptic plasticity is not driven by protein synthesis alone, and how could it? Logic dictates that constant synthesis of proteins in a limited space, even when only activity-driven, will eventually lead to crowding if a counter measure is not in place. That counter measure has been identified as protein degradation mediated by the ubiquitin proteasome system. In 2006, Fonseca et al. demonstrated that LTP is not solely dependent on protein synthesis, but also on protein degradation. They showed that blocking the proteasome led to as much a decrease in LTP as when blocking translation. Only when inhibiting protein synthesis and degradation at the same time, LTP was restored. This led them to conclude that synaptic protein degradation is essential for synaptic plasticity, counterbalancing protein synthesis and keeping protein levels in balance.

Protein degradation is generally achieved by post-translational modifications, meaning that proteins are modified by the attachment of cellular recognition tags that direct them to proteasomal degradation (Hershko and Ciechanover, 1998). Given their importance in synaptic plasticity, I will now first discuss the nature of these modifications in more detail.

Post-translational modifications

Only a few years ago the human genome project finished its efforts to sequence the human genome in its entirety (International Human Genome Sequencing, 2004). While analysis of the sequences advanced, it became clear that our genome does not contain an anticipated 50,000 to 90,000 genes (Antequera and Bird, 1993; Fields et al., 1994), but a mere 20,000 to 25,000 genes (International Human Genome Sequencing, 2004). This rather low number brought into question how so few proteins are able to fulfill the complexity of everyday cellular tasks in human cells. In comparison, the house mouse (*Mus musculus*) and the thale cress (*Arabidopsis thaliana*) have approximately the same number of genes (Arabidopsis Genome, 2000; Mouse Genome Sequencing et al., 2002). The phenomenon of alternative splicing was quickly identified as a means to increase protein diversity without the need to increase the number of genes. In alternative splicing, non-coding and coding parts of the pre-mRNA are excised to produce different mature mRNAs, often resulting in different isoforms of the same protein, potentially fulfilling a different or altered function (Black, 2003; Graveley, 2001; Maniatis and Tasic, 2002). In recent years, driven by technological advances, post-translational modifications (PTMs) have been identified to immensely contribute to structural and functional diversity of proteins (Jensen, 2004). PTMs are chemical modification of amino acids of proteins that are introduced during or after translation. These modifications can involve (i) structural changes, e.g. proteolytic cleavage and the formation of di-sulfide bridges, (ii) chemical changes such as amino acid conversions, (iii) the addition of functional groups, e.g. acetylation and alkylation, and (iv) the addition of other proteins and peptides, e.g. sumoylation, neddylation and ubiquitylation (Han and Martinage, 1992b). Most of these modifications are mediated by enzymatic activity and occur at specific amino acid sequences in the target proteins (Han and Martinage, 1992a; Han and Martinage, 1992b; Han and Martinage, 1993). The total number of types of post-translational modifications is estimated between 200 and 400 and all of them are able to change the structure and/or function of a protein (Farley and Link, 2009; Zhao and Jensen, 2009). In addition most proteins can be modified at more than one site, allowing for numerous combinations of PTMs to regulate protein function in many different ways. Some of the most common and also most studied PTMs include phosphorylation, acetylation, methylation, glycosylation, palmitylation, sumoylation and ubiquitylation (Khoury et al., 2011). Many, if

not all, PTMs affect synaptic proteins and have an impact on learning and memory in one way or another. A few of them will be briefly described in the following paragraphs, whereas ubiquitylation, which is especially relevant for this thesis will be explained in detail in the next section.

Phosphorylation is the reversible addition of a phosphate group to a serine, threonine, tyrosine or arginine residue (Han and Martinage, 1992b). Phosphorylation is mediated by kinases and can be reversed by phosphatases (Hunter, 1995). It is the experimentally most often identified modification of proteins with an extremely high turnover rate (Khoury et al., 2011). Phosphorylation is best known for its involvement in the activation and inactivation of enzyme activity and the modulation of molecular interactions in signaling pathways (Seo and Lee, 2004). It plays a major role in synaptic plasticity by controlling the activity state and function of numerous synaptic proteins, e.g. NMDA receptors, AMPA receptors, CaMKII and others (Lee, 2006). Dysregulation of phosphorylation is also assumed to be a trigger in the development of neurodegenerative diseases such as Parkinson's disease, where it precedes synuclein accumulation and Lewy body formation (Anderson et al., 2006).

Acetylation is the second most common protein modification. It occurs N-terminally or at lysine residues of amino acid sequences. It is estimated that 80 - 90% of all proteins in eukaryotes are acetylated (Walsh, 2006; Walsh et al., 2005). Acetylation is known to regulate many different cellular functions, including DNA recognition, gene regulation, protein-protein interaction and protein stability (Choi and Howe, 2009; Wang et al., 2011), but it is most prominently known as a histone modification enhancing transcriptional activity. By that means, acetylation also has a strong effect on synaptic plasticity, in particular late phase LTP and long-term memory, both of which are transcription-dependent (Sharma, 2010).

Sumoylation is a protein-based protein modification. SUMO (Small Ubiquitin-like MOdifier) is a collective term for three SUMO paralogues (SUMO 1, 2 and 3) of about 11.6 kDa that can be attached to lysine residues of other proteins (Martin et al., 2007). All three paralogues are abundantly expressed in the brain (Geiss-Friedlander and Melchior, 2007) and until recently they were considered to be mainly nuclear protein modifiers (Mahajan et al., 1997; Matunis, 1996). Several studies showed that cellular structures, such as dendrites, axons and synapses are also enriched in SUMO protein and in sumoylated proteins (Luo et al., 2013). Sumoylation can affect synaptic efficacy by altering protein-protein interaction,

and the activity and localization of modified proteins such as GluK2, CB1 and Arc in neurons (Lee et al., 2014; Martin et al., 2007). Sumoylation is dynamically regulated and was shown to be required for the normal expression of LTP and LTD (Tang et al., 2005; Wilkinson et al., 2008). Reversely, LTP induces an increase of SUMO1 in spines (Jaafari et al., 2013). Recently, it has been speculated that sumoylation plays a role in the development of neurodegenerative diseases, and inclusion bodies typical for Parkinson's disease and Alzheimer's disease are often SUMO immunoreactive (Dawson and Dawson, 2003; Dorval et al., 2007; Li et al., 2003).

Ubiquitylation

Ubiquitylation is the most common and most studied post-translational modification employing an entire protein as a modifier (Khoury et al., 2011). It plays a key role in many aspects of cellular life such as transcription, protein stability and intracellular transport (Hochstrasser, 2009). It is however mostly associated with its critical role in protein degradation. Ubiquitylation is the reversible attachment of ubiquitin, an 8.5 kDa protein, to a lysine residue of another protein (substrate) (Hershko, 1983; Hershko and Ciechanover, 1998). It is a process that demands the consecutive action of at least three different enzymes to finally attach one or multiple ubiquitin moieties to a lysine of the substrate protein (Streich et al., 2013). The three enzymes involved are: (i) an E1 ubiquitin-activating enzyme which covalently binds ubiquitin in an ATP-dependent manner, (ii) an E2 ubiquitin-conjugating enzyme which receives the activated ubiquitin from E1, and (iii) an E3 ubiquitin-protein ligase, which either directly transfers or facilitates the transfer of activated ubiquitin from E2 to the substrate protein (Figure 1). Two major types of ligases have been identified: HECT (Homologous to the E6-AP Carboxyl Terminus) and RING domain (Really Interesting New Gene domain) ligases (Pickart, 2004; Pickart and Eddins, 2004). Whereas E3 ligases of the HECT family form a thiol ester intermediate with ubiquitin and then directly transfer it to substrate proteins, E3 RING ligases do not directly transfer ubiquitin, instead they form a complex by interacting with a ubiquitin carrying E2 enzyme and the prospective substrate, thereby facilitating and catalyzing the transfer of ubiquitin (Hershko, 2005; Hershko et al., 2000; Pickart, 2004). Ubiquitin itself harbors 7 lysines (K6, K11, K27, K29, K33, K48, and K63) in its amino acid sequence, each of which can also be ubiquitylated, allowing the

formation of large ubiquitin chains. The type of ubiquitin chain and the number of ubiquitins then decide the fate of the substrate (Strieter and Korasick, 2012). Among other functions, mono-ubiquitylation for example is known to trigger endocytosis, change in localization and lysosomal degradation of proteins (Haglund and Dikic, 2012; Mosesson et al., 2009; Polo, 2012), whereas linear poly-ubiquitylation employing K48, and to a lesser degree K63, is generally known to target substrate proteins to the 26S proteasome for degradation (Hershko and Ciechanover, 1998). E3 ligases play a pivotal role in determining substrate specificity. This is reflected by the fact that the human genome alone encodes for 617 different E3 ligases (Li et al., 2008). E3 ligases usually only target a few very specific proteins, whereas E2 conjugating enzymes catalyze the ubiquitin transfer to the substrate and decide which of the ubiquitin lysines will be targeted for elongation (Berndsen and Wolberger, 2014; Strieter and Korasick, 2012).

It is worth noting that ubiquitylation is a highly dynamic and moreover reversible process (Reyes-Turcu et al., 2009). Ubiquitins attached to substrates can efficiently and specifically be removed or poly-ubiquitin chains be trimmed by de-ubiquitylation enzymes (DUBs). To date there are about 100 DUBs known (Komander et al., 2009), which is relatively few when compared to the more than 600 known E3 ligases (Li et al., 2008). However, considering that each DUB only needs to recognize certain consensus sites of ubiquitin-protein or ubiquitin-ubiquitin links, deubiquitylation can certainly be viewed as a very powerful antagonist of ubiquitylation.

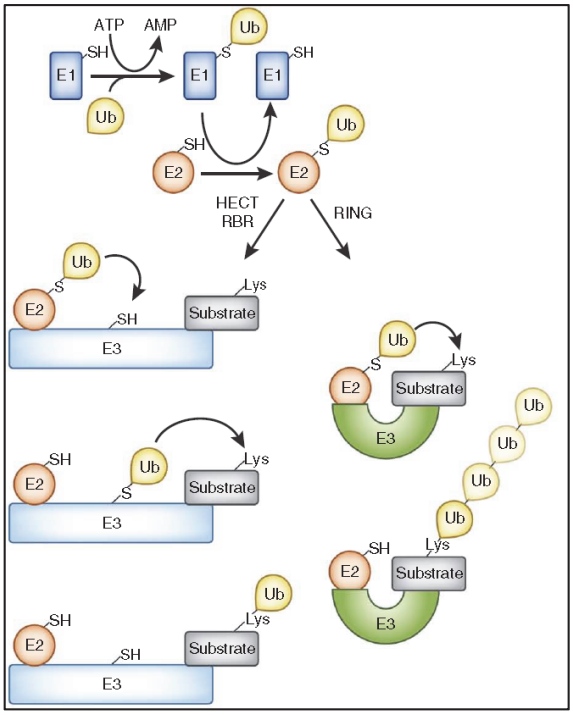

Figure 1. Ubiquitylation cascade. The ubiquitylation cascade begins with ATP-dependent charging of the E1 enzyme and results in the formation of a thioester bond between the ubiquitin C-terminus and the E1 active site cysteine. Ubiquitin is transferred to the E2 active site cysteine. An E3 ligase catalyzes the transfer of the ubiquitin from the active site cysteine of the E2 to a primary amine group on a lysine side chain or protein N-terminus. There are two main classes of E3 ligases: RING E3 ligases, which bind to both E2-Ub-thioester and substrate and thereby catalyze the ubiquitin transfer, and HECT ligases, which have active site cysteines and catalyze substrate ubiquitination in a two-step reaction involving formation of a thioester with the HECT followed by attack of the substrate lysine or N-terminus on the E3-Ub-thioester to form an isopeptide (or peptide) linkage between the ubiquitin C-terminus and lysine (or the protein N-terminus). Illustration and caption adjusted with permission from Berndsen and Wolberger (2014).

Ubiquitin ligases and the ubiquitin proteasome system in neurons

Ubiquitylation and several components of the ubiquitin proteasome system have been found to play a major role in plasticity, learning and memory, as well as in numerous neurodegenerative diseases (Dantuma and Bott, 2014; Mabb and Ehlers, 2010; Whalley, 2012). A common feature of diseases such as Alzheimer's, Parkinson's, and Huntington's is an aggregation/accumulation of certain proteins in the brain, mostly identified postmortem as amyloid plaques, Lewy bodies, neurofibrillary tangles and others. Accumulated proteins are often found to be highly ubiquitylated (Glickman and Ciechanover, 2002). Although it is still a matter of debate whether these ubiquitin-rich protein accumulations are cause or effect of the underlying diseases, it certainly demonstrates the involvement of the ubiquitin-proteasome system. For example mutations in the *PARK2* gene coding for the E3 ubiquitin ligase Parkin are responsible for about 50 % of all familial cases of Parkinson's disease and for 10 – 20 % of juvenile Parkinson's disease cases (Sandebring and Cedazo-Mínguez, 2012; Takahashi et al., 1994; Walden and Martinez-Torres, 2012). Another prominent example is the ubiquitin-protein ligase E3A (UBE3A) that, when defective in humans, causes Angelman syndrome, a neurodevelopmental disorder that is characterized by developmental delay and severe intellectual disabilities (Clayton-Smith and Laan, 2003; Kishino et al., 1997). Mouse models mimicking Angelman syndrome do not display such a severe phenotype, yet exhibit some deficits in LTP and learning (Bruinsma et al., 2015; Jiang et al., 1998; Silva-Santos et al., 2015). Although UBE3A and Parkin have been investigated extensively over the last decades and many ubiquitylation substrates suggested, it is not entirely clear to date what causative role, if any, they play in the development of Parkinson's disease and Angelman syndrome, respectively.

Many synaptic proteins, e.g. PSD-95, GKAP and SHANK, undergo activity dependent ubiquitylation (Ehlers, 2003; Mabb and Ehlers, 2010) and a small number of synaptic ubiquitin ligases have been identified. The number of identified synaptic E3 ligases is still growing, yet the identification of their substrates has proven to be rather difficult. A few ligase-substrate pairs, however, have successfully been identified and their role in plasticity and learning established. Ubiquitin ligase FBX2 for instance binds to the NR1 subunit of NMDA receptors and increases NR1 ubiquitylation in an activity-dependent manner (Kato et al., 2005). The presynaptic ubiquitin ligase SCRAPPER was shown to bind

and regulate RIM1, a presynaptic protein that is involved in vesicle release. SCRAPPER thereby indirectly regulates synaptic transmission (Takagi et al., 2012; Yao et al., 2007). Whereas overexpressing SCRAPPER in mice appears to have no effect on learning and behavior, knocking Scrapper out was lethal. Heterozygous *SCRAPPER* knockout mice however are viable and show increased freezing in a contextual fear memory paradigm (Yao et al., 2011). Another ubiquitin ligase, MDM2, was shown to bind and ubiquitylate PSD-95 in response to NMDA receptor activation (Colledge et al., 2003).

RING ligases and the TRIM protein family

E3 Ring ligases are the most diverse family of ligases that all share a common protein structure containing an N-terminal RING finger domain. The RING motif was first discovered when sequence databases were searched for the N-terminal domain of a gene termed *really interesting new gene 1* (*RING1*) and it consists of a conserved stretch of cysteine and histidine residues that bind two zinc ions. The RING domain is generally believed to confer ubiquitylation function to proteins that contain it (Deshaies and Joazeiro, 2009). While HECT ligases form a temporary thioester intermediate with ubiquitin before transfer to the substrate, RING ligases do not come in direct contact with ubiquitin, but rather bring the ubiquitin bound E2 and the substrate in proximity by binding to both, and thereby facilitate the ubiquitin transfer. The specificity of the reaction is provided by the E3 RING ligases pairing the E2s and their respective substrates (Glickman and Ciechanover, 2002; Hegde, 2010). RING finger E3 ligases can generally be divided into two groups: (i) large multisubunit RING finger E3 ligase complexes like SCF (Skp1/Cullin/Fbox) or APC/C (anaphase-promoting complex/cyclosome) that utilize multiple adaptors, cullin domains and RING domains to recruit substrates and ubiquitylate them, and (ii) single-subunit RING finger E3 ligases that contain the RING domain and substrate recognition sites in the same protein (Deshaies and Joazeiro, 2009; Mabb and Ehlers, 2010). One of the largest families of single-subunit RING finger E3 ligases are the TRIM (*tripartite motif*) proteins. TRIM family members have been shown to exert functions in a diversity of cellular processes, from development to antiviral immune responses, to finally playing a role in certain forms of cancer (Boulay et al., 2009; Pertel et al., 2011; Rajsbaum et al., 2014; Uchil et al., 2013). Yet, not in all cases is the specific function of a TRIM family member associated with its ubiquitin

ligase activity, nor has E3 ligase activity been demonstrated for every TRIM protein (Ozato et al., 2008). TRIM proteins are also known as RBCC motif-containing proteins, because the N-terminal region contains in addition to the RING domain one or two B-box domains and a coiled-coil region (Figure 2) (Meroni and Diez-Roux, 2005). The B-box domains also bind zinc ions and it is assumed that they contribute to the E3 ligase function, as was shown for TRIM18 (Han et al., 2011). The coiled-coil domain is required for homo- or heterodimerization and oligomerization, and it was shown to play an important role in cellular localization (Reymond et al., 2001). The coiled-coil domain is followed by a variable C-terminus that is used to classify TRIM proteins into subfamilies according to their domain composition (Reymond et al., 2001; Short and Cox, 2006). The number of subfamilies varies depending on domain classification and stringency. The most recent classification recognizes 11 subfamilies (Figure 2) (Ozato et al., 2008).

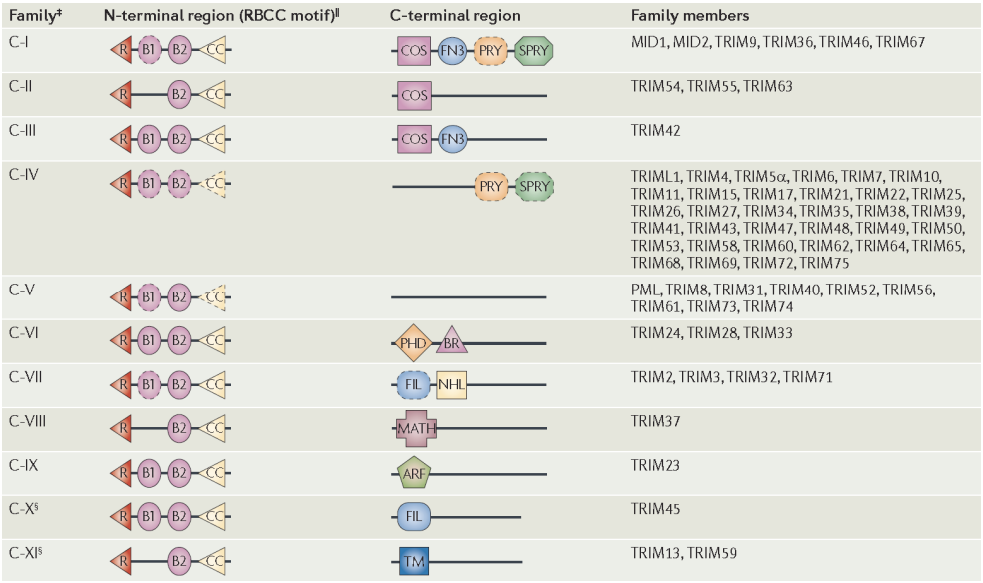

Figure 2 TRIM protein family. All members of the TRIM family contain the RBCC motif, consisting of a RING domain (R), 1 or 2 B-Box domains (B1, B2), and a coiled-coil domain (CC). TRIM protein family members are further grouped into 11 subfamilies according to their C-terminal composition. The RING domain is generally associated with the ability to facilitate ubiquitin transfer to substrate proteins. Coiled-coil domains are required for homo- and heterodimerization and oligomerization. TRIM3 belongs to subfamily VII, together with TRIM2, TRIM32 and TRIM71. All four members of this subfamily share a C-terminal NHL domain (NHL). Other illustrated domains are: ADP ribosylation factor-like (ARF), bromodomain (BR), C-terminal subgroup one signature (COS), fibronectin type 3 (FN3), filamin-type immunoglobulin (FIL), meprin and tumour-necrosis factor receptor-associated

factor homology (MATH), plant homeodomain (PHD), transmembrane (TM), splA kinase and ryanodine receptors domain (PRY, SPRY). Figure and caption adjusted with permission from Ozato et al. (2008).

TRIM3 and the TRIM-NHL subfamily

The TRIM-NHL subfamily of TRIM proteins, consisting of TRIM2, TRIM3, TRIM32 and TRIM71, share a stretch of 5 - 6 NHL repeats (first identified in protein NCL-1, HT2A and Lin-41) downstream of the RBCC domain (Slack and Ruvkun, 1998). TRIM32 is highly expressed in skeletal muscle (Horn et al., 2004; Kudryashova et al., 2005) and involved in two different human disorders, (i) limb-girdle muscular dystrophy type 2H (LGMD2H) and (ii) Bardet-Biedl syndrome (BBS). LGMD2H is caused by mutations in the NHL domain, whereas BBS is caused by an amino acid substitution in B-box 2 (Chiang et al., 2006; Cossee et al., 2009; Saccone et al., 2008). TRIM32 is an ubiquitin ligase that was shown to ubiquitylate many different proteins, e.g. X-linked inhibitor of apoptosis (XIAP) (Ryu et al., 2011), protein inhibitor of activated STAT (PIASy) (Albor et al., 2006) and muscle actin (Kudryashova et al., 2005). It was also recently shown that the NHL domain of TRIM32 positively regulates microRNA (miRNA) activity and plays a role in developmental timing and asymmetric cell division (Hammell et al., 2009; Schwamborn et al., 2009). TRIM71 is a close family member of TRIM32 and it was shown to associate and ubiquitylate AGO2 (Argonaute RISC Catalytic Component 2), a central protein in RNA mediated gene silencing (Rybak et al., 2009).

TRIM2 and TRIM3 are very similar and abundantly expressed in the brain (El-Husseini, 1999; Ohkawa et al., 2001). Both proteins interact with myosin V (Ohkawa et al., 2001; Reymond et al., 2001), yet a role in endosomal trafficking has not been demonstrated. TRIM2 further interacts with and ubiquitylates neurofilament light chain (NF-L). *Trim2* knockout mice are viable and born without apparent brain defects (Balastik et al., 2008). However they develop juvenile onset ataxia and exhibit spontaneous seizures. Brains of *Trim2* knockout mice show neurodegeneration from four months of age on, which is caused by increased levels of NF-L, leading to swollen axons and subsequent loss of neurons in the retina, cerebellum and spinal cord (Balastik et al., 2008). In a recently reported case of a patient with early-onset axonal neuropathy, two mutations in the *Trim2* gene as well as neurofilament accumulations were identified (Ylikallio et al., 2013), strengthening the

evidence that TRIM2 targets neurofilament light chain for degradation. TRIM3 is the subject of this thesis, and will be extensively introduced in the next paragraph.

Tripartite motif-containing protein 3 (TRIM3)

TRIM3, also called BERP (Brain Expressed Ring finger Protein), was first discovered in a RT-PCR (reverse transcription polymerase chain reaction) mRNA analysis of rat brain in 1999 (El-Husseini). It has the N-terminal RBCC motif (RING, B-box, coiled-coil) and a C-terminal domain consisting of six NHL repeats. With TRIM2 and TRIM32 it shares an immunoglobulin filamin-type (IG-FLMN) domain downstream of the RBCC motif. TRIM3 is highly expressed in the brain, particularly in cerebellum and hippocampus. Low levels of TRIM3 mRNA were also detected in other organs, e.g. lung, heart, liver and kidney (El-Husseini, 1999). When expressed in PC12 cells, TRIM3 localizes to the cytoplasm in a punctate pattern, but when a truncated TRIM3 protein lacking the NHL domain was expressed, cells remained small upon stimulation by nerve growth factor, formed clustered aggregates and failed to differentiate (El-Husseini, 1999), indicating that TRIM3 might play a role in cell differentiation. Another role for TRIM3 in intracellular transport or trafficking has also been suggested. Yeast-two-hybrid analysis showed that TRIM3 interacts with myosin Vb and alpha-actinin 4 (El-Husseini et al., 2000; El-Husseini, 1999). Yan et al. (2005) subsequently showed that TRIM3, alpha-actinin 4 and myosin V, together with the protein Hrs, form the cytoskeleton-associated recycling or transport (CART) complex, which is required for the efficient constitutive recycling of transferrin receptors and epidermal growth factor receptors in HeLa cells (Yan et al., 2005). Although these studies were all performed in non-neuronal cells, they might shed some light on the possible neuronal functions of TRIM3, as myosin Va and Vb were recently shown to be important motor proteins delivering AMPA receptor-containing cargo vesicles in neurons (Correia et al., 2008; Wang et al., 2008), and alpha-actinin plays a role in AMPA receptor transport in dendritic spines (Schulz et al., 2004). Recently, it was also reported that TRIM3 interacts with the orphan motor protein KIF21B, and that loss of TRIM3 reduces the motility of KIF21B in neurons (Labonte et al., 2013). Finally, Kanai et al. (2004) showed that TRIM3 is one of the major protein constituents of neuronal RNA transport granules associated with motor protein KIF5. Although these studies seem to suggest that TRIM3 is involved in cellular transportation, a

direct role for TRIM3 in the trafficking and/or recycling of AMPA receptors, or any other dendritic or synaptic cargo, has never been established.

Raheja et al. (2014) demonstrated convincingly that TRIM3 is indeed a RING domain ubiquitin ligase. In 2010 Hung et al. showed that TRIM3 is synaptically localized in neurons, and that overexpression of TRIM3 leads to a significant decrease in GKAP and SHANK1A levels in cultured cortical rat neurons. Importantly, the observed decrease was RING domain dependent. Overexpressing TRIM3 also caused a significant decrease in spine head width in cultured neurons, which would be in accordance with a decrease of synaptic scaffold proteins such as GKAP or SHANK. Although GKAP was suggested to be the direct ubiquitylation substrate of TRIM3, the two proteins were not shown to interact, and these very same authors subsequently showed that activity-dependent removal of GKAP from synapses *in vivo* does not likely depend on TRIM3 (Shin et al., 2012).

Ohkawa et al. (2001) showed that *Trim3* gene expression is coupled to activity. In order to trigger seizures, they lowered the seizure threshold of mice with the $GABA_A$ receptor antagonist pentylenetetrazole (PTZ) or with glutamate receptor agonist kainate. They observed that evoked seizures with both compounds increased mRNA expression of *Trim3*, but also of *Trim2*. In 2010 Cheung et al. demonstrated that *Trim3* deficient mice show increased resistance to PTZ-induced seizures, indicating that TRIM3 confers sensitivity to PTZ in mice. They argue that the PTZ insensitivity of *Trim3* deficient mice results from reduced surface expression of γ2-subunit-containing $GABA_A$ receptors, which also resulted in a decrease of miniature inhibitory postsynaptic currents. However, they failed to show a causal relationship between TRIM3 and GABA receptor surface expression.

Aim and outline of this thesis

The data presented in the introduction demonstrate that TRIM3 is a synaptically localized RING E3 ligase in the brain. Over the last decade TRIM3 has been investigated by several research groups, yet its role in neurons and especially at synaptic sites remains elusive. This study was aimed at understanding the precise role of TRIM3 in hippocampal and cerebellar function by making use of a newly generated *Trim3* knockout mouse and investigating it in a multidisciplinary manner. In **Chapter 2** a detailed analysis is provided of the morphological, cell physiological and behavioral phenotype of *Trim3* knockout mice. **Chapter 3** explores the possibility that TRIM3 is involved in mRNP trafficking. **Chapter 4** focuses on the identification of TRIM3 ubiquitylation substrates in the hippocampus and in the cerebellum, and in **Chapter 5** one of the identified substrates, ACTG1, is studied in more detail. Finally, in **Chapter 6** I summarize and discuss all data, and provide a working model in which TRIM3 and ACTG1 together contribute to the normal expression of hippocampal synaptic plasticity.

CHAPTER 2

The ubiquitin ligase TRIM3 affects hippocampal synaptic plasticity and learning in mice

Joerg Schreiber, Marlene J. Végh, Maarten Loos, Julia Dawitz, Tim Kroon, Chris I. de Zeeuw, Rhiannon R. Meredith, August B. Smit, and Ronald E. van Kesteren

Abstract

Post-translational protein modifications play an important role in cellular function. Ubiquitylation is one of the most common protein modifications. Poly-ubiquitylation in particular is a tightly controlled process targeting specific substrate proteins for subsequent proteasomal degradation. This specificity is achieved by E3 ubiquitin ligases recognizing and modifying only a certain set of substrate proteins. In recent years a number ubiquitin ligases were shown to regulate synaptic function and plasticity. Here, we show that TRIM3 is a synaptically localized E3 ligase in the hippocampus and the cerebellum. *Trim3* knockout mice show no morphological abnormalities in the hippocampus or the cerebellum, and anxiety, locomotion and motor coordination are unaffected. In contrast, hippocampal fear memory acquisition, long-term potentiation and spine densities are significantly enhanced in *Trim3* knockout mice. Our findings put forward TRIM3 as a synaptic E3 ligase that regulates hippocampal plasticity, learning and memory.

Introduction

Proteins can be viewed as molecular machines fulfilling a certain function in the cell. But as with the best machine, it is of no use, if it cannot be properly controlled. In the protein world, post-translational modifications are what switches, dials, buttons and levers are to real machines. The number of identified types of modifications ranges between 200 and 400, depending on which source is consulted (Farley and Link, 2009; Zhao and Jensen, 2009), all of which are able to change the function and fate of a protein in one way or another. The most common and also most studied post-translational modifications include phosphorylation, glycosylation, palmitylation, sumoylation and ubiquitylation (Khoury et al., 2011). The latter, ubiquitylation, is the main subject of this chapter.

Ubiquitylation is the attachment of ubiquitin, an 8.5 kDa protein, to a lysine residue of another protein, the substrate. This modification requires the consecutive activity of at least three different enzymes, an E1 ubiquitin-activating enzyme, which covalently binds ubiquitin in an ATP-dependent manner, an E2 ubiquitin-conjugating enzyme which receives activated ubiquitin from E1, and an E3 ubiquitin-protein ligase, which either directly transfers or facilitates the transfer of activated ubiquitin from E2 to the substrate protein. Substrate proteins, when poly-ubiquitylated, will be targeted to the proteasome for degradation

(Hershko and Ciechanover, 1998). E3 ligases play a key role in this process. They on the one hand recognize a specific substrate and a matching E2-carrying ubiquitin, and on the other hand catalyze ubiquitin transfer to the substrate (Berndsen and Wolberger, 2014). This specificity is reflected by the fact that the human genome encodes for 617 E3 ligases (Li et al., 2008). Recent studies show that a number of ubiquitin E3 ligases are found in or near synapses and that they target proteins involved in synaptic plasticity, learning and memory (Lin et al., 2011; Mabb et al., 2014; Takagi et al., 2012; Yao et al., 2007). Yet, a direct causal link between E3 ligase expression and learning behavior has not been established.

TRIM (tripartite motif) proteins are a large family (> 70 members in humans according to the HUGO Gene Nomenclature Committee) of structurally related proteins which all share an N-terminal RBCC (RING finger / B-box / coiled coil) region. TRIM proteins have a typical modular structure comprising multiple protein-protein interaction domains, and many have RING finger-dependent E3 ubiquitin ligase activity (Joazeiro and Weissman, 2000; Meroni and Diez-Roux, 2005; Reymond et al., 2001). Nine subfamilies of TRIM proteins are defined based on the nature of their C-terminal domains (Short and Cox, 2006). TRIM2, TRIM3 and TRIM32 form a subfamily that is characterized by a C-terminal IG-FLMN domain followed by six NHL repeats. TRIM2 and TRIM3 are structurally closely related and are predominantly expressed in the brain with largely overlapping expression patterns (El-Husseini, 1999; Ohkawa et al., 2001). TRIM32 is more distantly related and primarily expressed in skeletal muscle (Kudryashova et al., 2005). The NHL repeat domain of these proteins mediates interaction with myosins; TRIM2 and TRIM3 interact with unconventional class V myosins (El-Husseini, 1999; Ohkawa et al., 2001), whereas TRIM32 interacts with skeletal muscle Myosin II (Kudryashova et al., 2005). Myosins, however, are not ubiquitylation targets but rather are involved in determining subcellular localization. TRIM2 ubiquitiylates neurofilament light chain (NF-L) (Balastik et al., 2008), and TRIM32 ubiquitylates muscle actin (Kudryashova et al., 2009) and c-Myc in neuronal progenitors (Schwamborn et al., 2009). Hung et al. (2010) demonstrated that TRIM3 is indeed an E3 ubiquitin ligase, a finding that was later confirmed by Raheja et al. (2014) showing that TRIM3 ubiquitylates p21 in an *in vitro* assay.

Recently, *Trim2* and *Trim32* knockout mice were generated and analyzed (Balastik et al., 2008; Kudryashova et al., 2009), but neither protein seems a likely candidate E3 ligase for synaptic plasticity and learning processes. In this study we employed biochemical,

electrophysiological, behavioral and imaging techniques aimed to establish a potential role for TRIM3 in synaptic plasticity.

Material and Methods

Animals

Trim3$^{-/-}$ mice were maintained on a C57BL/6J background. In all experiments wildtype littermates were used as controls. Mice were individually housed on sawdust in standard Makrolon type II cages (26.5 cm long, 20.5 cm wide and 14.5 cm high) enriched with cardboard nesting material and a plastic tube under 12/12h dark/light cycle with access to water and food *ad libitum*. All animal experiments were approved by the animal ethics committee of the VU University Amsterdam, The Netherlands.

Immunohistochemistry

Mice were intracardially perfused with ice-cold paraformaldehyde (4 % in PBS, pH 7.4). Brains were removed, postfixed, embedded in gelatin (Mallinckrodt Baker, USA) and cryostat-sectioned at 40 µm. For immunostaining the following antibodies were used: Calbindin D28k (Swant, Bellinzona, Switzerland; 1:20,000) and TRIM3 (BD Biosciences, USA; 1:1,000). The antigens were visualized using VECTASTAIN ABC standard kit (Vector Laboratories, USA) or with secondary fluorescent Alexa Fluor 488 conjugated antibodies (Invitrogen, USA; 1:400). Nissl staining was used for gross morphological characterization of brain slices.

Golgi-Cox staining

Golgi-cox staining was performed using the FD Rapid GolgiStain Kit (FD NeuroTechnologies, USA). After staining, brains were microtome-sectioned at 100 µm. Neurons were photographed at 100 x magnification, and Z-stacks were generated using Image Pro Plus 6.2 software (Media Cybernetics Inc., USA). Morphological features were quantified using ImageJ 1.40g software (NIH, USA).

Immunofluorescence and confocal microscopy

Hippocampi were dissected from E18 wildtype mice, collected in Hanks balanced salts solution (HBSS; Sigma-Aldrich, USA) buffered with 7 mM HEPES (Invitrogen, USA) and incubated for 30 min in HBBS containing 0.25 % trypsin (Invitrogen, USA) at 37° C. After washing, neurons were triturated with fire-polished Pasteur pipettes, counted and plated in Neurobasal medium (Invitrogen, USA) supplemented with 2 % B - 27 (Invitrogen), 1.8 % HEPES, 1 % glutamax (Invitrogen, USA), 1 % Pen Strep (Invitrogen, USA) and 0.2 % 14.3 mM β-mercapto-ethanol. Cultures were plated on glass coverslips coated with poly-D-lysine (Sigma-Aldrich, USA) and treated with 5 % heat-inactivated horse serum (Invitrogen, USA). Neurons were plated at a seeding density of 250 cells/mm^2. Half of the medium was replaced with fresh medium every week. After 14 days in culture, neurons were fixed using 4 % paraformaldehyde and 10 % saccharose in PBS (pH 7.4). Neurons were stained with BERP (611732; BD Biosciences; 1:1,000) and MAP2 (AB5543, Abcam, 1:5,000) antibodies. Antigens were visualized using Alexa Fluor 488 and 568 (Molecular Probes; 1:400). Confocal microscopy was performed using a Zeiss LSM 510 (Zeiss, Germany).

Cellular fractionation

Brain tissue was obtained from C57BL/6 mice. Animals were sacrificed by cervical dislocation. Cortex, cerebellum and hippocampus were dissected and stored at -80° C. Cellular fractionation was performed as previously described (Klemmer et al., 2009). In brief, hippocampi were homogenized in a glass Potter homogenizer containing 5 ml of ice-cold homogenization buffer (320 mM sucrose in 5 mM HEPES, pH 7.4) at 900 rpm with 12 up and down strokes. Cell debris and nuclei were removed by centrifugation at 1,000 g for 10 min. The supernatant was centrifuged at 16,000 g for 30 min to obtain P2 fraction or at 100,000 g for 2 h to obtain crude synaptosome (P2 + M, Pellet 2 + microsomes) fraction enriched in synaptosomes and microsomes. For synaptosome and synaptic membrane isolation cleared homogenate was loaded on a sucrose gradient consisting of 0.85 M and 1.2 M sucrose. After ultracentrifugation at 100,000 *g*, 4° C for 2 h the synaptosome fraction was recovered at the interface of 0.85/1.2 M sucrose. Synaptosomes were then diluted with an equal volume of 5 mM HEPES buffer (pH 7.4) and brought to 15 ml using homogenization buffer, centrifuged at 25,000 g for 30 min. The pellet was resuspended in HEPES buffer and osmotically shocked while stirring slowly on ice for 15 min. The resulting synaptic

membrane fraction was recovered by ultracentrifugation using the sucrose step gradient as outlined above. Protein concentrations were measured using Bradford Protein-Assay (Bio-Rad Laboratories, USA) and equal amounts of protein were separated on a 10 % SDS-PAGE gel and transferred to PVDF membranes (Bio-Rad Immuno-Blot PVDF membrane, Bio-Rad Laboratories). Blots were blocked by immersing in 5 % nonfat dry milk in PBS-T (PBS plus 0.05 % Tween) for 1 h. Blots were then incubated with antibodies for BERP (611732, BD Biosciences, 1:250) and PSD-95 (73-028, Neuromab, 1:10) for 1 h at room temperature or overnight at 4° C, followed by a 1 h incubation with a secondary antibody conjugated to alkaline phosphatase. Proteins were visualized by ECF treatment (24 µl ECF substrate/cm^2) and scanned using an FLA-5000 scanner (Fujifilm, Japan).

Cell culture

Human embryonic kidney cells (HEK293) were maintained in Dulbecco's modified Eagle medium supplemented with 10 % fetal bovine serum and 1 % Penicillin-Streptomycin (all from Life Technologies Thermo Fisher Scientific Inc., USA) at 37° C and 5 % CO_2. Cells were transfected with myc-TRIM3, myc-ΔRBCC-TRIM3 or mock-transfected at 60 – 80 % confluence using polyethylenimine (PEI). After 48 h cells were washed with ice cold PBS and subsequently lysed in SDS-containing loading buffer. Samples were separated on 4 – 20 % gradient SDS-PAGE gel (Criterion TGX Stain-Free Gel, Bio-Rad Laboratories) and then transferred to PVDF membranes (Bio-Rad Immuno-Blot PVDF membrane, Bio-Rad Laboratories). Blots were blocked by either immersing the membrane in 5 % nonfat dry milk in TBS-T (TBS plus 0.025 % Tween) or 0.5 % BSA in TBS-T (TBS plus 0.025 % Tween) for 1 h. Blots were then incubated with antibodies for Actin (sc65634, Santa Cruz, 1:10,000) and Ubiquitin (BML-PW8810, Enzo Life Sciences, 1:100) for 1 h at room temperature or overnight at 4° C, followed by 1 h incubation with a secondary antibody conjugated to HRP. Proteins were visualized by ECL treatment (SuperSignal West Femto Chemiluminescent Substrate, Thermo Scientific) and scanned using the Odyssey Fc imager (Li-Cor, USA).

Spontaneous synaptic transmission

Mice of age 22 - 38 days were decapitated and brains rapidly removed and dissected in ice-cold carbogenated (95 % O_2/5 % CO_2) slicing solution (110 mM choline chloride, 26 mM $NaHCO_3$, 10 mM D-glucose, 11.6 mM Na-ascorbate, 7 mM $MgCl_2$, 3.1 mM Na-pyruvate,

2.5 mM KCl, 1.25 mM NaH_2PO_4, 0.5 $CaCl_2$). Horizontal hippocampal slices (300 µm) were prepared as previously described (Dawitz et al., 2011). Slices were stored for at least 1 h in a submerged-style holding chamber containing carbogenated artificial cerebrospinal fluid (aCSF; 125 mM NaCl, 26 mM $NaHCO_3$, 10 mM D-glucose, 3 mM KCl, 2.5 mM $MgCl_2$, 1.6 mM $CaCl_2$ and 1.25 mM NaH_2PO_4). Slices were then transferred to a recording chamber and perfused continuously with carbogenated aCSF (as in the holding chamber, but with 1.5 mM $MgCl_2$). CA1 pyramidal neurons were identified on the basis of cell soma location and basic firing properties recorded using the whole-cell patch-clamp technique. For recording excitatory synaptic currents patch pipettes (borosilicate glass, 3-5 MΩ resistance) were filled with 148 mM K-gluconate, 1 mM KCl, 10 mM HEPES, 4 mM Mg-ATP, 4 mM K_2-phosphocreatine, 0.4 mM GTP and 0.2 % biocytin, adjusted with KOH to pH 7.3. For inhibitory currents, intracellular solution contained 70 mM K-gluconate, 70 mM KCl, 10 mM HEPES, 4 mM Mg-ATP, 4 mM K_2-phosphocreatine, mM 0.4 GTP and 0.2 % biocytin, adjusted with KOH to pH 7.3. Neurons were allowed to stabilize for at least five minutes after a whole-cell configuration was achieved. For all measurements, eight-minute gap-free recordings were made at -70 mV holding potential in voltage-clamp mode. Spontaneous excitatory postsynaptic currents (sEPSCs) were measured in the presence of GABAa receptor blocker gabazine (10 µM), spontaneous inhibitory postsynaptic currents (sIPSCs) in the presence of glutamate receptor blockers DAPV (50 µM) and CNQX (10 µM). EPSCs and IPSCs were detected using Mini analysis software (Synaptosoft, USA). Amplitude, frequency, rise- and decay times of excitatory and inhibitory currents were measured and statistical significance was determined using a two-tailed t-test.

Spine analysis

Hippocampal slices were prepared from 8 - 10 weeks old mice and CA1 neurons recorded as described above. Cells were kept in whole-cell configuration for 10 - 15 min to fill with biocytin, after which a Giga-seal was obtained when retracting the pipette. After retraction of the pipette, slices were immediately fixed in 4 % paraformaldehyde in PBS for 1 - 2 days at 4° C. Slices were then washed four times for > 10 min in PBS and incubated with 0.5 % Triton X-100 in PBS, after which they were incubated for two days with 1:500 streptavidin-Alexa 488 conjugate (Life Technologies, Thermo Fisher Scientific, USA) and 0.1 % Triton X-100 in PBS. To-Pro-3 (Life Technologies) was added at 1:10,000 for the last 10 min of

incubation to counterstain for nuclei. Slices were then washed four times for > 15 min in PBS and mounted in Mowiol on glass slides. Labeled cells were imaged using a Nikon Ti-E A1R (Nikon, Tokyo, Japan) confocal microscope using a 10 x 0.45 NA air objective to check the position of the cells in CA1. Spines were imaged using a 100x 1.49 NA oil immersion objective at a resolution of 80 (x) x 80 (y) x 125 (z) nm/pixel. Approximately 80 µm of the first oblique dendrite and 80 µm of the first basal dendrite (either clockwise or counter clockwise from the apical dendrite) were imaged. For each labelled neuron one oblique and one apical dendrite were analyzed using NeuronStudio software (v0.9.92) (Rodriguez et al., 2008). Automatic dendrite tracing and spine recognition were used and spine densities were calculated. Statistical significance was determined using a two-tailed t-test.

Long-term potentiation

A planar multi-electrode recording setup (MED64 system; Alpha Med Sciences, Tokyo, Japan) was used to record field excitatory post-synaptic potential (fEPSP) and to elicit LTP as previously described (Shimono et al., 2002). Animals were decapitated and brains were rapidly removed and placed in ice-cold slice buffer (124 mM NaCl, 3.3 mM KCl, 1.2 mM KH_2PO_4, 7 mM $MgSO_4$, 0.5 mM $CaCl_2$, 20 mM $NaHCO_3$ and 10 mM glucose; constantly gassed with 95 % O_2/5 % CO_2). Coronal hippocampal slices were prepared using a vibrating microtome at 400 µm and then placed in a chamber containing aCSF (124 mM NaCl, 3.3 mM KCl, 1.2 mM KH_2PO_4, 1.3 mM $MgSO_4$, 2.5 mM $CaCl_2$, 20 mM $NaHCO_3$ and 10 mM glucose; constantly gassed with 95 % O_2/5 % CO_2). Slices were allowed to recover for one hour and then placed on 8 x 8 multi-electrode arrays containing P5155 probes (Alpha Med Sciences; inter-electrode distance 150 µm) pre-coated with polyethylenimine (PEI; Sigma-Aldrich, USA). After addition of 500 µl aCSF the array was placed in a moist chamber that was constantly gassed with 95 % O_2/5 % CO_2 for at least one hour before recording. Correct placement of the electrodes at the CA3 – CA1 region was done manually, monitored by a microscope (SZ61; Olympus, Japan). During recording, slices were constantly perfused with oxygenated aCSF containing 10 µM glycine at a flow rate of 2 ml/min at room temperature. fEPSPs were recorded from multiple electrodes in the stratum radiatum of CA1. An external concentric bipolar electrode (CBCBG75; FH-Company, Bowdoin, ME) in the Schaffer collateral pathway was used as the stimulating electrode using a homemade model 440b

isolated Bipolar Current Stimulator. Based on the stimulus–response curve, a stimulation intensity was used that evoked fEPSPs with a magnitude of 50 % of the maximum response (usually ~100 µA). After allowing a stable baseline of 10 min, LTP was evoked by a 2 x 100 Hz stimulus of 1 s each with a 15 s interval and fEPSP responses were recorded for 1 h after the tetanus. LTP was expressed as the change in the slope of the fEPSP relative to baseline and averaged for multiple electrodes (usually 5) located in the stratum radiatum. Statistical significance was determined using a two-tailed t-test on the fEPSP change from 10 – 20 min or 20 - 30 min after LTP induction.

Open field test

Mice were introduced into a corner of the white square open field (50 x 50 cm, walls 35 cm high) illuminated with a single white fluorescent light bulb from above (130 lx), and exploration was tracked for 10 min (12.5 frames/s; EthoVision 3.0, Noldus Information Technology, The Netherlands). EthoVision was used to calculate the total distance traveled as well as the time spent and the number of entries into the center square area (20 x 20 cm). The SEE software (Strategy for the Exploration of Exploration; (Kafkafi and Elmer, 2005) was used to smoothen path shape and calculate specific measures of locomotor behavior. SEE uses the distribution of speed peaks to parse the locomotor data and to slow local movements (so-called lingering episodes) and progression segments.

Light-Dark box

Mice were introduced into the dark compartment (< 10 lx; 25 x 25 x 30 cm, length x width x height) of a light-dark box and the lit was closed. After one minute the bright light was switched on, and the door to the brightly lit compartment (320 lx; same dimensions) was opened. Exploratory behavior of eight mice was video tracked simultaneously for 10 min (12.5 frames/s, EthoVision 3.0, Noldus Information Technology). The number of transitions into, and the total time spent in the light compartment were calculated using the hidden zone feature in EthoVision with the border of crossing into the light compartment defined two cm away from the door in the light compartment.

Elevated plus maze

Mice were introduced into the closed arm of an elevated plus maze (EPM, arms 30 x 6 cm, walls 35 cm high, elevated 50 cm above the ground), all facing the same closed end of the arm. The EPM was illuminated with a single white fluorescent light bulb from above (130 lx) and exploratory behavior was video tracked for five min (12.5 frames/s, EthoVision 3.0, Noldus Information Technology, The Netherlands). The border between center and arm entries was defined at two cm into each arm, producing the number of entries and total duration in the open arms, closed arms and the center platform.

Rotarod

Motor performance was tested using a rotarod device as previously described (van Hagen et al., 2007). In short, mice were placed on a rotating rod, and the latency to fall off the rod was recorded as a measurement of motor performance. Mice were initially trained to stay on a stationary rod and on a rod at a constant rotational speed of two rpm. Next, their latency to drop off was measured with increasing rotational speed (from 2 to 12 rpm in 2 min) during four different sessions.

Fear conditioning

Fear conditioning experiments were carried out as described (Misane et al., 2005; Stiedl et al., 2000) using a computerized fear conditioning system (TSE, 303410, Bad Homburg, Germany). In brief, mice were placed in an acrylic cage mounted into a constant illuminated (450 lux) fear conditioning box. After a 180 s exploration period, mice received a 2 s foot shock (0.7 mA) delivered through a metal floor grid. Mice were returned to their home cages 30 s after termination of the shock. Activity, exploration and freezing (lack of movement aside from respiration and heart beat) were measured automatically via infrared lasers before, during and after the shock. Contextual fear memory was measured as the time spent freezing after re-exposure of the animals to the conditioned context at various time points after receiving the shock.

Results

TRIM3 is a synaptic E3 ubiquitin ligase expressed in hippocampus and cerebellum

We first aimed to confirm that TRIM3 is an ubiquitin ligase. We generated expression constructs for full length TRIM3, and for mutant TRIM3 lacking the RING/B-box/coiled-coil domain (ΔRBCC- RIM3; Figure 1A). When we expressed these constructs in HEK293 cells and immunoblotted the cell lysates for ubiquitin, we observed a strong increase in high-molecular weight ubiquitin staining specifically in TRIM3-expressing cells (Figure 1B). These findings indicate that TRIM3, but not ΔRBCC-TRIM3, has ubiquitin ligase activity, and confirm previous work by Hung et al. (2010), who showed that TRIM3 can poly-ubiquitylate the protein GKAP *in vitro*. These same authors also showed that TRIM3 protein is enriched in biochemically isolated light membrane fractions from the cortex, suggesting synaptic localization. When we performed biochemical enrichment on hippocampal tissue and analyzed the different fractions for the presence of TRIM3, we observed a similar distribution, with relatively high TRIM3 protein levels in the microsome fraction and in the synapse (Figure 1C). TRIM3 staining on brain sections subsequently showed that TRIM3 is most strongly expressed in two brain regions, the hippocampus and the cerebellum. In the hippocampus TRIM3 is expressed throughout the CA region, but less in the dentate gyrus (Figure 1D). The TRIM3 antibody clearly also labeled the dendrites of CA pyramidal cells (Figure 1E). In the cerebellum TRIM3 protein is localized in the granular layer, the molecular layer and in the deep cerebellar nuclei (Figure 1F - H). A double staining for TRIM3 and Calbindin, a Purkinje cell marker, confirmed that TRIM3 is specifically expressed in molecular and granule cell layer, but not in Purkinje cells. TRIM3 protein staining in the cerebellum opposes that of TRIM2, which is absent in molecular and granular cell layer, but present in Purkinje cells. Absence of staining in *Trim3*$^{-/-}$ sections confirmed the specificity of the antibody (Figures 1D' - H'). We also stained cultured hippocampal neurons for TRIM3 and observed a punctate labeling in MAP2-positive dendrites, consistent with microsomal and/or synaptic localization and with the previous findings of Hung et al. (2010). Together these data confirm that TRIM3 is a synaptic ubiquitin ligase.

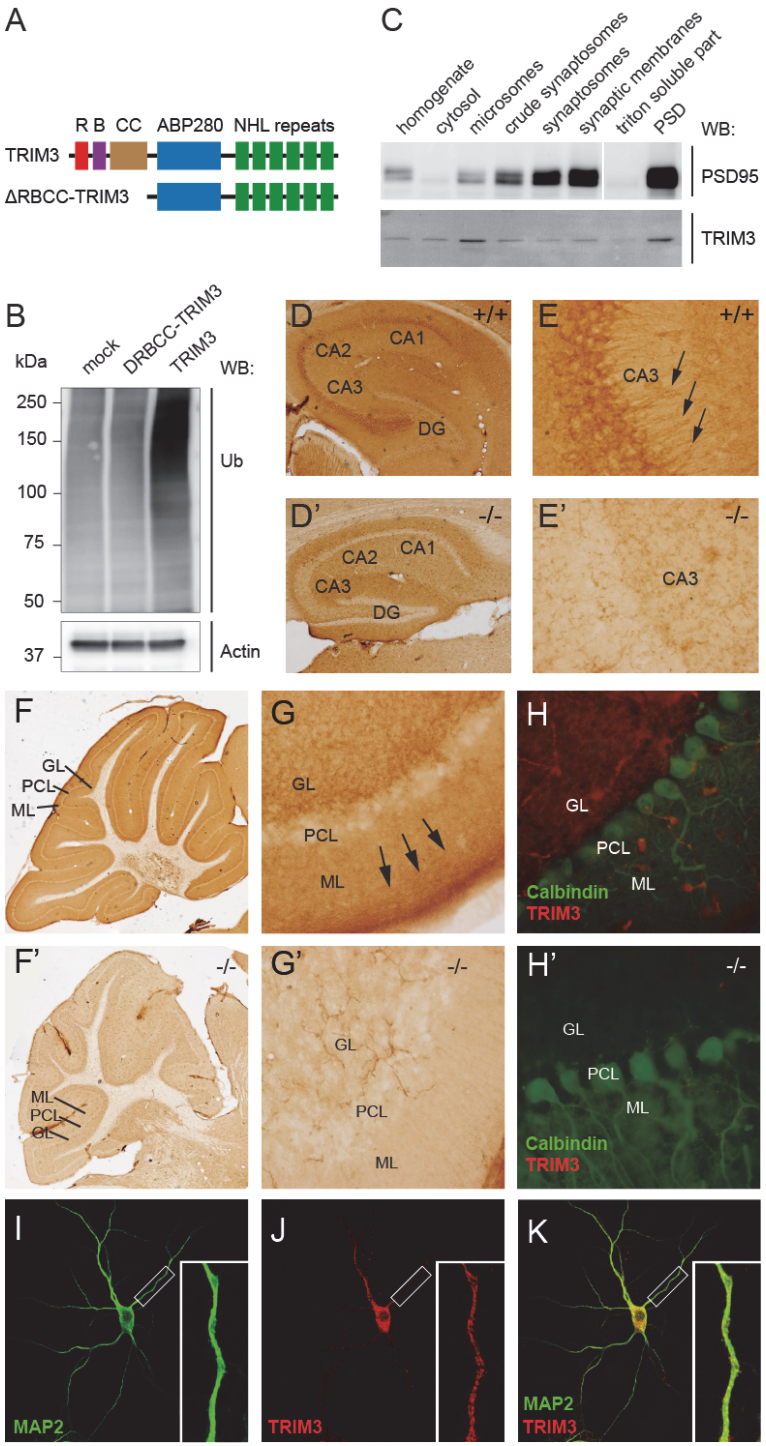
A
R B CC ABP280 NHL repeats
TRIM3
ΔRBCC-TRIM3
C
homogenate
cytosol
microsomes
crude synaptosomes
synaptosomes
synaptic membranes
triton soluble part
PSD
WB:
PSD95
TRIM3
B
kDa
mock
DRBCC-TRIM3
TRIM3
WB:
250
150
100
75
50
37
Ub
Actin
D
+/+
CA1
CA2
CA3
DG
E
+/+
CA3
D'
-/-
CA1
CA2
CA3
DG
E'
-/-
CA3
F
GL
PCL
ML
G
GL
PCL
ML
H
GL
PCL
ML
Calbindin
TRIM3
F'
-/-
ML
PCL
GL
G'
-/-
GL
PCL
ML
H'
-/-
GL
PCL
ML
Calbindin
TRIM3
I
MAP2
J
TRIM3
K
MAP2
TRIM3

Figure 1 TRIM3 is a synaptically localized ubiquitin ligase expressed in hippocampus and cerebellum. (A) Schematic diagram of full-length TRIM3 and ΔRBCC-TRIM3 constructs. Deletion of the RBCC domain abolishes E3 ligase activity (Hung et al., 2010). R, RING; B, B-box; CC, coiled-coil; ABP280, actin-binding protein 280 repeat; NHL repeat, NCL-1/HT2A/LIN-41 repeat. **(B)** TRIM3 induces poly-ubiquitylation in HEK293 cells. Lysates from HEK293 cells expressing full length TRIM3 or ΔRBCC-TRIM3 and mock-transfected cell lysates were subjected to WB analysis using an anti-ubiquitin (Ub) antibody. Increased poly-ubiquitylation is evidenced by a strong increase in high-molecular weight ubiquitin staining. Actin staining is shown as loading control. **(C)** TRIM3 is enriched in microsomal and synaptic fractions. Biochemical fractionation of hippocampal tissue followed by Western blot (WB) analysis showed that TRIM3 protein is enriched in the postsynaptic density fraction and in microsomes. Synaptic enrichment is evidenced by PSD95 staining. **(D - H)** Immunohistochemistry showed that TRIM3 protein is highly expressed in hippocampus and cerebellum. **(D - E)** In the hippocampus TRIM3 staining is found throughout the CA regions, but less in the dentate gyrus (DG) **(D)**. TRIM3 was primarily detected in CA pyramidal cell bodies, but also in dendrites (arrows in **E**). **(F - H)** In the cerebellum TRIM3 protein is expressed in the granule layer (GL) and molecular layer (ML), but not in the Purkinje cell layer (PCL). **(G)** In the molecular layer, TRIM3 labeling is strongest at the pial surface (arrows). **(H)** Trim3/Calbindin immunofluorescence double staining (red = TRIM3, green = calbindin) confirms the absence of TRIM3 protein in Purkinje cells. **(D' - H')** Staining of hippocampal and cerebellar sections from *Trim3*$^{-/-}$ animals confirmed the specificity of the TRIM3 labeling. **(I - K)** Immunocytochemistry revealed a punctuate staining of TRIM3 in dendrites of cultured primary hippocampal neurons. Neurons were cultured for 14 days and then labeled with antibodies against MAP2 (green; **I**) and TRIM3 (red; **J**). The overlay image clearly revealed TRIM3-positive puncta inside MAP2-positive dendrites **(K)**.

Trim3$^{-/-}$ mice have a hippocampal memory and plasticity deficit

Having confirmed that TRIM3 is a synaptically localized ubiquitin ligase in the hippocampus, we next tested whether loss of TRIM3 causes memory and plasticity deficits. We recently generated a *Trim3*$^{-/-}$ mouse (Labonte et al., 2013), which we here used for detailed morphological and functional analyses. Nissl staining revealed normal hippocampal morphology (Figure 2A), and Golgi-Cox staining did not indicate major differences in the dendritic morphology of CA1 and CA3 pyramidal neurons (Figures 2B - C) and dentate gyrus granule neurons (Figure 2D) between *Trim3*$^{-/-}$ mice and wildtype controls. The gross morphology and layering of the cerebellum are also intact in *Trim3*$^{-/-}$ mice (Figures 2E - F). Purkinje cell specific Calbindin staining further confirmed the integrity of the Purkinje cell layer (Figure 2H) and Golgi-Cox staining of Purkinje cells (Figure 2G) and cerebellar granule cells (Figure 2I) did not reveal major differences in cellular morphology.

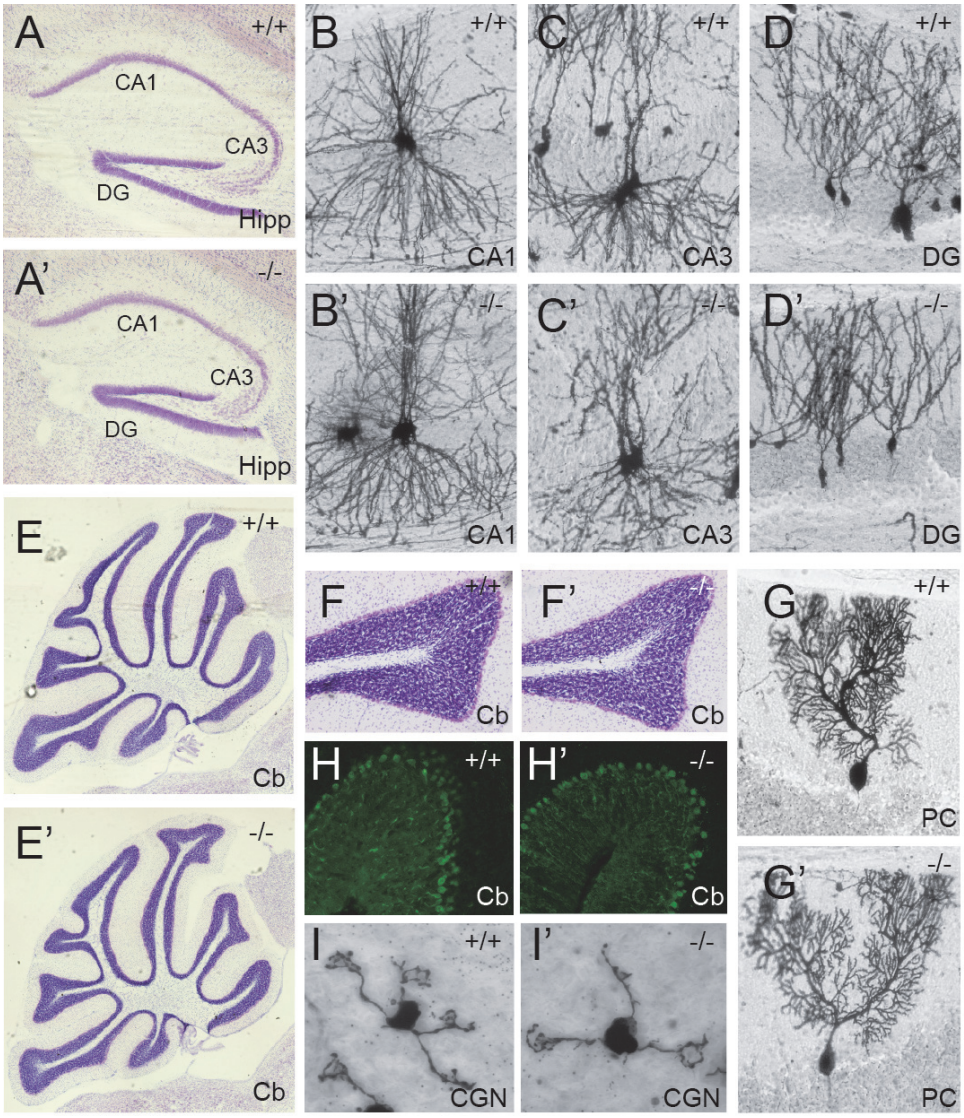

Figure 2 ***Trim3*$^{-/-}$ mice exhibit no brain morphological abnormalities (A)** Nissl staining showed normal gross morphology of the hippocampus in *Trim3*$^{-/-}$ mice **(A)** compared with wildtype controls **(A')** at four months of age. **(B - D)** Golgi-cox staining showed normal cellular morphology of CA1 (B) and CA3 **(C)** pyramidal neurons and of granule neurons in the dentate gyrus **(D)** in *Trim3*$^{-/-}$ mice compared with wildtype controls **(B' - D')**. CA; cornu amonis; DG, dentate gyrus. **(E - F)** Cerebellar morphology is normal in *Trim3*$^{-/-}$ mice. **(E)** Nissl staining showed normal gross morphology of the cerebellum **(H)** Calbindin staining confirmed normal appearance of the Purkinje cell layer. **(G - I)** Golgi-cox staining showed normal cellular morphology of Purkinje cells **(G)** and cerebellar granule neurons **(I).**

Behavioral analysis of *Trim3*$^{-/-}$ mice did not reveal important alterations in basal performance. We specifically assessed anxiety, locomotor behavior and motor coordination using open field, dark-light box, elevated plus maze and rotarod tests. In all tests, three months old *Trim3*$^{-/-}$ mice and wildtype controls scored comparable on all test parameters (Table 1). In a contextual fear memory task, however, we observed that *Trim3*$^{-/-}$ mice showed enhanced memory acquisition (Figure 3). Fear memory was measured as the amount of freezing that animals showed in an environment in which they had previously experienced a mild foot shock (Misane et al., 2005). Freezing was measured independently at 2 h (short-term memory) and at 24 h (long-term memory) after the shock using separate cohorts of animals (Figure 3A). At 24 h, *Trim3*$^{-/-}$ mice and wildtype littermates showed a similar increase in freezing behavior (Figure 3B), indicating that long-term memory consolidation occurred equally well in both genotypes. However, at 2 h after the shock *Trim3*$^{-/-}$ mice showed significantly higher freezing levels compared with wildtype controls ($p < 0.05$, n = 8/10, WT 16.6 ± 2.8, KO 28.4 ± 5.1 % freezing) (Figure 3B). Notably, the level of freezing in *Trim3*$^{-/-}$ mice was already at the level that was observed for both genotypes at 24 h after the shock. These data indicate that a fully consolidated fear memory is expressed much earlier in *Trim3*$^{-/-}$ mice compared with wildtype controls.

Table 1. Behavioral analysis of Trim3 knock-out mice.

		WT (n = 12)	KO (n=12)	
Test / test measure	unit	Mean ± SE	Mean ± SE	p-value
Open Field - Ethovision				
Number of entries into the center area		84.83 ± 4.07	91.67 ± 6.36	0.375
Time spent in the center area	s	314.5 ± 18.0	308.0 ± 18.4	0.803
Total distance traveled		5602 ± 264	5819 ± 345	0.622
Open Field - SEE analysis - velocity				
Lingering progression threshold speed	cm/s	12.05 ± 0.61	12.89 ± 0.83	0.418
Median of move segment max speed	cm/s	24.03 ± 0.69	25.01 ± 1.00	0.425
Quantile 95 of move segment max speed	cm/s	35.80 ± 0.89	35.54 ± 1.03	0.850
Lingering mean speed	cm/s	1.65 ± 0.10	1.66 ± 0.10	0.988
Median of lingering segment max speed	cm/s	3.17 ± 0.40	2.28 ± 0.60	0.231
Open Field - SEE analysis - acceleration				
Latency to max half speed	s	8.65 ± 3.84	5.88 ± 1.62	0.513
Median segment acceleration to max speed	cm/s^2	15.77 ± 0.69	15.44 ± 0.57	0.715
Open Field - SEE analysis - other				
Number of progression segments	segments	143.3 ± 10.7	142.0 ± 10.2	0.934
Median length of progression segments	cm	24.73 ± 0.96	28.40 ± 2.08	0.123
Median duration of progression segments	s	1.55 ± 0.05	1.63 ± 0.07	0.369
Quantile 5 of duration of progression segments	s	0.55 ± 0.03	0.57 ± 0.04	0.755
Quantile 95 of duration of progression segments	s	3.38 ± 0.10	3.62 ± 0.14	0.172
Number of stops per distance	segments/cm	0.03 ± 0.00	0.03 ± 0.00	0.386
Time proportion of lingering episodes		0.59 ± 0.03	0.58 ± 0.03	0.651
Median radius of turn	cm	77.69 ± 3.74	81.05 ± 3.41	0.513
Median turn rate	degrees/s	14.06 ± 0.58	13.83 ± 0.48	0.761
Light-Dark Box				
Number of entries into the light compartment		29.50 ± 3.30	38.00 ± 3.67	0.099
Time spent in the light compartment	s	301.1 ± 17.2	305.2 ± 16.7	0.863
Elevated Plus Maze				
Number of entries into the closed arms		22.00 ± 1.93	23.50 ± 1.81	0.576
Number of entries into the open arms		28.42 ± 2.94	32.75 ± 2.66	0.287
Number of entries into the middle		25.92 ± 2.53	29.58 ± 2.18	0.284
Time spent in the closed arms	s	419.8 ± 15.0	395.7 ± 7.9	0.171
Time spent in the open arms	s	159.7 ± 12.6	175.2 ± 8.3	0.315
Time spent in the middle	s	**84.64 ± 7.37**	**110.07 ± 7.87**	**0.028**
Total distance moved	cm	1552 ± 86	1608 ± 76	0.632
Rotarod				
Latency to fall (session 1)	s	163 ± 17	172 ± 23	0.761
Latency to fall (session 2)	s	217 ± 21	213 ± 20	0.892
Latency to fall (session 3)	s	238 ± 20	208 ± 24	0.351
Latency to fall (session 4)	s	224 ± 27	224 ± 20	0.999

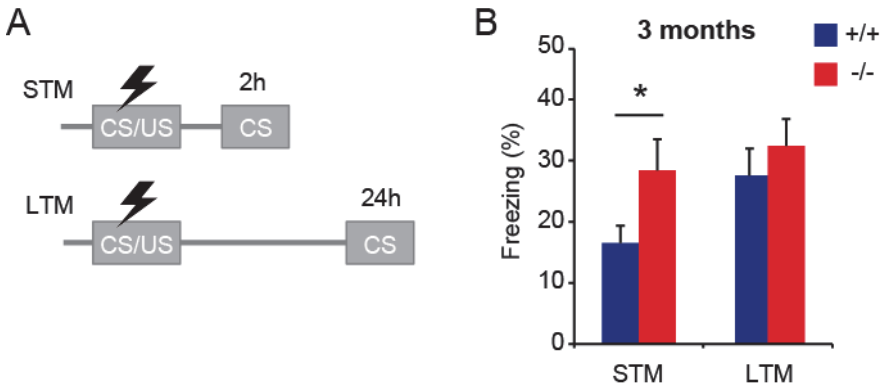

Figure 3 Contextual fear memory is enhanced in *Trim3*$^{-/-}$ mice. (A) Hippocampal memory performance was measured in a contextual fear memory task. Animals received a mild foot shock (unconditioned stimulus; US) in a novel context (conditioned stimulus; CS). Memory retrieval was tested either 2 h (short-term memory; STM) or 24 h (long-term memory; LTM) after conditioning by re-exposing animals to the shock-associated context (CS) and measuring the amount of freezing. STM and LTM were tested in two independent cohorts of mice. **(B)** Freezing behavior was significantly increased in *Trim3*$^{-/-}$ mice compared with wildtype littermates when re-exposed to the conditioned context 2 h after receiving the shock (STM), but not at 24 h (LTM), indicating enhanced consolidation of fear memory (means ± SEM, two-tailed t test, *$p < 0.05$, n = 8/10 per genotype).

Trim2$^{-/-}$ mice show a strong age-dependent neurodegenerative phenotype (Balastik et al., 2008). Because TRIM3 and TRIM2 are very similar, we wanted to exclude the possibility that the behavioral phenotype of *Trim3*$^{-/-}$ mice is also due to neurodegeneration and thus performed morphological and behavioral analyses in an independent cohort of eight month old animals. Gross hippocampal morphology was not affected in *Trim3*$^{-/-}$ mice at eight months of age (Supplemental Figure S1) and basal behavioral analyses did not reveal important alterations either (Supplemental Table S1). Importantly, enhanced memory consolidation after contextual fear conditioning was still observed in *Trim3*$^{-/-}$ mice at this age (Supplemental Figures S1 B - C), indicating that this phenotype is robust and unique, and not the result of other major morphological or behavioral alterations.

We then asked whether there are structural or physiological impairments in *Trim3*$^{-/-}$ mice that might explain the observed enhancement of fear memory consolidation. Spontaneous synaptic activity measurements in acute hippocampal slice preparations did not reveal significant differences between genotypes in either EPSC (Figure 4A) or IPSC (Figure 4B) amplitude (EPSC, WT: 12.11 ± 0.55, KO: 13.13 ± 1.01; IPSC, WT: 40.6 ± 5.1, KO: 33.71 ± 3.99 [pA]), frequency (EPSC, WT: 3.34 ± 0.95, KO: 1.98 ± 0.83; IPSC, WT: 12.37 ± 1.81, KO: 9.52 ± 2.14 [Hz]), rise time (EPSC, WT: 1.82 ± 0.14, KO: 1.96 ± 0.15; IPSC, WT: 1.50 ± 0.06, KO: 1.42 ± 0.05 [ms]) or decay time (EPSC, WT: 6.52 ± 0.47, KO: 6.85 ± 0.43; IPSC, WT: 16.26 ± 0.97, KO: 14.84 ± 1.12 [ms]).

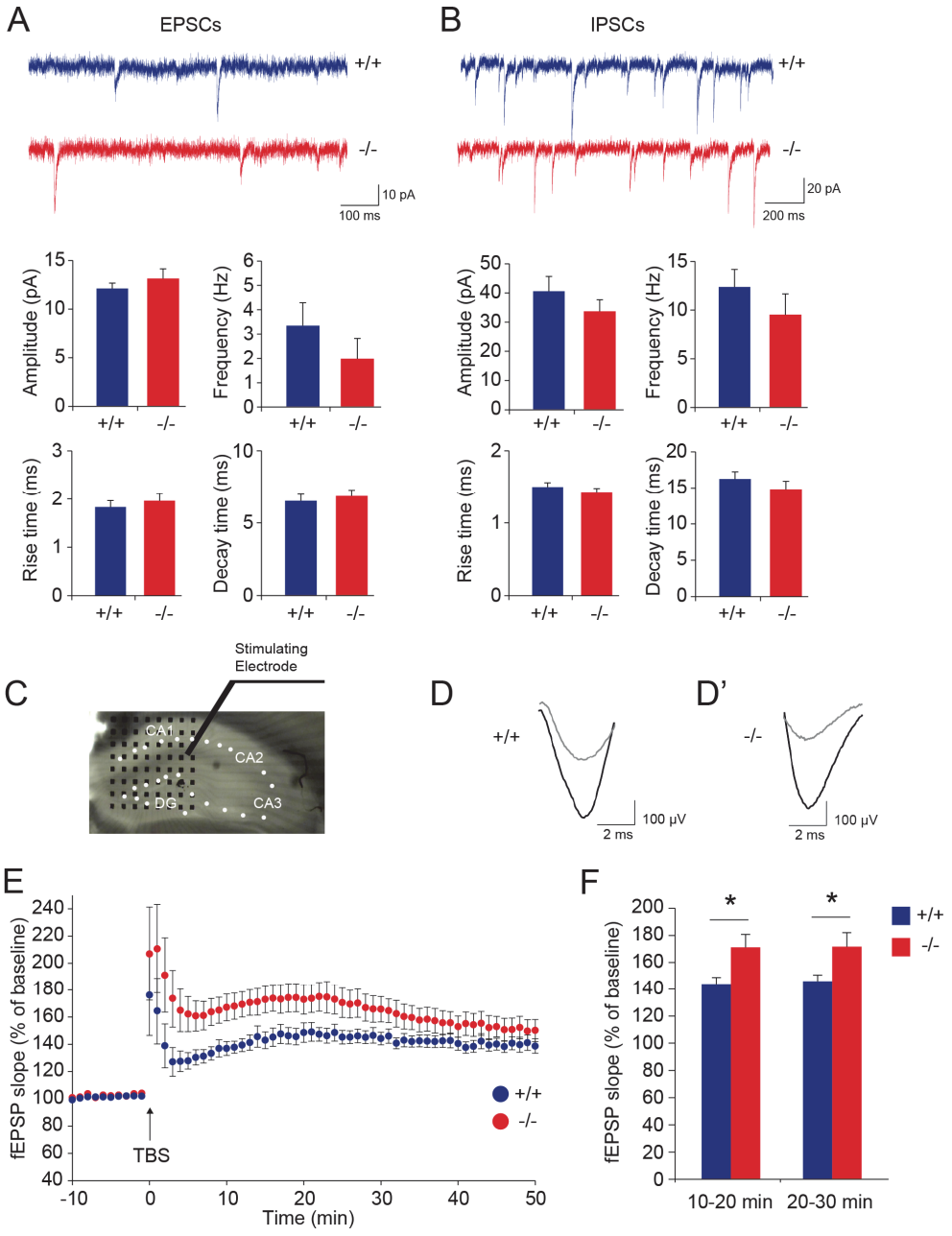

Figure 4 Hippocampal LTP, but not basal transmission, is increased in *Trim3*$^{-/-}$ mice. (A - B) Spontaneous excitatory **(A)** and inhibitory **(B)** synaptic transmissions are unaffected in *Trim3*$^{-/-}$ mice. Excitatory synaptic currents (mEPSC) **(A)** and inhibitory synaptic currents (mIPSCs) **(B)** were recorded from acute hippocampal slices. Frequency, amplitude, rise time and decay time of both

excitatory and inhibitory currents were unaffected in *Trim3*$^{-/-}$ mice compared to wildtype controls (means ± SEM, n = 6/8 for EPSCs, n = 10 for IPSCs). **(C - F)** Hippocampal LTP is enhanced after tetanus stimulation. **(C)** LTP was induced in acute hippocampal slices using a single stimulation electrode in the Schaffer collateral pathway and field excitatory postsynaptic potentials (fEPSPs) were recorded using an 8 x 8 multi-electrode array (black dots) in the CA1 area. **(D)** Example fEPSP traces from a wildtype control and a *Trim3*$^{-/-}$ mouse **(D')** before (grey) and after (black) tetanus stimulation indicate stronger potentiation in *Trim3*$^{-/-}$ mice. **(E)** Averaged fEPSP data show enhanced LTP in *Trim3*$^{-/-}$ animals compared to wildtype mice, in particular in the first 30 min after theta burst stimulation (TBS). **(F)** Quantification of the average amount of potentiation at 10 - 20 min and 20 - 30 min after TBS showed a significant increase in *Trim3*$^{-/-}$ mice compared to wildtype controls (means ± SEM, two-tailed t test, $*p < 0.05$, n = 12/13 per genotype).

Hippocampal long-term potentiation (LTP), however, was significantly enhanced in slices from *Trim3*$^{-/-}$ mice compared with wildtype controls. LTP was induced in acute hippocampal slices by theta burst stimulation of the Schaffer collateral pathway using a single stimulation electrode, and recorded in CA1 using an 8x8 multi-electrode array (Figure 4C). Potentiation was readily detected in slices from both genotypes (Figure 4D), but *Trim3*$^{-/-}$ slices showed on average a stronger potentiation compared with wildtype controls (Figure 4E). This increase in LTP was significant at 10 - 20 min and at 20 - 30 min after induction (10 – 20 min: WT 144 ± 4.8, KO 171.2 ± 9.6 %; 20 – 30 min: WT 146.1 ± 4.6, KO 171.7 ± 10.4 %) (Figure 4F). We next filled hippocampal CA1 neurons in slices from *Trim3*$^{-/-}$ mice and wildtype controls with biocytin and collected high-resolution confocal images of the first basal and oblique dendrite of each neuron (Figures 5A - E). Automated quantification of spine densities revealed that *Trim3*$^{-/-}$ dendrites on average have a higher spine density compared with wildtype control dendrites (WT 1 ± 0.03, KO 1.13 ± 0.06 %; 1.76 ± 0.05 spines/µm in WT and 1.99 ± 0.10 spines/µm in *Trim3*$^{-/-}$) (Figure 5F). Spine head diameter (Figures 5G - H) and spine length (Figures 5I - J) on the other hand were unaffected in *Trim3*$^{-/-}$ mice (diameter, WT 0.36 ± 0.01 µm, KO 0.36 ± 0.01 µm; length, WT 0.77 ± 0.02 µm and KO 0.81 ± 0.02 µm). Together these data indicate that increased LTP and increased spine densities in the hippocampus may provide the physiological and the structural basis for enhanced fear memory consolidation in *Trim3*$^{-/-}$ mice.

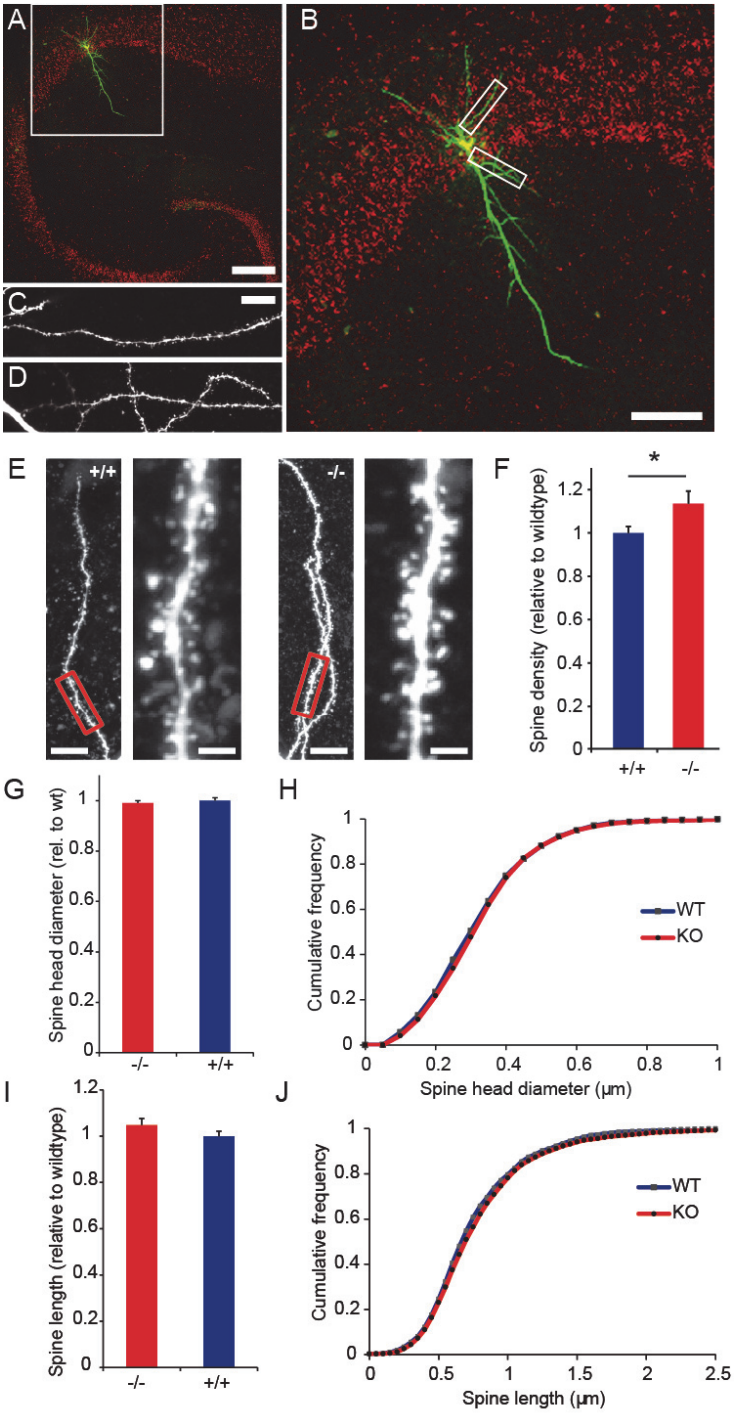
A
B
C
D
E
+/+
-/-
F
*
Spine density (relative to wildtype)
1.2
1
0.8
0.6
0.4
0.2
0
+/+
-/-
G
Spine head diameter (rel. to wt)
1
0.8
0.6
0.4
0.2
0
-/-
+/+
H
Cumulative frequency
1
0.8
0.6
0.4
0.2
0
0
0.2
0.4
0.6
0.8
1
WT
KO
Spine head diameter (µm)
I
Spine length (relative to wildtype)
1.2
1
0.8
0.6
0.4
0.2
0
-/-
+/+
J
Cumulative frequency
1
0.8
0.6
0.4
0.2
0
0
0.5
1
1.5
2
2.5
WT
KO
Spine length (µm)

Figure 5 Spine density is increased in *Trim3*$^{-/-}$ mice, while spine length and spine head diameter are unaffected. (A - B) Example of a confocal image of a patched hippocampal CA1 pyramidal cell filled with biocytin and stained with streptavidin-Alexa 488. **(A)** The image shows the location of cell bodies the in the hippocampus in red. Scale bar, 200 µm. **(B)** Zoom of **(A)** showing the first basal and oblique dendrite (boxed). Scale bar, 100 µm. **(C - D)** Maximum intensity z-projections from confocal stacks (resolution 80 x 80 x 125 nm/pixel, xyz) of the first basal and the first oblique dendrite of each cell were selected for spine density measurements. Images correspond to the boxes in **(B)**. **(E)** Representative images of dendrite segments from *Trim3*$^{-/-}$ mice and wildtype controls used for analysis. Scale bar, 10 µm (overview) and 2 µm (enlargement). **(F)** Average spine density was significantly higher in *Trim3*$^{-/-}$ mice compared to wildtype controls (means ± SEM, two-tailed t test, $*p < 0.05$, n = 6/11 per genotype). **(G - H)** Analysis of spine head diameter revealed no differences between wildtype animals and *Trim3*$^{-/-}$ mice. **(G)** Average spine head diameter did not differ between wildtype and *Trim3*$^{-/-}$ mice. **(H)** Cumulative frequency plot of spine head diameters of wildtype and *Trim3*$^{-/-}$ mice revealed no differences. **(I)** Spine length was slightly, but not significantly, increased in *Trim3*$^{-/-}$ mice (means ± SEM, two-tailed t test, $p > 0.05$, n = 6/11). **(J)** Frequency distributions of spine length did not differ between *Trim3*$^{-/-}$ and wildtype mice.

Discussion

In this study we aimed to elucidate the role of TRIM3 in learning and memory. We were able to demonstrate that TRIM3, like its two closest relatives TRIM2 and TRIM32, is an E3 ubiquitin ligase (Balastik et al., 2008; Hung et al., 2010; Kudryashova et al., 2005) and that in accordance with Raheja et al. (2014) the ability of TRIM3 to ubiquitylate is RING domain-dependent. TRIM3 is highly expressed in the brain, predominantly in the hippocampus and the cerebellum. The observed TRIM3 protein expression patterns are in accordance with *Trim3* mRNA expression reported previously (El-Husseini, 1999). Interestingly, we additionally observed dendritic TRIM3 protein staining of hippocampal pyramidal cells, suggesting postsynaptic localization, which is confirmed by biochemical enrichment analysis showing relatively high levels of TRIM3 in synaptic fractions. In the cerebellum however, high levels of TRIM3 staining were observed in the granular and molecular layers, indicating that the protein is synthesized in granule neurons and localized pre-synaptically in granule cell axons terminating on Purkinje cell dendrites in the molecular layer. Thus, the subcellular localization of TRIM3 may be different in the cerebellum compared with the hippocampus. The expression pattern of TRIM3 in the cerebellum is strikingly different from that of its paralogue TRIM2, which is highly expressed in Purkinje cells (Balastik et al., 2008; Ohkawa et al., 2001). Only in the deep cerebellar nuclei TRIM2 and TRIM3 expression appears to

overlap. TRIM2 mutant mice have a strong and progressive neurodegenerative phenotype (Balastik et al., 2008). At the age of 6 weeks TRIM2 mutant mice start to show intention tremor and gait ataxia due to the degeneration of cerebellar Purkinje cells, and at later stages they have episodes of spontaneous generalized seizures. Purkinje cell degeneration appears to be due to axonal swellings caused by the accumulation of neurofilament light chain protein, which was identified as the TRIM2 substrate. In strong contrast, *Trim3*$^{-/-}$ mice are morphologically and behaviorally indistinguishable from their wildtype littermates up to the age of 12 months. Locomotion and motor coordination were unaffected, and these mice did not develop seizures, nor did they show signs of neurodegeneration. Based on these findings we conclude that TRIM2 and TRIM3 have very different functions in the cerebellum. They are not only expressed in different cell types and at different subcellular locations, but also the neurodegenerative phenotype of TRIM2 mutant mice is not recapitulated in *Trim3*$^{-/-}$ mice. The exact cerebellar phenotype of *Trim3*$^{-/-}$ mice is at this moment still elusive, and we cannot exclude that fine motor skills or motor learning functions are affected.

In the hippocampus, TRIM2 and TRIM3 expression overlap completely, yet their specific contribution to hippocampal function has not been studied. We therefore decided to find evidence for a role of TRIM3 in the hippocampus. *Trim2* and *Trim32* knockout mice have both been thoroughly investigated, but no behavioral abnormalities were reported. *Trim3*$^{-/-}$ mice, in contrast to *Trim2*$^{-/-}$ mice, did not present with a neurodegenerative phenotype, which lead us to assume that also their behavior would hardly be affected. Indeed, observed basal behavior of our *Trim3*$^{-/-}$ mice was normal. Contextual fear conditioning on the other hand revealed a most striking and very specific phenotype. *Trim3*$^{-/-}$ mice showed fully consolidated fear memory already two hours after fear conditioning. This result was also reproducible in older mice. Interestingly we identified two underlying phenomena, alterations in spine density and LTP, which could potentially cause such a specific phenotype on a cellular level. *Trim3*$^{-/-}$ mice have significantly higher spine density in hippocampal pyramidal cells. Over the last two decades numerous studies suggested high spine densities to be direct correlates of different sorts of learning (Knafo et al., 2004; Moser et al., 1994; O'Malley et al., 1998). Following that reasoning, it is rational to assume that a stronger fear memory in *Trim3*$^{-/-}$ mice can be formed due to a higher number of spines and likely a higher number of functional synapses. In this regard it is worth noting that Hung et al. (2010) did not observe a change in spine density after overexpressing TRIM3 in cultured rat

hippocampal neurons. They did however observe a significant decrease in spine head width, which may indeed present a first step towards spine pruning, eventually resulting in lower spine density corroborating our finding.

The second mechanism potentially underlying increased fear memory in *Trim3*$^{-/-}$ mice is LTP. Cheung et al. (2010) reported a significant decrease in mIPSC amplitude in cortical neurons from TRIM3 deficient mice, a finding that we were not able confirm in hippocampal pyramidal cells. Recordings of spontaneous activity in slices of *Trim3*$^{-/-}$ mice did not show any differences in amplitude, frequency, rise time and decay time compared with recordings from wildtype animals. Intriguingly, we observed significantly enhanced LTP in hippocampal slices 10 – 30 minutes after stimulation, suggesting that TRIM3 or one of its ubiquitylation substrates plays a role in the induction and early phase of LTP, but not in the maintenance. This raises the question of how TRIM3 could directly affect the expression of LTP in the hippocampus. It is conceivable that TRIM3 is directly involved in AMPA receptor trafficking. The first demonstrated interactors of TRIM3 were myosin V (El-Husseini, 1999) and alpha-actinin-4. Both are known to be part of the CART complex (Yan et al., 2005), which is required for efficient recycling of transferrin receptors and epidermal growth factor receptors. Only recently, two studies identified myosin Va and Vb as important motor proteins delivering cargo vesicles containing AMPA receptors (Correia et al., 2008; Wang et al., 2008) and alpha-actinin was shown to play a role in AMPA receptor transport in dendritic spines (Schulz et al., 2004). In addition we had previously demonstrated that TRIM3 interacts with KIF21B, another motor protein, and increases its motility (Labonte et al., 2013).

Kanai et al. (2004) showed that TRIM3 is associated with yet another motor protein KIF5, which transports TRIM3 as part as of mRNP granules. This indicates that TRIM3 exerts its function localized, possibly at post-synaptic sites. Interestingly, we also detected high levels of TRIM3 in the microsomal fraction, suggesting that TRIM3 may be associated with vesicular structures. In line with these observations, TRIM3 is present in punctate structures along dendrites of cultured primary hippocampal neurons. The punctate TRIM3 staining we observed is likely to be TRIM3 as part of these transport granules. Whether or how TRIM3 may affect transport granule attributes, i.e. composition, localization and mobility is not clear and demands further investigation.

To summarize, loss of TRIM3 very specifically increases hippocampus dependent fear memory acquisition. This increase most likely results from higher spine density and increased LTP. However, at this stage it can only be speculated how, where and by what molecular mechanism TRIM3 influences memory consolidation, LTP and spine density. These questions need further investigation and will be addressed in the following chapters.

Supplementary

Supplemental Table S1. Behavioral analysis of *Trim3* knock-out mice at eight months of age.

Test / test measure	unit	WT (n = 14) Mean ± SE	KO (n = 12) Mean ± SE	p-value
Open Field - Ethovision				
Number of entries into the center area		37.29 ± 3.67	41.08 ± 4.06	0.493
Time spent in the center area	s	65.0 ± 6.4	85.8 ± 20.0	0.303
Total distance traveled	cm	4729 ± 341	5290 ± 303	0.238
Open Field - SEE analysis - velocity				
Lingering progression threshold speed	cm/s	**12.52 ± 0.67**	**14.83 ± 0.78**	**0.034**
Median of move segment max speed	cm/s	**21.55 ± 1.10**	**24.94 ± 1.09**	**0.040**
Quantile 95 of move segment max speed	cm/s	**30.22 ± 1.13**	**34.18 ± 1.33**	**0.031**
Lingering mean speed	cm/s	1.77 ± 0.10	1.84 ± 0.14	0.687
Median of lingering segment max speed	cm/s	4.41 ± 0.40	4.07 ± 0.35	0.540
Open Field - SEE analysis - acceleration				
Latency to max half speed	s	10.71 ± 2.87	13.01 ± 4.07	0.642
Median segment acceleration to max speed	cm/s^2	13.59 ± 0.36	14.55 ± 0.57	0.155
Open Field - SEE analysis - other				
Number of progression segments	segments	112.5 ± 8.3	114.8 ± 6.0	0.828
Median length of progression segments	cm	**23.83 ± 2.03**	**30.66 ± 1.99**	**0.026**
Median duration of progression segments	s	1.58 ± 0.08	1.76 ± 0.06	0.075
Quantile 5 of duration of progression segments	s	0.59 ± 0.05	0.67 ± 0.03	0.238
Quantile 95 of duration of progression segments	s	3.35 ± 0.15	3.68 ± 0.13	0.119
Number of stops per distance	segments/cm	0.03 ± 0.00	0.03 ± 0.00	0.109
Time proportion of lingering episodes		0.67 ± 0.03	0.63 ± 0.02	0.389
Median radius of turn	cm	75.43 ± 4.17	83.35 ± 5.29	0.245
Median turn rate	degrees/s	13.23 ± 0.54	13.45 ± 0.79	0.812

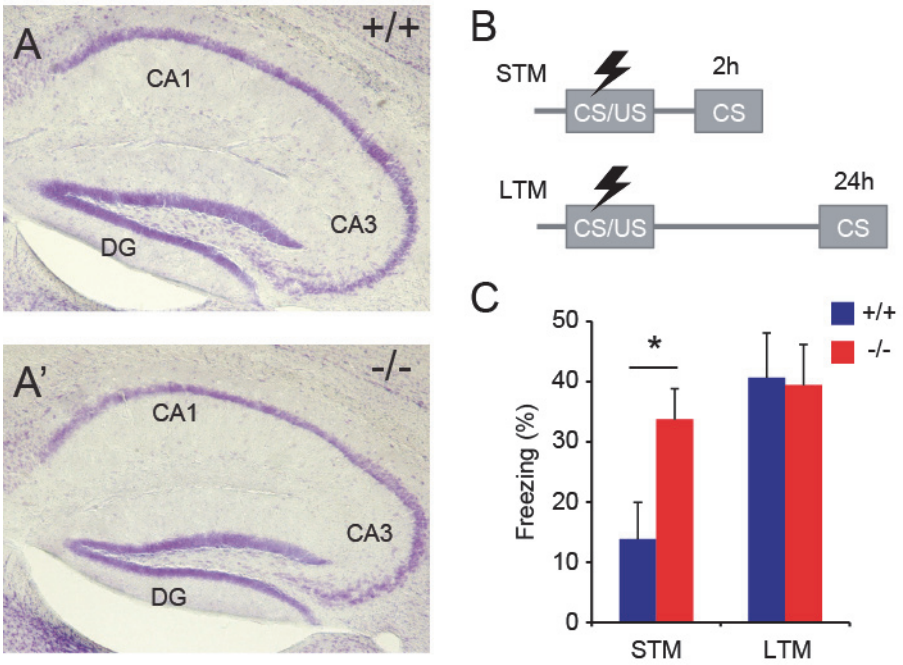

Figure S1 ***Trim3*$^{-/-}$ mice at the age of 8 months have normal hippocampal morphology and show enhanced contextual fear memory.** Nissl staining showed normal gross morphology of the hippocampus in eight months old *Trim3*$^{-/-}$ mice **(A)** compared with wildtype controls **(A')**. **(B)** Hippocampal memory performance in a contextual fear memory task. Animals received a mild foot shock (unconditioned stimulus; US) in a novel context (conditioned stimulus; CS). Memory retrieval was tested either 2 h (short-term memory; STM) or 24 h (long-term memory; LTM) after conditioning by re-exposing animals to the shock-associated context (CS) and measuring the amount of freezing. STM and LTM were tested in two independent cohorts of mice. **(C)** Freezing behavior was significantly increased in *Trim3*$^{-/-}$ mice compared with wildtype littermates when re-exposed to the conditioned context 2 h after receiving the shock (STM), but not at 24h (LTM), indicating enhanced consolidation of fear memory (means ± SEM, two-tailed t test, $*p < 0.05$, n = 5/7 per genotype).

CHAPTER 3

TRIM3 participates in mRNP granules, but is not essential for mRNP granule trafficking

Joerg Schreiber, Dorthe Labonté, Matthias Kneussel, August B. Smit, Ronald E. van Kesteren

Abstract

Over the last decades local protein synthesis in neurons has attracted a lot of research. The complexity of neuronal cell architecture, the long distances between cell somata and synapses, and the plasticity of the system require temporally and spatially controlled protein synthesis. The majority of messenger RNAs for local translation travels within messenger ribonucleoprotein (mRNP) particles. TRIM3 was shown to be part of RNA binding protein Pur-alpha (PURA) -containing mRNP particles. We have previously described the phenotype of TRIM3 deficient mice, showing enhanced memory consolidation, enhanced long-term potentiation and an increase in spine density. In this chapter we assessed whether observed changes of *Trim3*$^{-/-}$ mice might be explained by a role of TRIM3 in mRNP trafficking. By co-immunoprecipitation and overexpression experiments we first determined whether TRIM3 interacts with PURA and whether PURA is an ubiquitylation substrate of TRIM3. We then investigated mRNP trafficking in cultured neurons and analyzed mobility parameters in the presence or absence of TRIM3. We found that TRIM3 and PURA do not directly interact, but that they are part of the same mRNP granules. We furthermore found that TRIM3 is not essential for mRNP trafficking, but that the loss of TRIM3 increased travelled distance and velocity of a long distance sub-population of mRNP particles. We conclude that the observed characteristics of TRIM3 deficient mice are not caused by the role of TRIM3 in mRNP trafficking.

Introduction

Neurons are highly polarized cells, with dendritic trees and axons often extending far from the cell body. This specialized cellular architecture is on one hand the basis of many unique neuronal properties, but it also presents a very unique cellular challenge. How can axons, dendrites and even individual synapses be quickly and specifically supplied with all the needed proteins at times of high demand?

A leap towards answering that question came in 1982 when Steward and Levy showed that polyribosomes are found at the base of spines in hippocampal granule cells (Steward and Levy, 1982), opening the possibility of local mRNA translation into protein. In the following decades increasing evidence on local protein synthesis was gathered. Many

different mRNAs, such as *MAP2* (Garner et al., 1988), *CAMKIIα* (Burgin et al., 1990), *SHANK* (Bockers et al., 2004) and others were found to be localized in or near synapses of murine neurons. Recent studies even suggest that the number of different protein coding mRNAs in axons and dendrites is rather in the thousands than in single digits (Cajigas et al., 2012; Zivraj et al., 2010). In fact, Lécuyer et al. (2007) showed that in Drosophila embryos 71 % of all expressed genes encode mRNAs that are highly localized in non-nuclear subcellular compartments (Lecuyer et al., 2007), suggesting that local mRNA translation is not an isolated phenomenon in mammalian neurons, but rather a common theme.

In neurons, localized RNAs are often transported in messenger ribonucleoprotein (mRNP) granules containing mRNAs and a multitude of proteins, many of which are RNA binding proteins (Kiebler and DesGroseillers, 2000; Knowles et al., 1996; Kohrmann et al., 1999). One of the major components of neuronal mRNP granules is the RNA binding protein Pur-alpha (PURA) (Elvira et al., 2006; Kanai et al., 2004; Ohashi et al., 2002). PURA was shown to be essential for postnatal brain development. *Pura* knockout mice are normal at birth, but develop neurological problems after two weeks and die at the age of four weeks (Khalili et al., 2003). Immunohistochemical analysis of these mice revealed decreased neuron numbers in the hippocampus, and a profound reduction in synapse formation. Kanai et al. (2004) further demonstrated that PURA is essential for mRNA transport.

In their groundbreaking study, Kanai et al. (2004) identified 42 protein components of mRNP granules associated with motor protein KIF5. Using RNA interference they determined that not all of these proteins are essential for mRNP trafficking. The knock-down of PURA, hnRNP-U, PSF and STAUFEN, each significantly suppressed RNA dispersion in dendrites, but dendritic RNA localization was not affected when DDX3 or SYNGRIP were knocked down (Kanai et al., 2004). Based on their results, and on available functional data from other studies, they classified most mRNP proteins in five different groups: RNA transport, protein synthesis, RNA helicases, heterogeneous nuclear ribonucleoproteins and other RNA-associated proteins. Interestingly, the same study also identified TRIM2 and TRIM3 as part of mRNP granules. TRIM2 and TRIM3 were not studied in detail, and were simply classified as ‘other proteins’ with unknown functions. Given the role of TRIM3 in regulating plasticity, in particular the increased long-term potentiation (LTP) and spine density phenotype observed in *Trim3*$^{-/-}$ mice (see Chapter 2), we wondered whether this

phenotype might be related to the presence of TRIM3 in mRNP granules. The goal of this study was to identify a role for TRIM3 in dendritic mRNP trafficking as a possible explanation for the observed behavioral, structural and electrophysiological phenotype found in *Trim3*$^{-/-}$ mice as described in chapter 2.

Material and Methods

Animals

Trim3$^{-/-}$ mice were maintained on a C57BL/6J background. In all experiments wildtype littermates were used as controls. Mice were individually housed on sawdust in standard Makrolon type II cages (26.5 cm long, 20.5 cm wide and 14.5 cm high) enriched with cardboard nesting material and a plastic tube under 12/12h dark/light cycle with access to water and food *ad libitum*. All animal experiments were approved by the animal ethics committee of the VU University Amsterdam.

Synaptic protein isolation and quantification

Brain tissue was obtained from mice under control conditions (home cage) and two hours after contextual fear conditioning (shock; see Chapter 2 for details). Animals were sacrificed by cervical dislocation. Cerebellum and hippocampus were dissected and synapse-enriched fractions isolated as previously described (Klemmer et al., 2009). Protein concentrations were measured using Bradford Protein-Assay (Bio-Rad Laboratories, USA) and equal amounts of protein were loaded on a 4 - 20% gradient SDS-PAGE gel (Criterion TGX Stain-Free Gel, Bio-Rad Laboratories, USA). Total protein amounts were imaged after electrophoresis using Criterion Stain Free Imager (Bio-Rad Laboratories, USA). Gels were then transferred to polyvinylidene fluoride (PVDF) membranes (Bio-Rad Immuno-Blot PVDF membrane, Bio-Rad Laboratories, USA) and membranes were blocked by immersion in 5 % nonfat dry milk in TBS-T (TBS plus 0.025 % Tween, pH 7.4) for 1 h. Blots were then incubated with anti-PURA (ab79936, Abcam, 1:2,000) for 1 h at room temperature, followed by a 1 h incubation with a secondary antibody conjugated to HRP. Proteins were visualized by ECL (SuperSignal West Femto Chemiluminescent Substrate, Thermo Scientific, USA) and scanned using the Odyssey Fc imager (Li-Cor, USA). Protein quantities were calculated

by dividing the background corrected signal intensity of each protein band (ImageStudio Software v. 2.0.38, Li-Cor, USA) by the background corrected signal intensity of the corresponding stain-free gel protein lane (Image Lab 3.0, Bio-Rad, USA). Significance was tested using a two-tailed t test.

Cell culture and immunoprecipitation

Human embryonic kidney cells (HEK293) were maintained in Dulbecco's modified Eagle medium supplemented with 10 % fetal bovine serum and 1 % Penicillin-Streptomycin (all from Life Technologies Thermo Fisher Scientific Inc., USA) at 37° C and 5 % CO_2. Cells were co-transfected with myc-TRIM3 and GFP-PURA, myc-ΔRBCC-TRIM3 and GFP-PURA or GFP-PURA alone at 60 – 80 % confluency using polyethylenimine (PEI). Starting 12 h after transfection cells were sampled at three hour intervals for 12 hours. Cells were washed with ice cold PBS and subsequently lysed in SDS containing loading buffer. Samples were then separated and analyzed for PURA expression as described above. For immunoprecipitation (IP), HEK293 cells were co-transfected with myc-TRIM3 and GFP-PURA at 60 – 80 % confluence. At 48 h after transfection cells were washed with ice cold phosphate-buffered saline (PBS) and subsequently lysed in extraction buffer (1 % Triton X-100, 150 mM NaCl, 25 mM HEPES pH 7.4) supplemented with protease inhibitors (cOmplete Protease Inhibitor Cocktail, Roche Diagnostics) for 1 h at 4° C on a rotator. Insoluble material was pelleted at 20,000 g for 20 min and the supernatant used for IP. Antibodies used for IP were rabbit anti-PURA (ab79936, Abcam, 1:2,000) and rabbit anti-TRIM3 (epitope: CLRPGDLPPSPDDVK, GenScript). IPs and input were separated on an 8 % SDS-PAGE gel and transferred to PVDF membranes (Bio-Rad Immuno-Blot PVDF membrane, Bio-Rad Laboratories). Membranes were blocked by immersion in 5 % nonfat dry milk in TBS-T (TBS plus 0.025 % Tween, pH 7.4) for one hour, washed and incubated with antibodies for GFP (75-131, Neuromab, 1:2,000) and TRIM3 (epitope: CLRPGDLPPSPDDVK, GenScript, 1:1,000) for 1 h at room temperature, followed by a 1 h incubation with a secondary antibody conjugated to horseradish peroxidase (HRP). Proteins were visualized by ECL (SuperSignal West Femto Chemiluminescent Substrate, Thermo Scientific, USA) and scanned using the Odyssey Fc imager (Li-Cor, USA).

Co-Immunoprecipitation of TRIM3 from hippocampus and cerebellum

For an IP experiment 10 mg of synapse-enriched protein fractions (P2 + M) were extracted in an equal volume of 2 % Triton X-100, 150 mM NaCl, 25 mM HEPES pH 7.4, protease inhibitors (cOmplete Protease Inhibitor Cocktail, Roche Diagnostics) for 1 h on a rotator at 4° C. Insoluble material was then pelleted at 20,000 g for 20 min at 4°C. The pellet was then re-extracted in 1 % Triton X-100, 150 mM NaCl, 25 mM HEPES pH 7.4, protease inhibitors for 1 h. Insoluble material was again pelleted at 20,000 g for 20 min. Supernatants from the first and second extraction were pooled, centrifuged at 20,000 g for 20 min and the final supernatant served as input for IPs. Input from wildtype animals was split in two; one half was treated with RNase inhibitors (40 u/ml RiboLock, Thermo Scientific, USA) and the other with RNase A (R4642, Sigma-Aldrich). Input from *Trim3* knockout animals remained untreated. After 24h, 10 µg of anti-TRIM3 (epitope: QAPEGAHDPEDPHPC, GenScript) antibody was added to each sample and incubated overnight on a rotator at 4° C. On the next day, 30 µl of protein A/G beads (Protein A/G Plus-Agarose, Santa Cruz Biotechnology Inc., USA) were washed three times in washing buffer (0.1 % Triton X-100, 150 mM NaCl, 25 mM HEPES pH 7.4) and added to each IP. Beads were incubated for 120 min on a rotator at 4° C, then pelleted at 2.500 g and washed four times in ice-cold washing buffer. TRIM3 and interacting proteins were eluted by adding SDS containing loading buffer and boiling for five min. Samples were separated on SDS-PAGE and immunoblotted for PURA (ab79936, Abcam, 1:2,000).

Time-lapse video microscopy

Hippocampal primary neurons from *Trim3*$^{-/-}$ and wildtype mice were cultured on glass bottom dishes coated with 5 µg/ml ply-D-lysine. Cells were transfected with GFP-tagged PURA at DIV8 - 10. After 15 - 24 h cells were imaged. Imaging was performed in pre-warmed HEPES buffer with an inverse fluorescence microscope Axiovert 200M (Zeiss, Jena, Germany) at 37° C in the incubation chamber (Harnischmacher-Labortechnik, Kassel, Germany). MetaVue software (verion 6.2r6, Molecular Devices, Munich, Germany) was used to record cells for 5 min at 3 - 5 s intervals. Analysis of various trafficking parameters was performed with the Metamorph software. Significance was tested using a two-tailed t test.

Results

TRIM3 and PURA interaction and regulation

To test whether enhanced contextual fear memory and/or the increase in LTP observed in *Trim3*$^{-/-}$ mice might be explained by a role of TRIM3 in mRNP trafficking, we first determined whether TRIM3 interacts PURA, one of the major components of mRNP particles in neurons (Elvira et al., 2006; Kanai et al., 2004; Ohashi et al., 2002). We performed co-immunoprecipitation of TRIM3 from hippocampal and cerebellar synapse enriched fractions. To test whether the observed interaction is RNA-dependent, we treated co-immunoprecipitated fractions either with RNase inhibitors to preserve RNA, or with RNase A to break down RNA. Immunoblotting revealed that TRIM3 and PURA interact in an RNase-sensitive manner (Figure 1A - B), thus confirming that they indeed co-exist in mRNP particles, and that their interaction depends on the presence of RNA. Further evidence that TRIM3 and PURA do not directly interact came from co-expression experiments in heterologous cells. When we co-expressed TRIM3 and PURA in HEK293 cells and immunoprecipitated TRIM3 and PURA, PURA did not co-precipitate with TRIM3 and TRIM3 not with PURA (Figure 2A), confirming that the interaction observed in hippocampus and cerebellum is not direct. Given the fact that TRIM3 is an ubiquitin ligase (Raheja et al., 2014), we hypothesized that TRIM3 may negatively regulate PURA levels by ubiquitylation and subsequent proteasomal degradation. We therefore isolated hippocampal synaptosomal fractions from wildtype and *Trim3*$^{-/-}$ mice under basal conditions and two hours after contextual fear conditioning, the time point when enhanced memory consolidation was observed (see Chapter 2). We found no differences in PURA levels in *Trim3*$^{-/-}$ mice compared with wildtype controls, neither under basal conditions, nor at two hours after fear conditioning (Figure 1C - D). Moreover, when we co-expressed TRIM3 and PURA in HEK293 cells we observed a stable expression of PURA over time, independent of whether full length TRIM3 or ΔRBCC-TRIM3 were expressed (Figure 2B). Taken together these data demonstrate that PURA levels are not regulated by TRIM3.

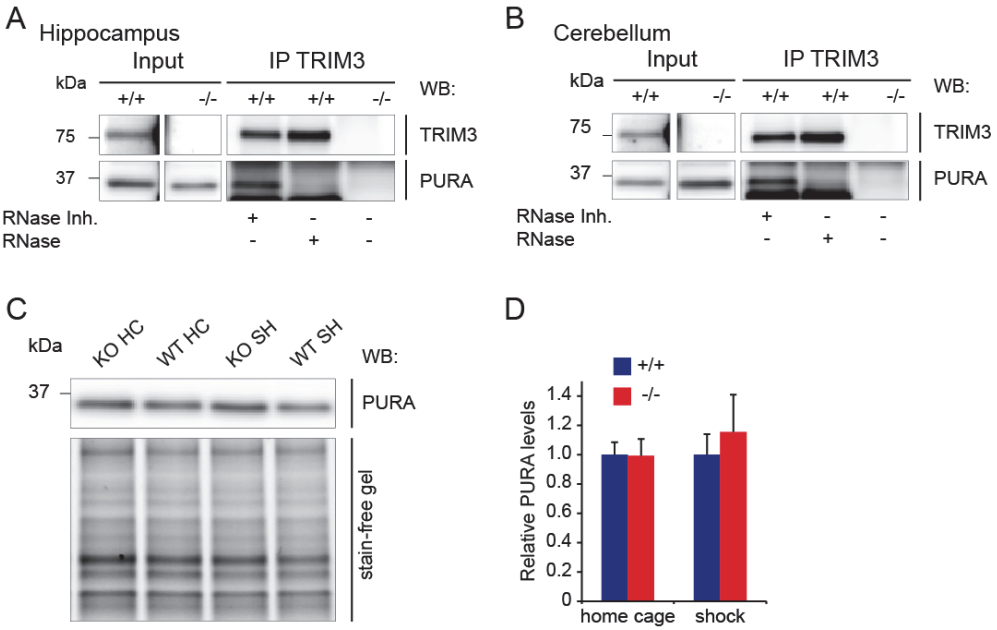

Figure 1 TRIM3 is present in PURA containing mRNP particles, but does not directly interact with PURA or affect PURA abundance. (A - B) TRIM3 interacts with PURA in an RNA-dependent manner. Hippocampal **(A)** and cerebellar **(B)** synapse-enriched fractions were prepared and treated either with RNase A or with RNase inhibitor. TRIM3 was immunoprecipitated and samples were immunoblotted and stained for TRIM3 and PURA. PURA was detected in RNase inhibitor treated samples, but not in RNase treated samples. Samples prepared from *Trim3*$^{-/-}$ mice served as negative control for the immunoprecipitation. **(C - D)** PURA levels are not altered in *Trim3*$^{-/-}$ mice. **(C)** Hippocampal synapse-enriched fractions were prepared from wildtype and *Trim3*$^{-/-}$ mice under control conditions (home cage, HC) and 2 h after contextual fear conditioning (shock, SH). Samples were immunoblotted and stained for PURA **(D)**. Normalized PURA levels were calculated by dividing Western blot (WB) signal intensities by the total protein intensities (stain-free gel) and expressed relative to wildtype levels. PURA levels did not differ between conditions (means ± SEM, n = 8 per genotype, 4 per condition).

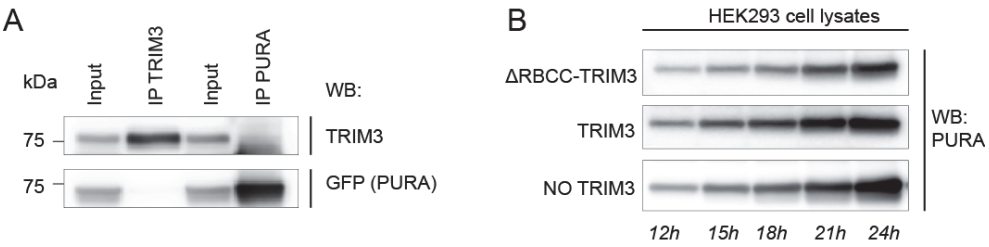

Figure 2 TRIM3 does not directly interact with PURA or affect PURA abundance in HEK293 cells. (A) TRIM3 and PURA do not interact when expressed in HEK293 cells. HEK293 cells were co-transfected with full length TRIM3 and GFP-PURA. Cells were lysed 48 h after transfection. TRIM3 and PURA were immunoprecipitated from lysates, immunoblotted and stained for TRIM3 and GFP (PURA). PURA did not co-immunoprecipitate with TRIM3, and TRIM3 not with PURA. **(B)** TRIM3 does not alter PURA levels in HEK293 cells. HEK293 cells were co-transfected with PURA and TRIM3, PURA and ΔRBCC-TRIM3, or PURA alone. Starting 12 h after transfection cells were lysed at 3 h intervals and lysates were immunoblotted and stained for PURA. No differences in PURA levels in TRIM3 expressing cells were observed at any time point.

TRIM3 and mRNP trafficking

We next asked whether TRIM3 is important for regulating mRNP trafficking. We expressed GFP-tagged PURA in cultured hippocampal neurons derived from *Trim3*$^{-/-}$ mice or wildtype controls and quantified the mobility of GFP-positive PURA-containing mRNP particles (Figure 3A). The total number of particles observed was not different between genotypes (WT: 0.173 ± 0.01 clusters/µm, *Trim3*$^{-/-}$: 0.155 ± 0.01 clusters/µm) (Figure 3B), nor was the percentage of mobile clusters (WT: 9.76 ± 1.37 %, *Trim3*$^{-/-}$: 10.01 ± 1.27 %) (Figure 3C). We then separated mobile clusters in clusters that moved > 5 µm over the 90 second imaging period (long-distance clusters) and clusters that moved < 5 µm (short-distance clusters). No difference was observed in the percentage of long- and short-distance moving clusters between genotypes (long distance, WT: 29.56 ± 5.83 %, *Trim3*$^{-/-}$: 26.09 ± 5.8 %; short distance, WT: 70.44 ± 5.83 %, *Trim3*$^{-/-}$: 73.91 ± 5.8 %) (Figure 3D). When we analyzed the kinetics of long-distance moving clusters separately, we observed no difference in the total distance moved (WT: 13.15 ± 0.86 µm, *Trim3*$^{-/-}$: 15.77 ± 1.57 µm) (Figure 3E), and a small but significant increase in *Trim3*$^{-/-}$ neurons compared with wildtype controls in the maximum velocity of clusters (WT: 0.72 ± 0.04 µm / s, *Trim3*$^{-/-}$: 0.91 ± 0.09 µm/s, $p < 0.05$) (Figure 3F) and the maximum distance they reached, measured from origin (WT: 8.15 ± 0.43 µm,

Trim3$^{-/-}$ 10.39 ± 1.16, $p < 0.05$) (Figure 3G). For short-distance moving clusters none of these parameters was significantly affected in *Trim3*$^{-/-}$ neurons (total distance: WT: 9.34 ± 0.53 µm, *Trim3*$^{-/-}$: 9.62 ± 0.58 µm; max. velocity: WT: 0.4 ± 0.03 µm/s, *Trim3*$^{-/-}$: 0.4 ± 0.03 µm/s; max. distance to origin: WT: 3.17 ± 0.11 µm, *Trim3*$^{-/-}$: 3.12 ± 0.11 µm) (Figures 3H - J). These findings indicate that, although present in mRNP particles and possibly affecting some kinetic parameters of a subpopulation of particles, TRIM3 is not essential for mRNP trafficking. We therefore conclude that TRIM3 likely travels on mRNP particles as cargo in order to exert its function at the synapse, possibly in the regulation of local mRNA translation.

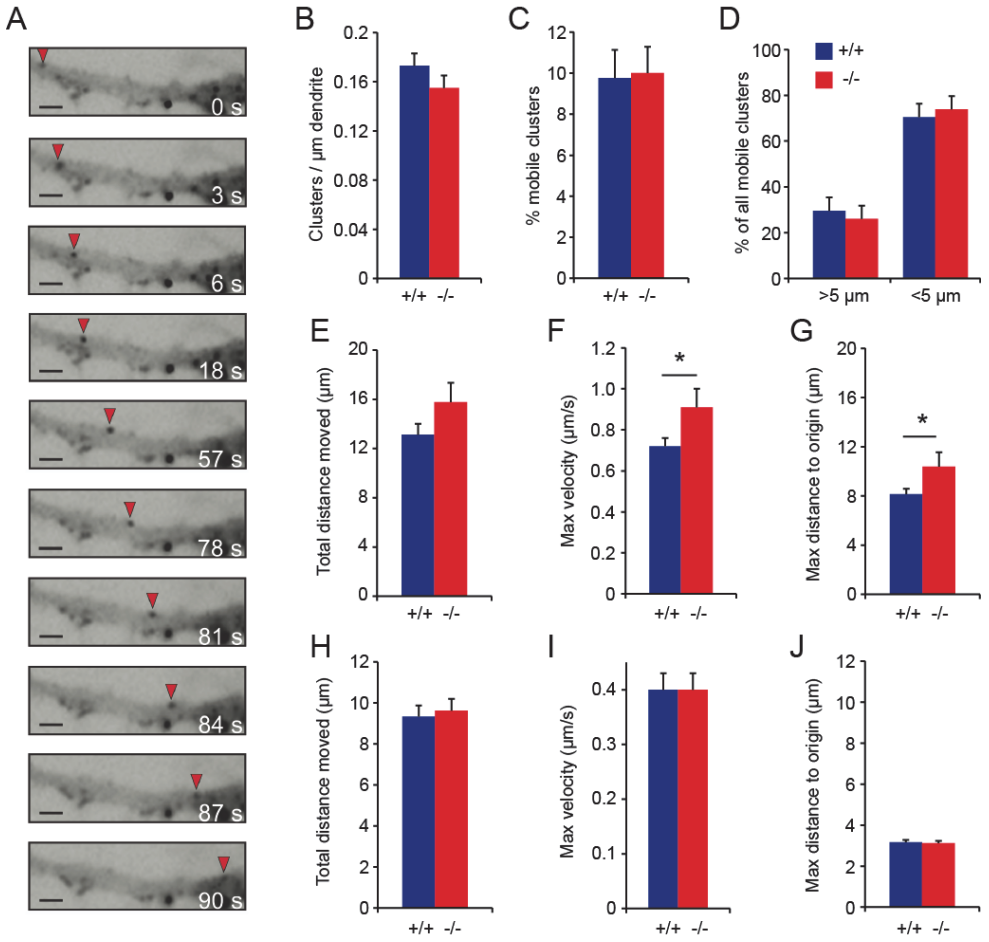

Figure 3 TRIM3 is not essential for mRNP particle trafficking. (A) Hippocampal neurons from *Trim3*$^{-/-}$ and wildtype mice were transfected with GFP-PURA at DIV8 - 10 and time-lapse imaged 15 – 24 h later. Example images of a mobile GFP-PURA cluster (red arrow) over a time span of 90 s are shown. Scale bars, 2 µm. **(B - C)** *Trim3*$^{-/-}$ neurons and wildtype control neurons expressed equal amounts of PURA clusters **(B)** and had equal fractions of mobile clusters **(C)**. **(D)** PURA clusters were divided in long-distance clusters that traveled < 5 µm from their site of origin, and short-distance clusters that traveled > 5 µm from their site of origin. *Trim3*$^{-/-}$ neurons and wildtype control neurons expressed equal amounts of short-distance and long-distance clusters. **(E - G)** Long-distance PURA clusters show slightly increased kinetics in *Trim3*$^{-/-}$ neurons. The total distance moved **(E)** did not change, but the maximum velocity **(F)** and the maximum distance reached from origin **(G)** were significantly increased in *Trim3*$^{-/-}$ neurons compared to wildtype neurons (means ± SEM, two-tailed t test, $*p < 0.05$, n = 27/40 clusters per genotype). **(H - J)** Short-distance PURA clusters show unaltered kinetics in *Trim3*$^{-/-}$ neurons. The total distance moved **(H)**, the maximum velocity **(I)** and the maximum distance reached from origin **(J)** did not differ significantly in *Trim3*$^{-/-}$ neurons compared wildtype neurons (means ± SEM, n = 76/80 clusters per genotype).

Discussion

TRIM3 is an ubiquitin ligase (Raheja et al., 2014) strongly expressed in the hippocampus and the cerebellum (Chapter 2). TRIM3 was shown to interact with myosin V (El-Husseini, 1999) and alpha-actinin-4 (El-Husseini et al., 2000), and shown to be part of the CART complex (cytoskeleton-associated recycling or transport complex) containing Hrs, actinin-4, TRIM3 (BERP) and myosin V (Yan et al., 2005). Myosin V is known to be involved in various sorts of intracellular transport (Reck-Peterson et al., 2000), and Yan et al. (2005) demonstrated that the CART complex is required for efficient recycling of transferrin receptors and epidermal growth factor receptors. It was furthermore demonstrated that TRIM3 interacts with motor protein KIF21B and affects its motility (Labonte et al., 2013). These data together led to the assumption that TRIM3 may be involved in cargo transport and trafficking.

One particular study indicated that TRIM3 is involved in the trafficking of mRNA (Kanai et al., 2004). Together with its paralog TRIM2, TRIM3 was found to be part of neuronal PURA containing mRNP granules associated with motor protein KIF5 (Kanai et al., 2004). These granules transport mRNA and associated translational machinery towards synapses (Erickson and Lykke-Andersen, 2011), however, the roles of TRIM proteins in these complexes has not been studied yet. We therefore aimed to identify the role of TRIM3 in mRNP trafficking in neurons. We employed co-immunoprecipitation of TRIM3 from synapse-enriched fractions of hippocampus and cerebellum, but also from HEK293 cells overexpressing TRIM3 and PURA, to determine protein-protein interactions. We also quantified PURA amounts in hippocampal synaptosomes of wildtype and TRIM3 deficient mice, as well as in HEK293 cells overexpressing PURA and full length TRIM3 or PURA and mutant TRIM3, missing its RING domain essential for ubiquitylation of substrate proteins (Deshaies and Joazeiro, 2009; Raheja et al., 2014). We furthermore expressed a GFP-tagged PURA in cultured hippocampal neurons and quantified the mobility of GFP-positive PURA-containing mRNP particles in the absence and the presence of TRIM3.

From our TRIM3 immunoprecipitation experiments from synapse-enriched fractions of hippocampus and cerebellum we can conclude that TRIM3 is part of the same mRNP particles as PURA. Both proteins co-immunoprecipitated under conditions preventing RNA degradation. When RNAs were degraded by the addition of RNase A, however, both proteins did not longer co-immunoprecipitate, indicating that their interaction is RNA

mediated, and not direct. Indeed, when PURA and TRIM3 were co-expressed in HEK293 cells and then immunoprecipitated, a direct interaction could not be observed. In addition we explored the possibility of PURA being a ubiquitylation substrate of TRIM3. If that were the case, PURA levels should be increased in TRIM3 deficient animals, or we should be able to decrease PURA amounts in heterologous cells when co-expressed with TRIM3. Neither in HEK293 cells nor in hippocampal synaptosomal preparations did we detect differences in PURA levels between conditions where TRIM3 was either present or absent. Taken together our findings indicate that (i) TRIM3 and PURA are indeed part of the same mRNP complex, (ii) TRIM3 and PURA do not directly interact, and (iii) PURA is not a likely TRIM3 substrate.

Since we did not observe alterations in PURA levels in synaptosome preparations from TRIM3 deficient mice, neither under basal conditions, nor upon induction of contextual fear memory, we may assume that mRNP granules in total are not affected by the absence of TRIM3. It is possible however that TRIM3 affects the trafficking of mRNP granules, for instance by modifying the tracks. It has been demonstrated, for instance, that posttranslational modification of the microtubule-associated protein MAP2, reduced the mobility of the motor protein KIF5 (Maas et al., 2009). From our time-lapse imaging experiment, where we overexpressed GFP-PURA in cultured hippocampal cells, we can however conclude that TRIM3 is not essential for mRNP integrity or trafficking. We observed equal amounts of total PURA-containing clusters per dendrite length and mobile PURA-containing clusters, confirming that TRIM3 is not essential for the existence for mRNP particles. When we separated all clusters in long distance (travel distance > 5 µm) and short distance (travel distance < 5 µm) clusters, we, however, detected two significantly different features of long distance particles. In TRIM3 deficient neurons, long distance clusters travelled further from their point of origin and they reached a higher maximal velocity. Taking into account that long distance clusters are only 26 – 30 % of all detected clusters, this certainly does not appear to be a substantial effect, but it may nonetheless give some insights into the role of TRIM3 in mRNP granules. Wilhelm and Vale (1993) brought forward four essential functions of mRNP granules: (i) assembly of mRNP particles, (ii) localization and transport via cytoskeletal motors, (iii) anchoring to local sites, and (iv) coordination of translation. Although Wilhelm and Vale had already speculated that recognition of local sites and anchoring would have to involve cytoskeletal (actin) elements, this matter has largely been

unaddressed over the last decades. This in mind, an interpretation of our trafficking phenotype could be that TRIM3 may serve as recognition or anchoring protein of certain cytoskeletal elements, allowing mRNP particles to recognize synapses or other local sites in need of local protein synthesis. Losing TRIM3 may reduce the ability of mRNP granules to recognize specific local sites, which may explain the longer distances travelled and the higher velocity. Further experiments are required to address this hypothesis.

If TRIM3 is not essential for mRNP trafficking, we should consider the possibility that it travels as cargo on mRNP granules to exert its function at the synapse. This raises the question of what its local function might be. Given that a large fraction of proteins identified in PURA containing mRNP particles, such as eEF1a1, eIF2a or RPL3 among others (Kanai et al., 2004), are involved in protein synthesis, it seems likely that TRIM3 also has a function in local mRNA translation. It is possible that TRIM3 acts as translational quality control as recently described (Duttler et al., 2013) or similar to the E3 ligase Not4 (Panasenko, 2014). It could also exert a function on local translation via modulation of the miRNA pathway, as was shown for several other NHL (NCL-1, HT2A, Lin-41) domain containing TRIM proteins such as *C. elegans* Nhl-2 (Hammell et al., 2009) or TRIM32 (Schwamborn et al., 2009). The NHL domain of TRIM3 might however also be responsible for its incorporation into mRNP granules in the first place. TRIM71, a TRIM3 paralog, and BRAT, a TRIM3 ortholog in *Drosophila*, were both shown to bind RNAs through their NHL domain (Kwon et al., 2013; Loedige et al., 2013; Loedige et al., 2014). Loedige et al. (2014) used structural homology modeling to predict that all NHL domain containing TRIM proteins have the potential to bind RNA. Further experiments are required to determine what the precise role of TRIM3 in mRNP complexes is. An obvious requirement for this is that we know which substrate proteins are (poly)-ubiquitylated by TRIM3.

CHAPTER 4

Identification of TRIM3 ubiquitylation substrates

Joerg Schreiber, Ka Wan Li, Pim van Nierop, Iryna Paliukhovich, August B. Smit, and Ronald E. van Kesteren

Abstract

Post-translational modification of proteins with ubiquitin plays an important regulatory role in many cellular processes, but is most widely known for its ability to target proteins for proteasomal degradation. Ubiquitylation is a tightly controlled and protein-specific process facilitated by a cascade of enzymes. Specificity is achieved by the last enzyme in that cascade, an E3 ubiquitin ligase. Several hundred ubiquitin ligases and several thousand ubiquitylated proteins have been identified, but it remains largely elusive which protein is ubiquitylated by which ligase. Experimental approaches aimed at identifying specific ligase-substrate pairs face several challenges, including the transient nature of the ligase-substrate interactions and the low steady state of ubiquitylated proteins due to de-ubiquitylation and proteasomal degradation. In this chapter we describe a mass spectrometry-based approach to identify potential substrates of the E3 ligase TRIM3 in two different brain areas, the hippocampus and the cerebellum. By combining results obtained from co-immunoprecipitation interaction proteomics and affinity purification of poly-ubiquitylated proteins, and including *Trim3* knockout tissue as a negative control, we were able to overcome most of the aforementioned challenges and put forward a high-confidence set of potential substrates of TRIM3 for further validation.

Introduction

Ubiquitin is a conserved 8.5 kDa protein containing 76 amino acids, which is found in all eukaryotic cells (Goldstein et al., 1975). By attaching ubiquitin to another protein, the fate and function of the latter can be changed entirely. Many functional alterations of mono-ubiquitylated proteins have been described, but when additional ubiquitins are added to the substrate-attached ubiquitin in a sequential manner (Hershko and Ciechanover, 1998), the substrate protein is poly-ubiquitylated and will be targeted to the 26S proteasome for degradation (Coux et al., 1996). The attachment of ubiquitin is catalyzed by a cascade of enzymes, including an E1 (ubiquitin activating enzyme), an E2 (ubiquitin conjugating enzyme) and an E3 ligase (ubiquitin ligating enzyme) (Hershko, 1983; Hershko and Ciechanover, 1998). Specificity of this enzymatic cascade is achieved by the E3 ligases that

recognize specific substrates and catalyze the ubiquitin transfer (Berndsen and Wolberger, 2014). Ubiquitylation has been the subject of many studies and many proteins are known to be ubiquitylated (Komander and Rape, 2012; Popovic et al., 2014). Recently, new enrichment strategies were developed that extended the number of known ubiquitylated proteins by several thousands. In all these studies antibodies were used that recognize the di-glycil remnant, which is left on lysine residues of ubiquitylated proteins after trypsin digestion. Taken together these studies identified more than 20,000 ubiquitylation sites and more than 5,000 ubiquitylated proteins (Kim et al., 2011; Udeshi et al., 2012; Wagner et al., 2011; Xu et al., 2010).

Despite these fascinating findings demonstrating how ubiquitous ubiquitylation is, there is currently no good way to directly identify specific E3-ligase-subtrate partners. In this chapter we establish a method to detect and identify poly-ubiquitylated substrates of the E3 ubiquitin ligase TRIM3. We make use of a recently generated *Trim3* knockout mouse (Labonte et al., 2013) to identify specific protein interactors of TRIM3 and detect proteins that are differentially poly-ubiquitylated between *Trim3*$^{-/-}$ and wildtype mice. We employ Tandem Ubiquitin Binding Entities (TUBEs) (Hjerpe et al., 2009; Lopitz-Otsoa et al., 2012) to specifically identify proteins that are poly-ubiquitylated and would therefore be targeted for proteasomal degradation. By combining TRIM3 interaction data and data of enriched poly-ubiquitylated proteins we aimed to identify a limited number of high-confidence substrates of TRIM3.

Material and Methods

Animals

Trim3$^{-/-}$ mice were maintained on a C57BL/6J background. Wildtype littermates were used as controls in all experiments. Mice were individually housed on sawdust in standard Makrolon type II cages (26.5 cm long, 20.5 cm wide and 14.5 cm high) enriched with cardboard nesting material and a plastic tube under 12/12h dark/light cycle with access to water and food *ad libitum*. All animal experiments were approved by the animal ethics committee of the VU University Amsterdam, The Netherlands.

Synaptic protein isolation and quantification

Brain tissue was obtained from C57BL/6J mice. Animals were sacrificed by cervical dislocation. Cerebellum and hippocampus were dissected and stored at -80° C. Synapse-enriched protein fractions (P2 + M, pellet 2 + microsomes) were isolated as previously described (Klemmer et al., 2009). Protein concentrations were measured using Bradford Protein-Assay (Bio-Rad Laboratories, USA) and equal amounts of protein were loaded on a 4 - 20 % gradient SDS-PAGE gel (Criterion TGX Stain-Free Gel, Bio-Rad Laboratories, USA). Total protein amounts were imaged after electrophoresis using Criterion Stain Free Imager (Bio-Rad Laboratories, USA). Gels were then transferred to PVDF membranes (Bio-Rad Immuno-Blot PVDF membrane, Bio-Rad Laboratories, USA) and blots were blocked by either immersing the membrane in 5 % nonfat dry milk in TBS-T (TBS plus 0.025 % Tween, pH 7.4) or 0.5 % BSA in TBS-T (TBS plus 0.025 % Tween, pH 7.4) for 1 h. Blots were then incubated with the antibody of interest for 1h at room temperature or overnight at 4° C, followed by a 1h incubation with a secondary antibody conjugated to HRP. Proteins were visualized by ECL treatment (SuperSignal West Femto Chemiluminescent Substrate, Thermo Scientific, USA) and scanned using the Odyssey Fc imager (Li-Cor, USA). Antibodies used: rabbit anti-TRIM3 (CLRPGDLPPSPDDVK, GenScript, 1:1,000), rabbit anti-TRIM3 (QAPEGAHDPEDPHPC, GenScript, 1:500), goat anti-RNF22 (ab4215, Abcam, 1:500), mouse anti-poly-ubiquitin (FK1, BML-PW8805, Enzo Life Sciences, 1:1,000), mouse anti-SAPAP1 (75-236, Neuromab, 1:1,000), mouse anti-SHANK1 (75-064, Neuromab, 1:1,000), mouse anti-GLUR1 (75-327, Neuromab, 1:10,000), mouse anti-GLUR2 (75-002, Neuromab, 1:1,000), mouse anti-NR2B (73-097, Neuromab, 1:10), rabbit anti-HOMER1 (AP7302c, Abgent, 1:200), rabbit anti-AP2A1 (11401-1-AP, Proteintech, 1:1,500), rabbit anti-DNM3 14737-1-AP, Proteintech, 1:800), rabbit anti-ACTN4 (19096-1-AP, Proteintech, 1:1,500), mouse anti-AP2M1 (611350, BD Biosciences, 1:10,000), rabbit anti-ANXA5 (NB100-1930, Novus Biologicals, 1:2,000), rabbit anti-NME1 (ABS95, Millipore, 1:2,000)

Co-Immunoprecipitation of TRIM3 and interactors

For each immunoprecipitation (IP) experiment 10 mg of P2 + M from wildtype or *Trim3*$^{-/-}$ mice (control for co-immunoprecipitation specificity) were extracted in an equal volume of Triton X-100 containing extraction buffer (2 % Triton X-100, 150 mM NaCl,

25 mM HEPES pH 7.4, protease inhibitors (Complete Protease Inhibitor Cocktail, Roche Diagnostics) for 1 h on a rotator at 4° C. Insoluble material was then pelleted 20,000 g for 20 min at 4° C. The pellet was then re-extracted in 1 % Triton X-100 extraction buffer (1 % Triton X-100, 150 mM NaCl, 25 mM HEPES pH 7.4, protease inhibitors) for 1h. Insoluble material was again pelleted at 20,000 g for 20 min. Supernatants from the first and second extraction were then pooled, centrifuged at 20,000 g for 20 min and the final supernatant served as input for the immunoprecipitation.

Three different antibodies raised against TRIM3 were used for immunoprecipitations (IPs): goat anti-RNF22 (ab4215, Abcam), rabbit anti-Trim3 (epitope: CLRPGDLPPSPDDVK-NH2, GenScript) and rabbit anti-Trim3 (epitope: QAPEGAHDPEDPHPC, GenScript). All IPs were performed with 10 µg of antibody, which were added to the final supernatant and incubated overnight on a rotator at 4° C. Next day 30 µl of protein A/G beads (Protein A/G Plus-Agarose, Santa Cruz Biotechnology Inc.) were washed 3 times in washing buffer (0.1 % Triton X-100, 150 mM NaCl, 25 mM HEPES pH 7.4) and added to each IP. Beads were incubated for 120 min on a rotator at 4° C, then pelleted at 2,500 g and washed four times in ice-cold washing buffer. TRIM3 and interacting proteins were eluted off the beads by adding SDS containing loading buffer and boiling for 5 min. Samples were separated on SDS page and immunoblotted or in-gel digested (Chen et al., 2011b) for mass spectrometry analysis.

Extraction efficiency optimization for poly-ubiquitylated proteins

In order to increase the extraction yield of poly-ubiquitylated proteins from brain material, 13 combinations of four different detergents (n-Dodecyl-β-D-maltoside (DDM), sodium deoxycholate (DOC), Tween 20, IGEPAL CA-630) in different concentrations were tested. Equal amounts of input material were extracted twice for one hour at 4° C on a rotator and remaining insoluble material pelleted at 20,000 g. Pooled Supernatants and remaining pellets were separated on a 0.5 % 2,2,2-Trichloroethanol containing 10 % SDS-PAGE. Total protein amounts were imaged after electrophoresis using Criterion Stain Free Imager (Bio-Rad Laboratories). Gels were then transferred to PVDF membranes (Bio-Rad Immuno-Blot PVDF membrane, Bio-Rad Laboratories) and blots were blocked by immersing the membrane 0.5 % BSA in TBS-T (TBS plus 0.025 % Tween, pH 7.4) for 1 hour. Blots were

then incubated with mouse anti-poly-ubiquitin (FK1, BML-PW8805, Enzo Life Sciences, 1:1,000) antibody for 1 h at room temperature, followed by a one hour incubation with a secondary antibody conjugated to HRP. Poly-ubiquitylated proteins were visualized by ECL treatment (SuperSignal West Femto Chemiluminescent Substrate, Thermo Scientific, USA) and scanned using the Odyssey Fc imager (Li-Cor, USA). Extraction efficiency was scored by measuring and ranking stain-free gel signal intensities of supernatants, pellets and by measuring western blot poly-ubiquitin signal intensities. Scored ranks were averaged and the most efficient poly-ubiquitin extraction selected for TUBEs pull-down.

Enrichment of poly-ubiquitylated proteins

Tandem ubiquitin binding entities (TUBEs) immobilized to agarose beads were purchased from LifeSensors (Malvern, PA). For each affinity purification experiment, 20 mg of hippocampal P2 + M protein fraction was added to 100 µl of TUBEs slurry. Purification of bound proteins was performed according to the manufacturer's protocol with minor modifications. Not NP40, but a combination of 0.5 % Na-deoxycholate (DOC) and 1 % n-dodecyl-β-D-maltoside (DDM) in 25 mM HEPES, 150 mM NaCl (pH 7.2) was used as solubilizing detergent. Deubiquitylation and proteasomal degradation were minimized by adding 10 mM N-ethylmaleimide (NEM), 20 µM MG132 (Tocris Bioscience) and protease inhibitors (Roche) to all extraction buffers. Tris was replaced by HEPES as the buffering agent. Purified proteins were washed three times in extraction buffer, one time in high-salt buffer (500 mM NaCl) and one time in no-salt buffer. Proteins were then eluted in 0.15 % trifluoroacetic acid (TFA) and lyophilized for further analysis.

Trypsin digestion

Immunoprecipitated protein samples were separated on SDS-PAGE and in-gel trypsin-digested as previously described (Chen et al., 2011a). TUBEs-purified proteins were re-solubilized in 50 mM NH_4HCO_3 / 10 % acetonitrile, brought to 2 mM DTT and heated to 60° C for 20 min. Proteins were then alkylated with 8 mM iodoacetamide for 1 h. Alkylation was stopped by bringing samples to 8 mM DTT. Samples were then brought to a final concentration of 25 mM NH_4HCO_3, 8 % acetonitrile and 2 mM DTT, and digested with

trypsin (mass spectrometry grade; Promega, Fitchburg, WI, USA) overnight at room temperature. Digestion was stopped by adding 1 % TFA. Peptides were purified over a C18 column and lyophilized.

Nano-LC MS/MS

Peptides were re-dissolved in 20 µl 0.1 % TFA and subjected to nano-LC MS/MS. Peptides were delivered with a FAMOS autosampler at 30 µL/min to a Pepmap C18 trap column (5 mm x 300 µm i.d.; Dionex, Sunnyvale, CA, USA) and separated on an Alltima analytical capillary C18 column (150 mm x 100 µm i.d.) at 400 nl/min using the LCPacking Ultimate system. The peptides were separated using a linearly increasing concentration of acetonitrile from 5 – 35 % in 80 min, from 35 – 45 % in 7 min, from 45 – 90 % in 2 min and then held at 90 % for an additional 11 min. The eluent was mixed with matrix (7 mg α-cyano-hydroxycinnaminic acid in 1 mL 70 % acetonitrile, 0.1 % trifluoroacetic acid, 10 mM ammonium monobasic phosphate) delivered at a flow rate of 1.5 µL / min, and deposited off-line to the Applied Biosystems metal target every 15 s for a total of 384 spots, using an automatic robot (Probot from Dionex, Thermo Fisher Scientific, USA). A 5800 proteomics analyzer (Applied Biosystems, SCIEX, USA) was used for peptide analysis. Collision-induced dissociation (CID) was performed at 2 kV, the collision gas was nitrogen. MS / MS spectra were collected from 2500 laser shots. The peptides with signal to noise ratio above 50 at the MS mode were selected for MS/MS experiment; a maximum of 25 MS/MS were allowed per spot. The precursor mass window was 200 relative resolution (FWHM, full width at half maximum).

Peptide data analysis and Protein inference

MS / MS spectra were annotated against a concatenated target-decoy database of Uniprot mouse reference proteome sequences (version 02 / 2012) using ProteinPilot software (v3.0; Applied Biosystems, Foster City, CA, USA) using the Paragon algorithm (v3.0.0.0) (Shilov et al., 2007). Database searches were performed with trypsin-specificity and alkylation of cysteine residues by iodoacetamide. For each spectrum the best scoring peptide sequence was selected as spectrum annotation. Protein inference was performed using IsoformResolver software (Meyer-Arendt et al., 2011) aiming for consistent protein assignment of peptides

across experiments. False discovery rate (FDR) for peptide and protein identification were established using Mayu (Reiter et al., 2009). Peptide-spectrum matches were truncated at 5 % FDR and protein identifications were truncated at 1 % FDR. Proteins were quantified according to their normalized spectral intensity value (Griffin et al., 2010), their peptide ratio (wildtype / *Trim3*$^{-/-}$) and their spectral count ratio (wildtype / *Trim3*$^{-/-}$). Values contributed by peptides shared by different proteins were apportioned according to the spectral intensity values obtained from unique peptides of the respective proteins. Apportioned values were then transformed as follows: all values were divided by the lowest value in the sample, the value of 1 was added to each value to allow log transformation, and all resulting values were log2 transformed. Candidate TRIM3 interactors were defined as all proteins that were immunoprecipitated with at least two out of three antibodies from wildtype tissue and that showed at least a 2-fold (log2) enrichment compared with samples obtained from *Trim3*$^{-/-}$ tissue. For candidate TRIM3 substrates we selected all proteins that were identified in at least two out three TUBEs affinity purification replicates from wildtype tissue, and had an average enrichment of at least 2-fold (log2) compared with samples obtained from *Trim3*$^{-/-}$ tissue. An arbitrary cut-off for the highest ranking 100 potential TRIM3 interactors and the highest ranking 300 poly-ubiquitylated was applied. Highest ranked interactors and poly-ubiquitylated proteins were then cross-referenced to identify potential TRIM3 substrates.

Fear conditioning

Fear conditioning experiments were carried out as described (Misane et al., 2005; Stiedl et al., 2000) using a computerized fear conditioning system (TSE, 303410, Bad Homburg, Germany). In brief, mice were placed in an acrylic cage mounted into a constant illuminated (450 lx) fear conditioning box. After a 180 s exploration period, mice received a 2 s foot shock (0.7 mA) delivered through a metal floor grid. Mice were returned to their home cages 30 s after termination of the shock. Animals were sacrificed 24 h after the shock and brains dissected and processed for biochemical analysis of synaptosomes.

Results

Several candidate synaptic proteins are not regulated by TRIM3 *in vivo*

In search for a synaptic role of TRIM3 we asked which synaptic proteins are likely candidate substrates for poly-ubiquitylation by TRIM3. It was recently reported that TRIM3 can poly-ubiquitylate the postsynaptic scaffold protein GKAP *in vitro*, leading to a significant reduction in the levels of both GKAP and its associated scaffold SHANK1 (Hung et al., 2010). These findings were, however, challenged by the same authors who subsequently showed that the activity-dependent removal of GKAP from synapses *in vivo* does not likely require TRIM3 (Shin et al., 2012). To test GKAP and SHANK1 as potential TRIM3 substrates *in vivo* we quantified their levels in hippocampal synapse-enriched fractions from *Trim3*$^{-/-}$ mice and wildtype controls, both under basal conditions (Figures 1A and 1B) and 2 h after fear conditioning (Figures 1C and 1D). We did not observe an increase in GKAP or SHANK1 protein levels in *Trim3*$^{-/-}$ mice as would be expected if these proteins underwent TRIM3-dependent poly-ubiquitylation and proteasomal degradation (Figure 1). In addition to GKAP and SHANK, iTRAQ proteomics analysis performed in our lab identified 12 synaptic proteins of which the levels were increased in synapse-enriched preparations from *Trim3*$^{-/-}$ mice compared to wildtype controls (unpublished data), including the known TRIM3 interactor alpha-actinin-4 (El-Husseini et al., 2000). Using quantitative immunoblotting on the same synapse-enriched fractions we could also rule these proteins out as ubiquitylation substrates of TRIM3 (Figure S1).

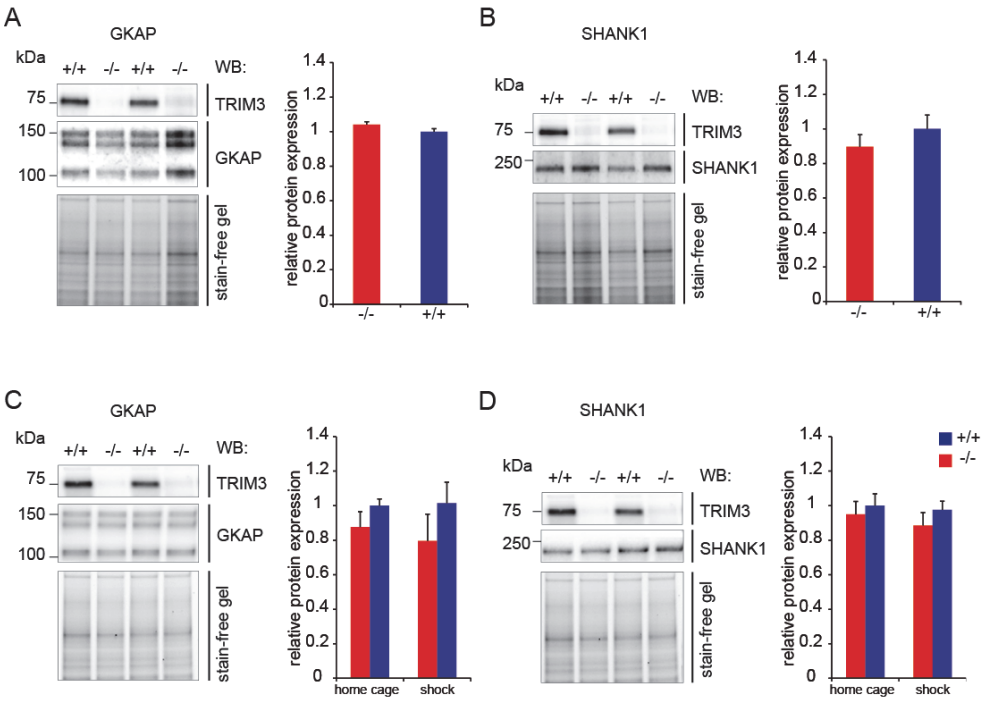

Figure 1 GKAP and SHANK1 levels are not affected in Trim3$^{-/-}$ mice. (A - B) Hippocampal synapse-enriched fractions (P2 + M) were prepared from wildtype and *Trim3*$^{-/-}$ mice. Samples were immunoblotted for GKAP **(A)** and SHANK1 **(B)**. Protein levels of GKAP and SHANK1 are not affected by loss of TRIM3 in the synapse enriched fraction P2 + M (means ± SEM, two-tailed t test, $p > 0.05$, $n = 8$ per genotype). **(C - D)** Synaptosomes were prepared from wildtype and *Trim3*$^{-/-}$ mice under control conditions (home cage) and 2 hours after contextual fear conditioning (shock). Samples were immunoblotted and stained for GKAP **(C)** and SHANK1 **(D)**. Normalized protein levels were calculated by dividing Western blot (WB) signal intensities by the total protein intensities (stain-free gel) and expressed relative to wildtype levels. GKAP and SHANK1 levels did not differ between conditions (means ± SEM, two-tailed t test, $p > 0.05$, $n = 4$ per genotype).

Identification of TRIM3 ubiquitylation substrates

To identify potential TRIM3 substrate proteins we reasoned that a bona fide substrate should (i) physically interact with TRIM3, even if only transiently or weak, and (ii) be less poly-ubiquitylated in *Trim3*$^{-/-}$ mice. To detect differentially ubiquitylated proteins between wildtype and *Trim3*$^{-/-}$ mice we used TUBEs (Tandem Ubiquitin Binding Entities). TUBEs are recombinant proteins based on the E1 ubiquitin activating enzyme UBE1 and RAD23A, a protein that is essential for the delivery of poly-ubiquitylated proteins to the proteasome.

TUBEs have a very high affinity to poly-ubiquitin (Hjerpe et al., 2009; Lopitz-Otsoa et al., 2012) and thus would strongly enrich for proteins that are poly-ubiquitylated and targeted for proteasomal degradation. TUBEs furthermore have a protective function. Ubiquitylation is a reversible process, and a large number of de-ubiquiylation enzymes cleave ubiquitin from substrate proteins. Moreover, de-ubiquitylation is enhanced in cell lysates (Komander et al., 2009). TUBEs, by binding to poly-ubiquitylated proteins, protect proteins from de-ubiquitylation and proteasomal degradation, thereby allowing identification of transient poly-ubiquitylation events at any moment in time, even when poly-ubiquitylated proteins are of low abundances.

We first optimized TUBEs methodology to (i) increase the yield of the TUBEs pull-down and (ii) demonstrate the efficacy and reproducibility of the TUBEs approach. To increase the yield, we first aimed to optimize extraction efficiency and solubility of poly-ubiquitylated proteins from synapse-enriched fractions. We tested four different detergents (Tween-20, n-Dodecyl β-D-maltoside (DDM), deoxycholate (DOC) and IGEPAL CA-630) in 11 different combinations and concentrations (Table 1 and Figure 2). Extraction efficiency was scored by analyzing (i) protein amounts of the soluble and insoluble fractions after extraction on SDS-PAGE and (ii) by poly-ubiquitin staining intensity after immunoblotting (Figure 2). Detergent combinations of DDM + DOC and CA-630 + DOC scored highest on SDS-PAGE and immunoblot (Figure 2, conditions 5 and 8), and we chose to perform all following experiments with a combination of 1 % DDM and 0.5 % DOC.

Table 1 Extraction optimization for poly-ubiquitylated proteins from synapse-enriched cellular fractions. Synapse-enriched fractions were extracted twice for 1 h in HEPES buffer (25 mM HEPES, 150 mM NaCl, pH 7.2) containing different detergents as indicated in the table. Soluble and insoluble fractions were resolved on SDS-PAGE, then imaged and immunoblotted for poly-ubiquitin. Signal intensities of all samples from SDS-PAGE and western blot were scored and a combined rank was assigned to each extraction procedure.

Extraction Buffers		**Rank**			
First Extraction	**Second Extraction**	**Soluble**	**Insoluble**	**Poly-Ub Blot**	**Combined**
DDM 1 %	0.5 % DOC	1	2	4	1
CA-630 1 %	0.5 % DOC	6	4	2	2
0.5 % Tween, 0.5 % CA-630	0.5 % DOC	4	1	10	3
CA-630 1 %, 0.1 % DOC	CA-630 1 %, 0.1 % DOC	7	3	6	4
DOC 0.5 %, 0.1 % CA-630	DOC 0.5 %, 0.1 % CA-630	3	5	9	5
0.5 % Tween, 0. 5% CA-630, 0.1 % DOC	0.5 % Tween, 0.5 % CA-630, 0.1 % DOC	8	10	1	6
0.5 % Tween, 0.5 % CA-630	0.5 % Tween, 0.5 % CA-630	5	7	7	7
CA-630 1 %	CA-630 1 %	2	6	11	8
DOC 0.5 %	DOC 0.5 %	9	8	3	9
DDM 1 %	DDM 1 %	11	9	5	10
DDM 1 %, 0.1 % DOC	DDM 1 %, 0.1 % DOC	10	11	8	11

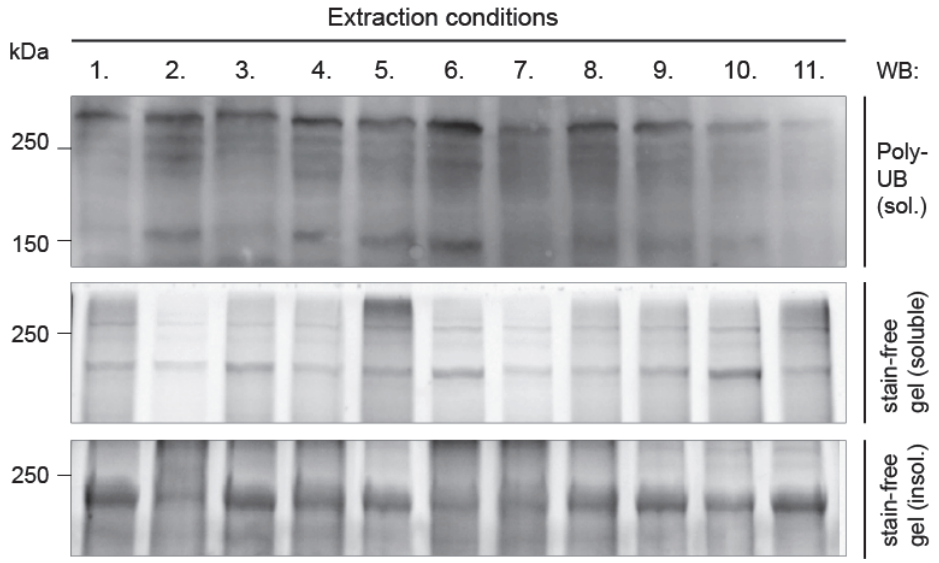

Figure 2 Exemplary immunoblot and stain-free gel images of different extraction conditions on synapse-enriched cellular fractions. Synapse-enriched fractions were extracted twice in buffers containing different detergents. Soluble (middle panel) and insoluble fractions (bottom panel) were resolved on SDS-PAGE, then imaged and immunoblotted for poly-ubiquitin (top panel – only soluble fractions). Signal intensities of all samples from SDS-PAGE and western blot were scored and a combined rank was assigned to each extraction procedure. (Extraction conditions (left to right): **1.** DOC 0.5 %/0.1 % CA-630, **2.** DDM 1 %, **3.** 0.5 % Tween-20/0.5 % CA-630, **4.** DOC 0.5 %, **5.** DDM 1 %/0.5% DOC, **6.** 0.5 % Tween-20/0.5 % CA-630/0.1 % DOC, **7.** DDM 1 %/0.1 % DOC, **8.** CA-630 1 %/0.5 % DOC, **9.** CA-630 1 %/0.1 % DOC, **10.** 0.5 % Tween-20/0.5 % CA-630/0.5 % DOC, **11.** CA-630.

TUBEs efficacy was demonstrated by showing that TUBEs pull-down, but not a pull-down with empty agarose beads, resulted in a strong enrichment of poly-ubiquitylated proteins detected by immunoblotting (Figure 3A). Moreover, the coomassie-stained gel revealed that the TUBEs-enriched protein fraction contained many individual proteins that were not detected in the control pull-down samples (Figure 3B). We then performed three TUBEs pull-down replicates on independent synapse enriched samples and identified proteins using mass spectrometry. On average we were able to detect 3150 peptides mapping to 577 proteins with at least one unique peptide. Reproducibility at the protein level was 79.4 % between replicates (Figure 3C).

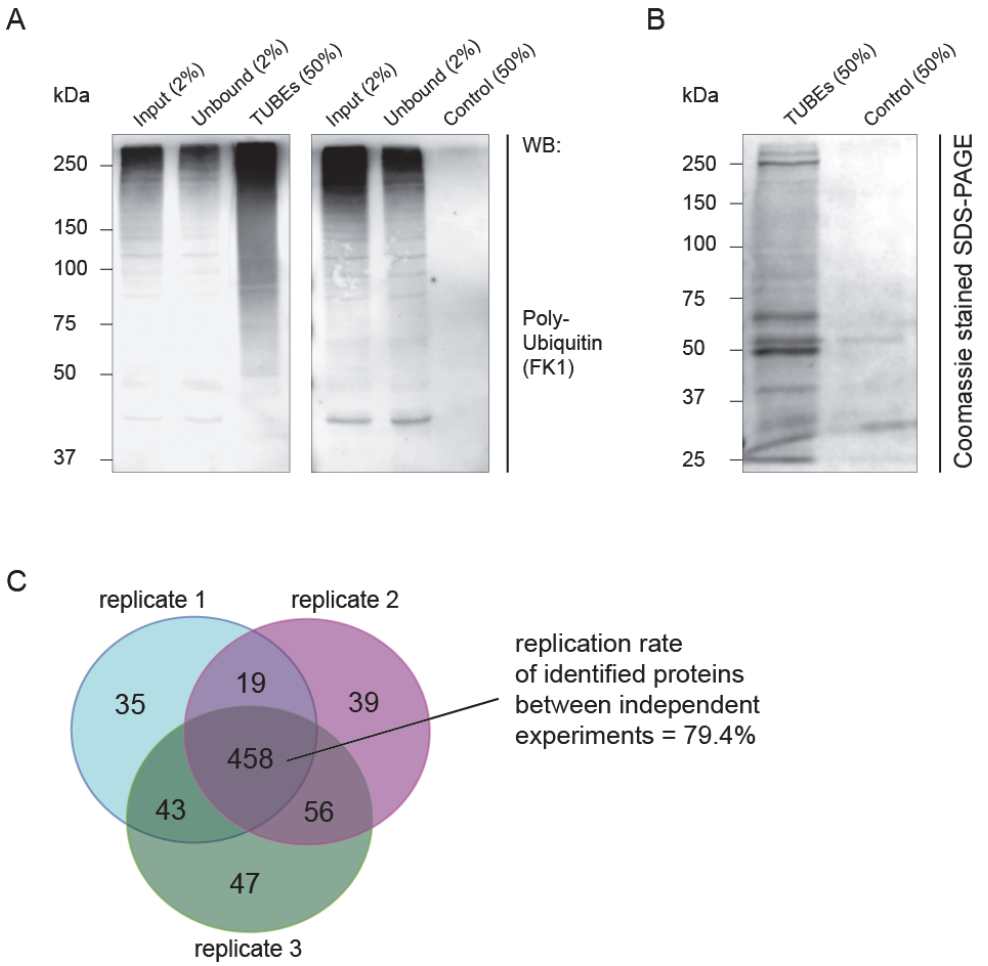

Figure 3 Validation of the TUBEs pull-down approach. (A) TUBEs immobilized to agarose beads were added to 2 mg of hippocampal protein extract and incubated for 2 h in the presence of MG132 and protease inhibitors. Input, unbound fraction, TUBEs pull-down (50 %) and control pull-down (agarose beads only) were resolved on SDS-PAGE and immunoblotted for poly-ubiquitin. A strong enrichment for poly-ubiquitylated proteins (50 - 250 kDa) was observed in the TUBEs pull-down fraction (left), but not in the control pull-down fraction (right). **(B)** When resolved on SDS-PAGE and coomassie-stained for total protein content, the TUBEs pull-down appeared to be highly enriched in proteins compared with the control pull-down sample. **(C)** Venn diagram indicating reproducibility of TUBEs pull-down between three independent replicate experiments.

We then designed a substrate identification strategy (Figure 4) in which we immunoprecipitated TRIM3 from hippocampal and cerebellar synapse-enriched fractions using three different antibodies, and in parallel performed affinity purification of poly-

ubiquitylated proteins from synapse-enriched fractions using TUBEs in triplicate. In both experiments, *Trim3*$^{-/-}$ tissue fractions were used as negative controls. Proteins from co-immunoprecipitates and TUBEs pull-downs were then identified and quantified using mass spectrometry, and results from both experiments compared to find proteins that specifically co-imunoprecipitated with TRIM3 from wildtype tissue and not *Trim3*$^{-/-}$ tissue, and which were more ubiquitylated in wildtype tissue compared with *Trim3*$^{-/-}$ tissue.

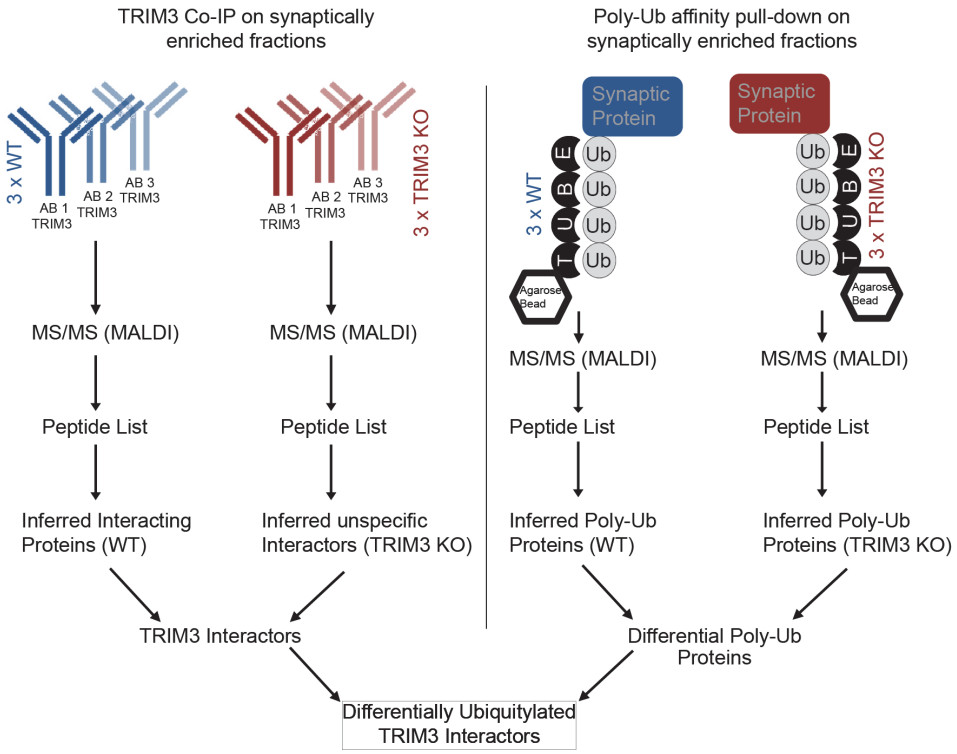

Figure 4 Strategy to identify TRIM3 ubiquitylation substrates. Hippocampal synapse-enriched protein fractions were used as input for both immunoprecipitation (left) and poly-ubiquitin affinity pull-down (right). Immunoprecipitation was performed with three independent antibodies raised against different epitopes of TRIM3 (AB1 epitope: QAPEGAHDPEDPHPC, AB2 epitope: CLRPGDLPPSPDDVK, AB3 epitope: AKREDSPGPEVQP). Samples from *Trim3*$^{-/-}$ mice served as a control for co-immunoprecipitation specificity. Poly-ubiquitin affinity pull-down was performed using TUBEs. Three independent replicates were performed. The parallel use of *Trim3*$^{-/-}$ and wildtype tissue allowed for identification of differentially poly-ubiquitylated proteins. All samples were analyzed by quantitative mass spectrometry and potential TRIM3 substrates were identified by ranking and comparing results from all six samples (see *Material and Methods* for details).

Using immunoprecipitation we identified 110 potential TRIM3 interactors in hippocampus and 186 in cerebellum (Tables S1 - S2) that consistently co-immunoprecipitated with TRIM3 using two or three antibodies, specifically from wildtype tissue. Several proteins were identified that were previously reported to interact with TRIM3. Myosin Vb, for instance, is a known interactor of TRIM3 (El-Husseini, 1999), and we found myosin Vb and TRIM3 to interact in the hippocampus (Table S1). In contrast, in the cerebellum we found myosin 18b (Table S2) to interact with TRIM3. We also detected numerous proteins reported to be present in mRNP particles alongside TRIM3 (Kanai et al., 2004). While Kanai et al. (2004) used whole brain homogenate for mRNP isolation, our data show a more differentiated picture. Whereas TRIM2 co-precipitated with TRIM3 from both hippocampus and cerebellum, Eef1a2 only co-precipitated from hippocampus and HSPA2 co-precipitated with TRIM3 only from cerebellum.

Using the TUBE approach, we identified a total of 1015 poly-ubiquitylated proteins in the hippocampus and 1018 in cerebellum. To limit the number of potential substrates we introduced a cut-off at the 100 highest-ranked potential TRIM3 interactors and the 300 most-enriched poly-ubiquitylated proteins in hippocampus and cerebellum of wildtype animals. In order to identify potential TRIM3 ubiquitylation substrates we compared potential interactors with enriched poly-ubiquitylated proteins and created an overlap of proteins present in both. Overlapping proteins were considered likely ubiquitylation substrates (Figure 5).

The overlap between TRIM3 interactors and potential TRIM3 substrates was very little and yielded a limited list of potential substrates. In the hippocampus we identified five proteins that met both criteria: gamma-actin (ACTG1), immunoglobulin-like and fibronectin type III domain-containing protein 1 (IGFN1), kalirin (KALRN), ADP/ATP translocase 1 (SLC25A4) and macoilin (TMEM57) (Figure 5A). ACTG1 ranked the highest in both criteria. In the cerebellum we identified seven proteins: vimentin (VIM), GRB10 interacting GYF protein 2 (GIGYF2), GM8765, heat shock protein 90kDa alpha – class B member 1 (HSP90AB1), adenylate cyclase 1 (ADCY1), synaptosomal-associated protein – 25kDa (SNAP25) and neuroplastin (NPTN).

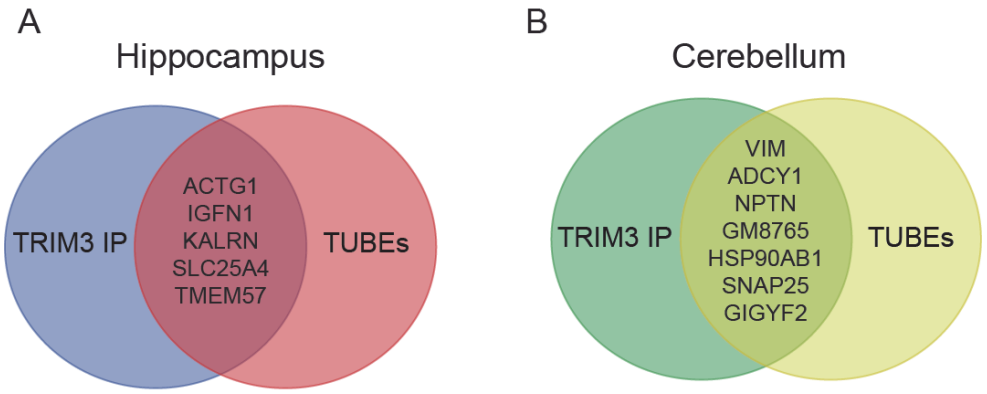

Figure 5 Combination of co-immunopricipation and TUBEs pull-down reveals potential TRIM3 ubiquitylation substrates. (A) Venn diagram indicating the five proteins that were identified in the hippocampus as potential TRIM3 substrates with the highest confidence based on combined co-immunopreciptation and differential TUBEs pull-down. **(B)** Venn diagram indicating the seven proteins that were identified in the cerebellum as potential TRIM3 substrates. For both brain regions a cut-off was set for the highest ranking 100 TRIM3 interactors and the highest ranking 300 TUBEs pull-down proteins that were more poly-ubiquitylated in wildtype mice compared to *Trim3*$^{-/-}$ mice (see *Materials and Methods* for inclusion criteria).

Discussion

In this chapter we excluded several synaptic proteins as TRIM3 ubiquitylation substrates and developed an experimental approach to identify true TRIM3 substrates. We were able to identify candidate TRIM3 ubiquitylation substrates by using a dual mass spectrometry approach combining co-immunoprecipitation and enrichment of poly-ubiquitylated proteins. Many synaptic proteins, including CaMKIIα, PSD-95, GKAP and receptors for AMPA, NMDA and GABA are known to be ubiquitylated (Lin and Man, 2013; Na et al., 2012). TRIM3 was shown to poly-ubiquitylate GKAP in an *in vitro* overexpression assay, leading to a significant reduction in the levels of both GKAP and its associated scaffold SHANK1 (Hung et al., 2010). If TRIM3 indeed targeted GKAP and/or SHANK1 *in vivo* for proteasomal degradation, *Trim3*$^{-/-}$ mice should have higher levels of both proteins. We found no such increase in hippocampal synapse-enriched fractions from *TRIM3*$^{-/-}$ mice, independent of whether these mice underwent hippocampal stimulation (i.e., fear conditioning) or not. Moreover, Shin et al. (2012) showed that the activity-dependent removal of GKAP form

synapses *in vivo* does not necessarily require TRIM3. Together, these findings led us to conclude that TRIM3 does not target GKAP or SHANK1 for proteasomal degradation.

We therefore set out to identify true TRIM3 substrates. Due to the nature of the ubiquitylation process, its reversibility by DUBs (Wilkinson, 2000) and the low steady-state levels of ubiquitylated substrate proteins (Pickart, 2004; Pickart and Eddins, 2004), no direct way to identify substrate proteins of E3 ligases *in vivo* has been developed to date. Indirect methods used to identify substrate proteins often involve overexpression of tagged proteins of the ubiquitin proteasome pathway, such as ubiquitin itself in cell lines (Beers and Callis, 1993; Lee et al., 2011; Peng et al., 2003). Other used methods include yeast two-hybrid (Drury et al., 1997; Thomas et al., 1995), protein microarrays (Loch et al., 2011) and co-precipitation (Yaron et al., 1998). A major drawback of all of these methods is that they do not extend beyond establishing physical interaction between two proteins, and normally result in long lists of candidate proteins that still need to be validated as substrates. With our approach, combining enrichment of poly-ubiquitylated proteins from brain tissue using TUBEs and the identification of TRIM3 interactors using co-immunoprecipitation, and using *Trim3*$^{-/-}$ mice as specificity controls, we were able identify a small number of potential substrate proteins that interact with TRIM3 and are significantly less ploy-ubiquitylated in *Trim3*$^{-/-}$ mice. Our approach is also superior to using di-glycil antibodies (Wagner et al., 2011) for quantitative detection of ubiquitylation for three reasons: (i) di-glycil antibodies are not able to differentiate between the type of ubiquitylation (mono-, multiple-mono-, poly-ubiquitylation), (ii) they only detect peptides with di-glycil modified lysines, making it impossible to detect isoforms of proteins sharing the majority of peptides, and (iii) other modifications such as neddylation, leaving the same glycin-gylcin remnant after trypsin digestion, will be falsely identified as ubiquitylation.

The fact that we find non-overlapping protein sets as candidate TRIM3 substrates in hippocampus and cerebellum suggests that TRIM3 has different functions according to its localization. This is further supported by our finding that TRIM3 is localized post-synaptically in hippocampus and axonally / pre-synaptically in cerebellum (Chapter 2). Of the 12 proteins that we identified (five in hippocampus and seven in cerebellum) three are of particular interest because they are components or regulators of the neuronal cytoskeleton. In the hippocampus we identified kalirin as a potential substrate. Kalirin is a guanine exchange factor for several key actin-modulatory GTPases including RhoG, RhoA and Rac (May et

al., 2002; Penzes et al., 2001). Kalirin was shown to be involved in the maintenance of hippocampal pyramidal cell dendrites and dendritic spines (Ma et al., 2003). A kalirin isoform, kalirin-7, was reported to be localized in dendritic spines and a knock-down using RNAi resulted in a loss of spines (Zhong et al., 2006). Cahill et al. (2009) created a *Kalirin* knockout mouse, and observed a robust reduction in spine density in cortex, deficits in working memory and sociability and increased locomotor activity. An even higher-ranking candidate TRIM3 substrate in the hippocampus was gamma-actin. Interestingly, TRIM3 contains a long actin-binding protein-like repeat (El-Husseini, 1999) and its close paralog TRIM32 was reported to ubiquitylate actin in muscle (Kudryashova et al., 2005). Although a role for gamma-actin in regulating actin stability has been suggested (Belyantseva et al., 2009; Bergeron et al., 2010), no specific contribution of actin-gamma to synaptic stability or plasticity has been reported, yet. We will further discuss the role of actin-gamma as a potential TRIM3 substrate in Chapter 5.

In the cerebellum we identified the intermediate filament protein vimentin as a potential TRIM3 substrate. It is interesting to note that TRIM2, the closest relative of TRIM3, was shown to also target intermediate filaments, in particular neurofilament light chain, for proteasomal degradation in cerebellar Purkinje cells (Balastik et al., 2008). Consequently, *Trim2*$^{-/-}$ mice show a strong neurodegenerative phenotype (Balastik et al., 2008). While TRIM2 and TRIM3 may thus both target intermediate filament proteins in the cerebellum, they most likely do so in different neurons as TRIM3 expression was detected primarily in cerebellar granule neurons, and not in Purkinje cells (Chapter 2). Despite these intriguing observations, one should keep in mind that vimentin expression is normally associated with developing neurons, and vimentin appears to be depleted as an important intermediate filament constituent in adult neurons (Yabe et al., 2003). This could disqualify vimentin as a likely TRIM3 substrate, but could also imply that TRIM3 is somehow involved in the developmental decrease of vimentin levels.

To summarize, we showed that neither GKAP nor SHANK1 protein levels are affected by TRIM3, and we also excluded several other synaptic proteins as candidate TRIM3 substrates. We further developed a novel method that is sensitive enough to detect a small, but distinct set of potential substrate proteins of TRIM3, demonstrating the feasibility of this approach. We conclude that this approach could be applied to any ubiquitin ligase for which appropriate controls, e.g., knockout animal, are available.

Supplementary

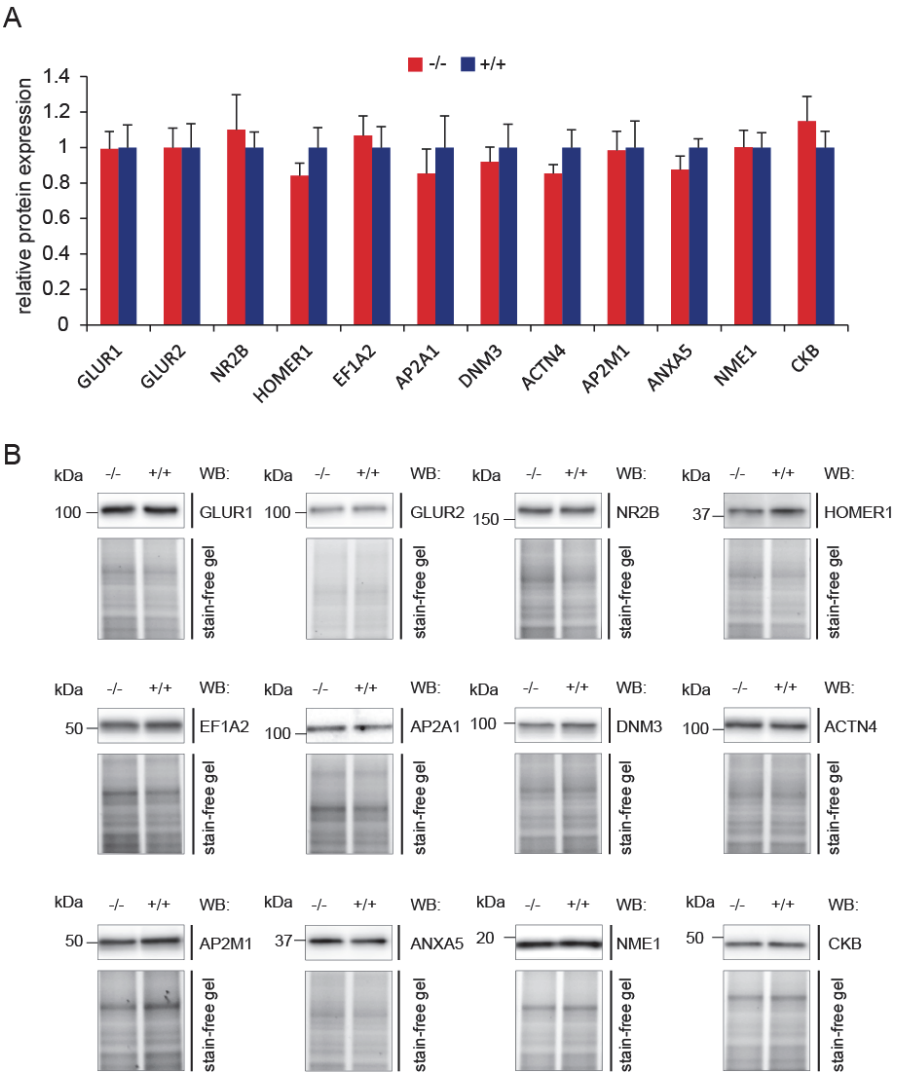

Figure S1 (A - B) Quantitated protein expression **(A)** and quantitative western blot images **(B)** for GLUR1, GLUR2, NR2B, HOMER1, EF1A2, AP2A1, DNM3, ACTN4. AP2M1, ANXA5, NME1 and CKB on hippocampal synaptosomal samples (n = 5 per genotype, WT = +/+, TRIM3 KO = -/-) from mice under home cage conditions. All data points show mean ± SEM, two-tailed t test, all non-significant, n = 5. Quantities are presented relative to WT samples set to a value of 1. [GLUR1: WT 1 ± 0.13, KO 0.99 ± 0.10; GLUR2: WT 1 ± 0.13, KO 1 ± 0.11; NR2B: WT 1 ± 0.09, KO 1.10 ± 0.20; HOMER1: WT 1.00 ± 0.11, KO 0.84 ± 0.07; EF1A2: WT 1 ± 0.12, KO 1.07 ± 0.11; AP2A1: WT 1 ± 0.18, KO 0.85 ± 0.14; DNM3: WT 1 ± 0.13, KO 0.92 ± 0.08; ACTN4: WT 1 ± 0.10, KO 0.85 ± 0.05; AP2M1: WT 1 ± 0.15, KO 0.99 ± 0.11; ANXA5: WT 1 ± 0.05, KO 0.88 ± 0.08; NME1: WT 1 ± 0.08, KO 1 ± 0.10; CKB: WT 1 ± 0.09, KO 1.15 ± 0.1]

Table S1 TRIM3 interactors in hippocampus detected with at least 2 out of 3 antibodies and at least one unique peptide.

Gene symbol	Protein name	Antibody Count	Average # peptides
1700013D24Rik	MCG1037134	2	1.5
Aard	Alanine and arginine-rich domain-containing protein	2	1
Actg1	Uncharacterized protein	2	1
Acy3	Aspartoacylase-2	2	1
Agrn	Isoform 2 of Agrin	2	2
Akap8l	A-kinase anchor protein 8-like	2	1
Als2	Alsin	2	1
Amigo2	Amphoterin-induced protein 2	2	1
Ankzf1	Ankyrin repeat and zinc finger domain-containing protein 1	2	2
Antxr1	Isoform 2 of Anthrax toxin receptor 1	2	1.33
Atp4a	Potassium-transporting ATPase alpha chain 1	2	1.33
Blzf1	Isoform 2 of Golgin-45	2	1.33
Bnc1	Uncharacterized protein	2	1.67
Brca2	Breast cancer type 2 susceptibility protein homolog	2	3
Bsn	Isoform 2 of Protein bassoon	2	1
Cand1	Cullin-associated NEDD8-dissociated protein 1	2	1.33
Cbs	Isoform 2 of Cystathionine beta-synthase	2	1
Cdca7l	Cell division cycle-associated 7-like protein	2	1
Cdh23	Isoform 2 of Cadherin-23	2	1
Celsr2	Isoform 2 of Cadherin EGF LAG seven-pass G-type receptor 2	2	2.5
Copa	Coatomer subunit alpha	2	1
Ctnnal1	Alpha-catulin	2	1.33
D1Pas1	Putative ATP-dependent RNA helicase Pl10	2	2
Daam2	Disheveled-associated activator of morphogenesis 2	2	1
Dcaf13	DDB1- and CUL4-associated factor 13	2	1.5
Def6	Isoform 2 of Differentially expressed in FDCP 6	2	1
Eef1a2	Elongation factor 1-alpha 2	2	1
Elmo3	Isoform 2 of Engulfment and cell motility protein 3	3	1.33
Epg5	Ectopic P granules protein 5 homolog	2	1
Eppk1	Epiplakin	2	1
Erbb2ip	Isoform 1 of Protein LAP2	2	1.67
Exog	Nuclease EXOG_ mitochondrial	2	1.33
Fhdc1	FH2 domain-containing protein 1	2	2

Gene symbol	Protein name	Antibody Count	Average # peptides
Gadl1	Glutamate decarboxylase-like protein 1	2	1
Galntl4	Putative polypeptide N-acetylgalactosaminyltransferase-like protein 4	2	1
Gatad2a	Transcriptional repressor p66 alpha	2	1
Gm5771	MCG140783	2	1.5
Golga1	Isoform 2 of Golgin subfamily A member 1	2	1
Grn	Granulins	2	1
Hkdc1	Putative hexokinase HKDC1	2	1
Hmcn1	Uncharacterized protein	2	2
Igfn1	Immunoglobulin-like and fibronectin type III domain-containing protein 1	2	2.5
Ino80	Isoform 2 of DNA helicase INO80	2	1.33
Kalrn	Isoform 2 of Kalirin	2	3
Kiaa1009	Protein QN1 homolog	2	1.33
Kif6	Uncharacterized protein	2	1
Lilra6	Uncharacterized protein	2	1
Magi1	Membrane-associated guanylate kinase_ WW and PDZ domain-containing protein 1	2	2
Map2	Microtubule-associated protein 2	2	1
Map3k3	Mitogen-activated protein kinase kinase kinase 3	2	1
Mast1	Microtubule-associated serine/threonine-protein kinase 1	2	1.5
Mbd3	Uncharacterized protein	2	1
Mpdz	Isoform 2 of Multiple PDZ domain protein	2	1
Mup20	Major urinary protein 20	2	1
Myo5b	Isoform 3 of Unconventional myosin-Vb	2	1
Naalad2	N-acetylated-alpha-linked acidic dipeptidase 2	2	1.5
Nadsyn1	Glutamine-dependent NAD(+) synthetase	2	1.5
Narg2	NMDA receptor-regulated protein 2	2	1
Nfatc1	Isoform Beta of Nuclear factor of activated T-cells_ cytoplasmic 1	2	1.5
Nsun4	Isoform 4 of Sperm head and tail associated protein	2	1
Odz2	Teneurin-2	2	1.5
Pde4a	cAMP-specific 3'_5'-cyclic phosphodiesterase 4A	2	1
Polr3c	DNA-directed RNA polymerase III subunit RPC3	2	1
Pop1	Processing of 1_ ribonuclease P/MRP family_ (S. cerevisiae)	2	1
Ppp1r12b	Protein phosphatase 1 regulatory subunit 12B	2	1
Prkaa1	5'-AMP-activated protein kinase catalytic subunit alpha-1	2	1
Prkaa2	5'-AMP-activated protein kinase catalytic subunit alpha-2	2	1

Gene symbol	Protein name	Antibody Count	Average # peptides
Ptprd	Protein tyrosine phosphatase_ receptor type_ D	2	2.5
Rab10	Ras-related protein Rab-10	2	1
Rab33b	Ras-related protein Rab-33B	3	1.33
Rab39a	Ras-related protein Rab-39A	2	1
Rab39b	Ras-related protein Rab-39B	3	1.67
Rec8	Meiotic recombination protein REC8 homolog	2	1
Rictor	Rapamycin-insensitive companion of mTOR	2	1.5
Rif1	Isoform 2 of Telomere-associated protein RIF1	2	2.5
Rock2	Uncharacterized protein	2	2
Rplp0	60S acidic ribosomal protein P0	2	1
Safb	Scaffold attachment factor B1	2	1
Safb2	Scaffold attachment factor B2	2	1.67
Scube2	Signal peptide_ CUB and EGF-like domain-containing protein 2	2	1
Serbp1	Isoform 2 of Plasminogen activator inhibitor 1 RNA-binding protein	2	2
Sh2d3c	Isoform 2 of SH2 domain-containing protein 3C	2	1
Sh3d21	Isoform 2 of SH3 domain-containing protein 21	2	1
Skint6	Selection and upkeep of intraepithelial T-cells protein 6	2	2
Slc1a3	Excitatory amino acid transporter 1	2	1
Slc27a4	Long-chain fatty acid transport protein 4	2	1
Smtn	Isoform L2 of Smoothelin	3	1.33
Smurf1	E3 ubiquitin-protein ligase SMURF1	2	1
Snx2	Sorting nexin-2	2	1.5
Spnb4	Uncharacterized protein	2	2
Spta1	Spectrin alpha chain_ erythrocyte	2	2.5
St6galnac1	Alpha-N-acetylgalactosaminide alpha-2_6-sialyltransferase 1	2	1.5
St6galnac6	Isoform 2 of Alpha-N-acetylgalactosaminide alpha-2_6-sialyltransferase 6	3	1.33
Stard9	StAR-related lipid transfer protein 9	2	2
Sult1e1	Estrogen sulfotransferase_ testis isoform	2	1
Syne3	Isoform 2 of Nesprin-3	2	1
Synj2	Isoform 2 of Synaptojanin-2	2	1.5
Sytl2	Isoform 2 of Synaptotagmin-like protein 2	2	1
Tmem57	Macoilin	2	1
Tnrc18	Trinucleotide repeat-containing gene 18 protein	2	2.5
Trim2	Tripartite motif-containing protein 2	2	12
Ube1ay	Ubiquitin-like modifier-activating enzyme 1 Y	2	1

Gene symbol	Protein name	Antibody Count	Average # peptides
Ythdc2	Probable ATP-dependent RNA helicase YTHDC2	2	1.5
Zc3h13	Uncharacterized protein	2	2
Zfp937	Novel zinc fingerprotein	2	1
Znf879	Zinc finger protein 879	2	1
Znfx1	NFX1-type zinc finger-containing protein 1	2	1

Table S2 TRIM3 interactors in cerebellum detected with at least 2 out of 3 antibodies and at least one unique peptide.

Gene symbol	Protein name	Antibody Count	Average # peptides
1110002E22Rik	Uncharacterized protein	2	3
5430421N21Rik	Uncharacterized protein	2	4.33
A430107O13Rik	RIKEN cDNA A430107O13 gene	2	1
Abca9	ATP-binding cassette sub-family A member 9	2	1.5
Abcb4	Multidrug resistance protein 3	2	3
Adcy1	Adenylate cyclase type 1	2	1
Ahnak	Uncharacterized protein	2	4
Ahr	Aryl hydrocarbon receptor	2	1
AI481877	Likely orthologue of H. sapiens chromosome 9 open reading frame 84	2	2
Akap13	Uncharacterized protein	2	4.5
Akap9	Uncharacterized protein	2	2.5
Ank1	Isoform Br2 of Ankyrin-1	2	3.5
Ankrd12	Ankyrin repeat domain 12_ isoform CRA_a	2	2
Ankrd50	Ankyrin repeat domain 50 (Fragment)	3	3
Ano6	Anoctamin-6	2	2
Anxa1	Annexin A1	2	1
Ap2m1	AP-2 complex subunit mu	3	3
Arhgef10l	Isoform 4 of Rho guanine nucleotide exchange factor 10-like protein	2	1.5
Atp2b1	MCG13663_ isoform CRA_a	2	1.33
Atp4a	Potassium-transporting ATPase alpha chain 1	2	3.33
Atp5j2	ATP synthase subunit f_ mitochondrial	2	1.5
Atp7a	Copper-transporting ATPase 1	2	2.5
Baz2a	Isoform 2 of Bromodomain adjacent to zinc finger domain protein 2A	2	1

Gene symbol	Protein name	Antibody Count	Average # peptides
Brwd1	Isoform B of Bromodomain and WD repeat-containing protein 1	2	2
C030017K20Rik	RIKEN cDNA C030017K20 gene (Fragment)	2	1.5
C87977	Expressed sequence C87977 (Fragment)	2	1
Ccdc109b	Uncharacterized protein	2	1
Ccdc165	Isoform 3 of Coiled-coil domain-containing protein 165	2	3
Ccdc79	Isoform 2 of Coiled-coil domain-containing protein 79	2	1.5
Cd163l1	RIKEN cDNA E430002D04_ isoform CRA_a	2	2
Cdh23	Isoform 2 of Cadherin-23	3	2
Cenpe	Centromere-associated protein E	3	2.67
Cep112	Centrosomal protein of 112 kDa	2	3
Cep55	Isoform 2 of Centrosomal protein of 55 kDa	2	1
Cep95	Centrosomal protein of 95 kDa	2	1
Chchd7	Coiled-coil-helix-coiled-coil-helix domain-containing protein 7	2	2
Col22a1	Uncharacterized protein	2	3.5
Col4a3	Collagen alpha-3(IV) chain	2	2.5
Col6a3	Uncharacterized protein	2	3.5
Creb5	Cyclic AMP-responsive element-binding protein 5	2	1
Cul5	Uncharacterized protein	3	2.33
Cyth3	Cytohesin 3 (Fragment)	2	1
Ddah2	N(G)_N(G)-dimethylarginine dimethylaminohydrolase	2	1
Ddx50	ATP-dependent RNA helicase DDX50	2	1.5
Dgcr6	Isoform 2 of Protein DGCR6	2	1.33
Dido1	Death-inducer obliterator 1	2	2
Dnah5	Dynein heavy chain 5_ axonemal	2	2.5
Dnahc9	Dynein_ axonemal_ heavy chain 9	2	3.5
Dnmt1	DNA (cytosine-5)-methyltransferase 1	2	4
Dusp13	Uncharacterized protein	2	1.5
Dync1h1	Cytoplasmic dynein 1 heavy chain 1	2	6
Dync2h1	Isoform 2 of Cytoplasmic dynein 2 heavy chain 1	2	2.5
Eea1	Early endosome antigen 1	2	3
Eftud1	Elongation factor Tu GTP-binding domain-containing protein 1	2	3
Egln2	Egl nine homolog 2	2	1.33
Eif4g1	Isoform 2 of Eukaryotic translation initiation factor 4 gamma 1	2	1.5
Erlin2	Erlin-2	2	1.5

Gene symbol	Protein name	Antibody Count	Average # peptides
Fam184b	Protein FAM184B	2	2.5
Fastk	Uncharacterized protein	3	1.33
Gas8	Growth arrest-specific protein 8	2	1
Gigyf2	PERQ amino acid-rich with GYF domain-containing protein 2	2	2
Gm14548	Uncharacterized protein	2	2
Gm597	Uncharacterized protein	2	1
Gm8765	Predicted	2	2
Golga3	Isoform 1 of Golgin subfamily A member 3	2	1.5
Gpsm1	Isoform 2 of G-protein-signaling modulator 1	2	2.5
Gripap1	GRIP1-associated protein 1	2	1
Heatr1	HEAT repeat containing 1	2	2
Helb	Helicase (DNA) B	2	1.5
Hinfp	Histone H4 transcription factor	2	1
Hivep3	Uncharacterized protein	2	2.67
Hsf1	Isoform 1 of Heat shock factor protein 1	2	2
Hsp90ab1	Heat shock protein HSP 90-beta	2	1.5
Hspa2	Heat shock-related 70 kDa protein 2	3	1.67
Iars	Isoleucine--tRNA ligase_ cytoplasmic	2	1.5
Inpp5j	Phosphatidylinositol 4_5-bisphosphate 5-phosphatase	2	3
Kdm2b	Lysine-specific demethylase 2B	2	4.5
Kif18a	Kinesin-like protein KIF18A	2	1
Kif23	Uncharacterized protein	2	1
Kif26a	Kinesin-like protein KIF26A	3	2
Klhl28	Kelch-like protein 28	2	1.5
Lipe	Uncharacterized protein	2	2
Lman1	Protein ERGIC-53	2	1.5
Mag	Isoform S-MAG of Myelin-associated glycoprotein	2	2.67
Map7d3	Isoform 2 of MAP7 domain-containing protein 3	2	1
Mcf2l	Guanine nucleotide exchange factor DBS	2	3.5
Mmrn2	Multimerin-2	2	1
Mon2	Isoform 2 of Protein MON2 homolog	2	1.33
Mpnd	MPN domain-containing protein	2	2
Msh3	Uncharacterized protein	2	1.5
Msn	Moesin	2	2
Mtap4	Microtubule-associated protein (Fragment)	2	1

Gene symbol	Protein name	Antibody Count	Average # peptides
Myo18b	Uncharacterized protein	2	4
Narg2	NMDA receptor-regulated protein 2	2	1
Ncoa4	Nuclear receptor coactivator 4	2	1.5
Ndst1	Bifunctional heparan sulfate N-deacetylase/N-sulfotransferase 1	2	1.5
Nfasc	Neurofascin	2	2.5
Nfatc1	Nuclear factor of activated T-cells_ cytoplasmic 1	3	1.67
Nktr	NK-tumor recognition protein	2	1.5
Nlgn1	Isoform 2 of Neuroligin-1	2	1
Nox1	Isoform 2 of NADPH oxidase 1	2	2
Noxin	Nitric oxide-inducible gene protein	2	2.5
Npas1	Neuronal PAS domain-containing protein 1	2	1
Npcd	Neuronal pentraxin chromo domain	2	2.5
Nptn	Neuroplastin	2	2.67
Nudt6	Nudix (Nucleoside diphosphate linked moiety X)-type motif 6	2	1
Numa1	Uncharacterized protein	2	3.67
Obscn	Obscurin	2	1.5
Odf2	Outer dense fiber of sperm tails 2	2	1.5
Odz3	Isoform 2 of Teneurin-3	2	5.5
Olfr1213	Olfactory receptor 1213	2	1
Osbpl3	Oxysterol-binding protein-related protein 3	2	1
Pdap1	28 kDa heat- and acid-stable phosphoprotein	2	1
Pdss2	Decaprenyl-diphosphate synthase subunit 2	2	1.5
Pik3cg	Phosphatidylinositol-4_5-bisphosphate 3-kinase catalytic subunit gamma isoform	2	2
Plcb2	1-phosphatidylinositol-4_5-bisphosphate phosphodiesterase beta-2	2	1.5
Plcb4	Phospholipase C beta 4	2	1.5
Plch2	1-phosphatidylinositol-4_5-bisphosphate phosphodiesterase eta-2	2	3.5
Plekha7	Isoform 2 of Pleckstrin homology domain-containing family A member 7	2	3.5
Plekhg4	Uncharacterized protein	2	1
Polm	Polymerase (DNA directed)_ mu	3	1.67
Polr3b	DNA-directed RNA polymerase III subunit RPC2	2	1.5
Ppp1r13b	Apoptosis-stimulating of p53 protein 1	2	2.5
Prmt10	Putative protein arginine N-methyltransferase 10	2	1.5
Rab33b	Ras-related protein Rab-33B	2	2.33
Rab39a	Ras-related protein Rab-39A	2	1.5

Gene symbol	Protein name	Antibody Count	Average # peptides
Rad54l	DNA repair and recombination protein RAD54-like	2	1.5
Ranbp9	Isoform 2 of Ran-binding protein 9	2	1
Rasgrf1	Ras-specific guanine nucleotide-releasing factor 1	2	1.5
Rgs16	Regulator of G-protein signaling 16	2	1
Ric8a	Synembryn-A	2	1
Rif1	Isoform 2 of Telomere-associated protein RIF1	2	4
Ros1	Proto-oncogene tyrosine-protein kinase ROS	2	2.5
Rsbn1	Round spermatid basic protein 1	2	1
Rsph9	Radial spoke head protein 9 homolog	2	1.5
Safb2	Scaffold attachment factor B2	2	1
Scaper	Uncharacterized protein	2	2
Scin	Adseverin	2	3.5
Sdk2	Protein sidekick-2	2	3.5
Sec1	Galactoside 2-alpha-L-fucosyltransferase 3	2	1.5
Sec14l2	SEC14-like protein 2	2	1
Sema6a	Isoform 2 of Semaphorin-6A	2	1.5
Serpinf2	Alpha-2-antiplasmin	2	2
Shisa6	Protein shisa-6 homolog	2	1
Slc38a10	Isoform 2 of Putative sodium-coupled neutral amino acid transporter 10	2	3
Smu1	WD40 repeat-containing protein SMU1	2	2.33
Snap25	Synaptosomal-associated protein 25	2	1.33
Snrnp200	Activating signal cointegrator 1 complex subunit 3-like	2	3.67
Snx25	Uncharacterized protein	2	1
Sorbs1	Sorbin and SH3 domain-containing protein 1	2	3.5
Sp140	Sp140 nuclear body protein	2	3.5
Srgap1	SLIT-ROBO Rho GTPase-activating protein 1	2	1
St6galnac1	Alpha-N-acetylgalactosaminide alpha-2_6-sialyltransferase 1	2	2
Synj1	Synaptojanin-1	3	2.33
Taok2	Serine/threonine-protein kinase TAO2	2	2.5
Tarsl2	Probable threonine--tRNA ligase 2_ cytoplasmic	2	1
Tbc1d8b	TBC1 domain family member 8B	2	1.5
Tbc1d9	TBC1 domain family member 9	2	2
Tbx10	Isoform 2 of T-box transcription factor TBX10	2	1
Tfap2b	Transcription factor AP-2-beta	2	1.5
Tm6sf1	Transmembrane 6 superfamily member 1	2	1

Gene symbol	Protein name	Antibody Count	Average # peptides
Trim21	E3 ubiquitin-protein ligase TRIM21	3	2.33
Trpm1	Uncharacterized protein	2	1.5
U2af1l4	Splicing factor U2AF 26 kDa subunit	2	1
Ush2A	Isoform 3 of Usherin	3	1.67
Utp15	U3 small nucleolar RNA-associated protein 15 homolog	2	2.5
Vdac1	Isoform Mt-VDAC1 of Voltage-dependent anion-selective channel protein 1	2	1
Vim	Vimentin	2	1.5
Vti1b	Uncharacterized protein	2	1
Vwf	von Willebrand factor	2	1.5
Wdr35	Isoform 2 of WD repeat-containing protein 35	2	1
Wfs1	Wolframin	2	1.5
Wipi2	WD repeat domain phosphoinositide-interacting protein 2	2	1.5
Wwc2	Protein WWC2	2	2.33
Zfp292	Isoform 2 of Zinc finger protein 292	2	2
Zfp420	MCG144734_ isoform CRA_a	2	1.5
Zfp804b	Uncharacterized protein (Fragment)	2	2
Zfyve26	Zinc finger FYVE domain-containing protein 26	2	2
Znf354a	Zinc finger protein 354A	2	1
Znf827	Zinc finger protein 827	2	3
Zscan10	Isoform 2 of Zinc finger and SCAN domain-containing protein 10	2	2.5

CHAPTER 5

TRIM3 ubiquitylates gamma-actin in an activity-dependent manner

Joerg Schreiber, Marion J. M. Sassen, August B. Smit, and Ronald E. van Kesteren

Abstract

Stimulus-dependent structural and physiological synaptic plasticity require remodeling of the actin cytoskeleton. Two actin isoforms, β-actin and γ-actin, are expressed in neurons, yet their specific contribution to plasticity is unknown. We demonstrate that the E3 ubiquitin ligase TRIM3 co-localizes with, interacts with, and regulates γ-actin in hippocampal neurons. *Actg1* mRNA transcripts and TRIM3 protein are both present in messenger ribonucleoprotein granules responsible for the dendritic targeting of mRNAs. TRIM3 regulates γ-actin through poly-ubiquitylation, most likely co-translationally in dendritic spines. We furthermore demonstrate the importance of γ-actin in learning and memory by showing that hippocampus-specific *Actg1* knockout mice have enhanced fear memory. These findings show for the first time that γ-actin is involved in regulating neuronal plasticity mechanisms underlying memory formation, and identify TRIM3 as an important upstream regulator of γ-actin-dependent plasticity.

Introduction

Synaptic plasticity has been widely established as the underlying mechanism of learning and memory formation. Many studies have shown that protein synthesis is an essential mechanism regulating protein content of synapses and thereby affecting synaptic strength and learning (Fonseca et al., 2006a; Frey et al., 1988; Huang et al., 1996). Synaptic protein degradation mediated by the ubiquitin proteasome system, was already proposed as a plasticity mechanism in the 1980s (Lynch and Baudry, 1984), but has only recently come into focus. In 2006 Fonseca et al. (Fonseca et al., 2006b) demonstrated that long-term potentiation (LTP) is not solely dependent on protein synthesis, but also on protein degradation. They showed that blocking the proteasome leads to a similar decrease in LTP as blocking translation. Only when inhibiting protein synthesis and degradation at the same time, LTP was restored. This led the authors to conclude that a delicate balance in synaptic protein synthesis and degradation is essential for synaptic plasticity. Since then numerous studies have been published highlighting the importance of synaptic E3 ubiquitin ligases targeting specific synaptic proteins for degradation. One of the first to be identified was

ubiquitin ligase E3A (UBE3A), which was recently demonstrated to ubiquitylate Arc (activity-regulated cytoskeleton-associated protein) and thereby affect AMPA receptor internalization (Greer et al., 2010). AMPA receptor subunits themselves (Lin et al., 2011; Schwarz et al., 2010), as well as many other key components of synapses such as PSD-95, SHANK and NMDA receptors are also subject to ubiquitin-mediated degradation (Colledge et al., 2003; Ehlers, 2003; Kato et al., 2005).

In the previous chapters we demonstrated that TRIM3 is a synaptic E3 ubiquitin ligase, that when knocked out, causes enhanced LTP in the hippocampus, enhanced contextual fear memory consolidation and higher spine density in hippocampal pyramidal neurons. After demonstrating that GKAP and SHANK are not TRIM3 ubiquitylation substrates, as was recently proposed by Hung et al. (2010), we hypothesized that the electrophysiological, structural and behavioral phenotype in TRIM3 deficient mice is most likely caused by an as yet unidentified synaptic ubiquitylation substrate of TRIM3. Using a mass-spectrometry-based substrate identification assay we then identified gamma-actin (ACTG1), one of six known actin isoforms in mammals (Vandekerckhove and Weber, 1978), as the most likely ubiquitylation substrate of TRIM3. Two closely related TRIM3 paralogs, TRIM2 and TRIM32, also ubiquitylate cytoskeletal proteins (Balastik et al., 2008; Kudryashova et al., 2005) and TRIM3 itself contains an actin binding protein-like repeat (El-Husseini, 1999).

Cytoskeletal proteins such as actins are often viewed as stable and rigid cellular structures, yet in neurons, and especially in synapses and dendritic spines, the actin skeleton is highly dynamic (Hotulainen and Hoogenraad, 2010). Actin remodeling contributes to the structural changes observed during synaptic plasticity, i.e., spine growth and new synapse formation (Matsuzaki et al., 2004; Okamoto et al., 2004), and plays a key role in membrane insertion, clustering and internalization of postsynaptic receptors (Allison et al., 1998; Charrier et al., 2006), all of which are essential to the expression of physiological plasticity, i.e. long-term potentiation (LTP) or long-term depression (LTD) (Choquet and Triller, 2003; Malinow and Malenka, 2002; Shepherd and Huganir, 2007). Moreover, beta-actin is known to be locally translated, indicating that also tight control of local actin levels plays an important role in the expression of synaptic plasticity (Buxbaum et al., 2014; Leung et al., 2006).

In this chapter we aim to validate ACTG1 as an ubiquitylation substrate of TRIM3, and to establish regulation of ACTG1 by TRIM3 as a potential mechanisms underlying

synaptic plasticity. We first use a biochemical approach to demonstrate that TRIM3 and ACTG1 co-localize and interact in hippocampal synapses. We then show that TRIM3 poly-ubiquitylates ACTG1 in an activity dependent manner. Using an mRNP-precipitation-qPCR approach we furthermore demonstrate that *Actg1* mRNA is present in TRIM3-containing mRNP granules. We finally highlight the importance of ACTG1 in learning by showing that forebrain-specific *Actg1* knockout mice show enhanced memory in a contextual fear memory paradigm.

Material and Methods

Animals

The generation of *Trim3*$^{-/-}$ mice was described previously (Labonte et al., 2013). *Actg1*$^{lox/lox}$ mice (Perrin et al., 2010) (kind gift of Dr. James Ervasti) were crossed with *CamkIIa-Cre* mice (Mantamadiotis et al., 2002) in order to generate *Actg1*-cKO mice. All mice were maintained on a C57BL/6J background. In all experiments wildtype littermates were used as controls. Mice were individually housed on sawdust in standard Makrolon type II cages (26.5 cm long, 20.5 cm wide and 14.5 cm high) enriched with cardboard nesting material under 12/12 h dark/light cycle with access to water and food *ad libitum*. All animal experiments were approved by the animal ethics committee of the VU University Amsterdam, The Netherlands.

Cellular fractionation and synaptic protein isolation

Brain tissue was obtained from wildtype and *Trim3*$^{-/-}$ mice. Animals were sacrificed by cervical dislocation. Hippocampi were dissected and synaptic fractions isolated as previously described (Klemmer et al., 2009). Protein concentrations were measured using Bradford Protein-Assay (Bio-Rad Laboratories, USA) and equal amounts of protein were loaded on a 4 – 20 % gradient SDS-PAGE gel (Criterion TGX Stain-Free Gel, Bio-Rad Laboratories, USA). Total protein amounts were imaged after electrophoresis using Criterion Stain Free Imager (Bio-Rad Laboratories, USA). Gels were then transferred to PVDF membranes (Bio-Rad Immuno-Blot PVDF membrane, Bio-Rad Laboratories, USA) and blots were blocked by immersion in 5 % nonfat dry milk in TBS-T (TBS plus 0.025 % Tween, pH 7.4) for 1 h. Blots were then incubated with the antibody of interest for 1 h at room temperature, followed

by 1 h incubation with a secondary antibody conjugated to HRP. Proteins were visualized by enhanced chemiluminescence (ECL) (SuperSignal West Femto Chemiluminescent Substrate, Thermo Scientific, USA) and scanned using the Odyssey Fc imager (Li-Cor, USA). Antibodies used: ACTG1 (clone 2A3, ab123034, Abcam, 1:10,000), TRIM3 (CLRPGDLPPSPDDVK, GenScript, 1:1,000), SYP (sc-9116, Santa Cruz, 1:2,000), PSD-95 (73-028, Neuromab, 1:10).

Cell culture and Immunoprecipitation

Human embryonic kidney cells (HEK293) were maintained in Dulbecco's modified Eagle medium supplemented with 10 % fetal bovine serum and 1 % Penicillin-Streptomycin (all from Life Technologies Thermo Fisher Scientific Inc., USA) at 37° C and 5 % CO_2. Cells were co-transfected with GFP-TRIM3, GFP-ΔRBCC-TRIM3 or mock transfected at 60 – 80 % confluence using polyethylenimine (PEI). For initial screening cells were sampled starting 12h after transfection at three hour intervals for 12 h. Cells were washed with ice cold PBS and subsequently lysed in SDS containing loading buffer. For quantitative analysis cells were lysed 48 h after transfection. Samples were then separated on a 4 - 20% gradient SDS-PAGE gel (Criterion TGX Stain-Free Gel, Bio-Rad Laboratories, USA), total protein amounts imaged using Criterion Stain Free Imager (Bio-Rad Laboratories, USA) and then transferred to PVDF membranes (Bio-Rad Immuno-Blot PVDF membrane, Bio-Rad Laboratories, USA). Blots were blocked by immersing the membrane in 5 % nonfat dry milk in TBS-T (TBS plus 0.025 % Tween, pH 7.4) for 1 h, washed and incubated with antibodies for ACTG1 (clone 2A3, ab123034, Abcam, 1:10,000) and ACTB (A5441, Sigma-Aldrich, 1:10,000) for 1 h at room temperature, followed by a 1 h incubation with a secondary antibody conjugated to HRP. Proteins were visualized by ECL (SuperSignal West Femto Chemiluminescent Substrate, Thermo Scientific, USA) and scanned using the Odyssey Fc imager (Li-Cor, USA) for Western blot analysis. Protein quantities were calculated by dividing the background corrected signal intensity of each Western blot protein band (ImageStudio Software v. 2.0.38, Li-Cor, USA) by the background corrected signal intensity of the corresponding stain-free gel protein lane (Image Lab 3.0, Bio-Rad, USA). Significance was testes using a two-tailed t test. Values are presented as mean ± SEM expressed relative to wildtype samples.

For immunoprecipitation HEK293 cells were co-transfected with GFP-TRIM3 or mock transfected at 60 - 80% confluence. 48 h after transfection cells were washed with ice cold PBS (see above) and subsequently lysed in extraction buffer (1 % Triton X-100, 150 mM NaCl, 25 mM HEPES pH 7.4) supplemented with protease inhibitors (Complete Protease Inhibitor Cocktail, Roche Diagnostics) for 1 h at 4° C on a rotator. Insoluble material was pelleted at 20,000 g for 20 min and the supernatant used for immunoprecipitations (IPs). Antibodies used for IPs were: ACTG1 (clone 2-4, sc65634, Santa Cruz) and TRIM3 (CLRPGDLPPSPDDVK, GenScript). IPs and input were separated on a 4 – 20 % gradient SDS-PAGE gel (Criterion TGX Stain-Free Gel, Bio-Rad Laboratories) and immunoblotted as described earlier using antibodies for ACTG1 (clone 2-4, sc65634, Santa Cruz) and TRIM3 (CLRPGDLPPSPDDVK, GenScript).

Ubiquitylation assay in HEK293 cells

HEK293 cells were transfected with myc-TRIM3, myc-ΔRBCC-TRIM3 or mock transfected at 60 - 80% confluence using polyethylenimine (PEI). 48 h after transfection cells were either washed with ice cold PBS and subsequently lysed in extraction buffer (2 % SDS, 150 mM NaCl, 2 mM DTT, 25 mM HEPES pH 7.4) supplemented with protease inhibitors (Complete Protease Inhibitor Cocktail, Roche Diagnostics) or first treated with 20 µM MG132 (Tocris Bioscience, 1748) and 500 nM TPA (12-O-Tetradecanoylphorbol-13-acetate, Sigma-Aldrich, P1585) for four hours and then lysed. Samples were then sonicated, boiled for 10 min and again sonicated. Extracts were diluted to a SDS concentration of 0.1 % with Triton X-100 containing extraction buffer (1 % Triton X-100, 150 mM NaCl, 25 mM HEPES pH 7.4). Insoluble material was pelleted at 20,000 g for 20 min and the supernatant used for immunoprecipitations (IPs). 25 µg of ACTG1 antibody (clone 2A3, ab123034, Abcam) were added to each sample and incubated overnight on a rotator at 4° C. Next day 50 µl of protein A / G beads (Protein A/G Plus-Agarose, Santa Cruz Biotechnology Inc.) were washed three times in washing buffer (0.1% Triton X-100, 150 mM NaCl, 25 mM HEPES pH 7.4) and added to each IP sample. Beads were incubated for 120 min on a rotator at 4° C, then pelleted at 2,500 g and washed four times in ice-cold extraction buffer (1 % Triton X-100, 150 mM NaCl, 25 mM HEPES pH 7.4). ACTG1 was eluted off the beads by adding SDS containing loading buffer and heating to 55° C for 10 min. IPs and input were separated on a 4 – 20 %

gradient SDS-PAGE and immunoblotted. Blots were blocked in 0.5 % BSA in TBS-T (TBS plus 0.025 % Tween) for 1h. Blots were then incubated with antibodies for Ubiquitin (FK2, BML-PW8810, Enzo Life Sciences, 1:100) and ACTG1 (clone 2-4, sc65634, Santa Cruz, 1:200) for 1 h at room temperature, followed by a 1 h incubation with a secondary antibody conjugated to HRP. Proteins were visualized by ECL (SuperSignal West Femto Chemiluminescent Substrate, Thermo Scientific, USA) and scanned using the Odyssey Fc imager (Li-Cor, USA). ACTG1 protein bands at 42 kDa blots were scanned for two minutes, ACTG1 bands of higher molecular weight for 10 - 20 min. Ubiquitylation was quantified by dividing the background corrected ubiquitin signal intensity (50 - 150 kDa) by the background corrected ACTG1 signal intensity (42 kDa) of the corresponding lane (ImageStudio Software v. 2.0.38, Li-Cor, USA). Experiments were performed in three independent replicates. Significance was tested using a two-tailed t-test.

Hippocampal primary neuron culture

Hippocampi were dissected from E18 wildtype and *Trim3*$^{-/-}$ mice and collected in Hanks balanced salts solution (HBSS; Sigma-Aldrich, USA), buffered with 7 mM HEPES (Invitrogen). Hippocampi were incubated for 30 min in trypsinated HBBS at 37° C. After washing, neurons were triturated with fire-polished Pasteur pipettes, counted and plated in Neurobasal medium (Invitrogen, USA) supplemented with 2 % B-27 (Invitrogen), 1.8 % HEPES, 1 % glutamax (Invitrogen, USA), 1 % Pen Strep (Invitrogen) and 0.2 % 14.3 mM β-mercapto-ethanol. Cultures were plated on poly-D-lysine (Sigma-Aldrich)-coated and 5 % heat-inactivated horse serum (Invitrogen)-treated glass coverslips. Neurons were plated at a seeding density of 250 cells/mm^2. Half of the medium was replaced with fresh medium every week. After 14 days in culture, neurons were either lysed in SDS-containing loading buffer directly or first treated with 20 µM MG132 and 500 nM TPA for 4 h and then lysed. Samples were separated on SDS-PAGE and immunoblotted for ACTG1 (clone 2-4, sc65634, Santa Cruz, 1:1,000), TRIM3 (CLRPGDLPPSPDDVK, GenScript, 1:1,000), ACTB (A5441, Sigma-Aldrich, 1:10,000) and TUBB3 (T8660, Sigma-Aldrich, 1:2,000). Protein quantities were calculated by dividing the background corrected signal intensity of each Western blot protein band (ImageStudio Software v. 2.0.38, Li-Cor, USA) by the background corrected signal intensity of the corresponding stain-free gel protein lane (Image Lab 3.0, Bio-Rad, USA). Significance was tested using a two-tailed t-test.

Co-Immunoprecipitation of TRIM3 from Hippocampus

For immunoprecipitation (IP) experiments 10 mg of hippocampal P2 + M from wildtype and *Trim3*$^{-/-}$ mice were extracted in equal volumes of Triton X-100-containing extraction buffer (2 % Triton X-100, 150 mM NaCl, 25 mM HEPES pH 7.4, protease inhibitors (Complete Protease Inhibitor Cocktail, Roche Diagnostics) for 1 h on a rotator at 4° C. Insoluble material was then pelleted at 20,000 g for 20 min at 4° C. The pellet was then re-extracted in 1 % Triton X-100 extraction buffer (1% Triton X-100, 150 mM NaCl, 25 mM HEPES pH 7.4, protease inhibitors) for one hour. Insoluble material was again pelleted at 20,000 g for 20 min. Supernatants from the first and second extraction were then pooled, centrifuged at 20,000 g for 20 min and the final supernatant served as input for the immunoprecipitation. Input was treated with RNase A (R4642, Sigma-Aldrich). After 24 h 10 µg of Trim3 antibody (epitope: QAPEGAHDPEDPHPC, GenScript) or ACTG1 antibody (clone 2-4, sc65634, Santa Cruz) were added to each sample and incubated overnight on a rotator at 4° C. Next day 30 µl of protein A/G beads (Protein A/G Plus-Agarose, Santa Cruz Biotechnology Inc.) were washed three times in washing buffer (0.1 % Triton X-100, 150 mM NaCl, 25 mM HEPES pH 7.4) and added to each IP sample. Beads were incubated for 120 min on a rotator at 4° C, then pelleted at 2,500 g and washed four times in ice-cold washing buffer. TRIM3 and interacting proteins were eluted off the beads by adding SDS-containing loading buffer and boiling for 5 min. Samples were run on SDS-PAGE and immunoblotted for TRIM3 (epitope: QAPEGAHDPEDPHPC, GenScript, 1:1,000) and ACTG1 (clone 2-4, sc65634, Santa Cruz, 1:10,000).

RNA Immunoprecipitation

Immunoprecipitations were performed in triplicate from wildtype and *Trim3*$^{-/-}$ mice hippocampi as described above. All IP buffers contained 40 units RiboLock RNase inhibitor (R4642, Sigma-Aldrich) per milliliter. Antibodies used for IPs were TRIM3 (epitope: QAPEGAHDPEDPHPC, GenScript) and PURA (05-1361, Millipore). After immunoprecipitation RNA was isolated using Trizol (Thermo Fisher Scientific) following manufacturer's instructions, DNase-treated and reverse transcribed to cDNA using random hexanucleotide primers. Gene expression levels of *Actg1*, *Actb* and *Slc1a3* were analyzed using an ABI Prism® SDS 7900 (Applied Biosystems) system with SYBR Green as the reporter dye. Per 10 µl reaction a cDNA equivalent of 20 ng RNA was used with 300 nM

gene specific primers (*Actg1* Fw 5' A C C A A C A G C A G A C T T C C A G G A T 3', *Actg1* Rev 5' A G A C T G G C A A G A A G G A G T G G T A A 3'; *Actb* Fw 5' A A G A T C A A G A T C A T T G C T C C T C C T G 3', *Actb* Rev 5' A G C T C A G T A A C A G T C C G C C T 3'; *Slc1a3* Fw 5' G T G G A C T G G T T T C T G G A C C G 3', *Slc1a3* Rev 5' T C A T G T C G G G A C A A G T G C T C 3'). Levels of mRNA were compared using the $\Delta\Delta^{-Ct}$ method (Winer et al., 1999). Expression levels were normalized to the mean of *Actb*.

Fear conditioning

Fear conditioning experiments were carried out as described (Misane et al., 2005; Stiedl et al., 2000) using a computerized fear conditioning system (TSE, 303410, Bad Homburg, Germany). In brief, mice were placed in an acrylic cage mounted into a constant illuminated (450 lx) fear conditioning box. After a 180 s exploration period, mice received a 2 s foot shock (0.7 mA) delivered through a metal floor grid. Mice were returned to their home cages 30 s after termination of the shock. Base-line behavior, activity, exploration and freezing were automatically measured by infrared laser beams before, during and after foot shock. Contextual fear memory was tested by measuring freezing (lack of movement aside from respiration and heart beat) at re-exposure of the animals to the conditioning box at and 24 h and 72 h after the foot shock.

Results

TRIM3 interacts and co-localizes with ACTG1

In our assay to identify potential substrates of TRIM3 we found gamma-actin to be a strong interactor that is also specifically ubiquitylated in wildtype mice, but not in *Trim3*$^{-/-}$ mice. To establish whether ACTG1 levels are regulated by TRIM3 we first validated whether the two proteins physically interact. Expression of TRIM3 in HEK293 cells and immunoprecipitation of either TRIM3 or endogenously expressed ACTG1, resulted in co-immunoprecipitation of ACTG1 and TRIM3, respectively, only from TRIM3-expressing cells, but not from mock-transfected cells (Figure 1A). Similarly, immunoprecipitation of TRIM3 from wildtype hippocampal synapse-enriched fractions, but not from *Trim3*$^{-/-}$ fractions, yielded ACTG1 and

vice versa (Figure 1B). Cellular fractionation of hippocampal tissue followed by immunoblotting for TRIM3, ACTG1 and markers for pre- and postsynaptic structures subsequently showed that TRIM3 and ACTG1 co-localize in all fractions, including postsynaptic fractions (Figure 1C). Thus, TRIM3 and ACTG1 physically interact in heterologous cells and in hippocampal synaptic protein fractions, and co-localize at synaptic sites.

TRIM3 regulates ACTG1 levels

We then asked whether TRIM3 also regulates ACTG1 protein levels. We first transfected HEK293 cells with TRIM3, ΔRBCC-TRIM3 or mock transfected them. When we sampled cells, we observed that ACTG1 protein amounts decreased with time in cells expressing TRIM3, whereas they increased in mock transfected or ΔRBCC-TRIM3 expressing cells (Figure 1D), indicating that TRIM3 may negatively regulate ACTG1 levels in HEK293 cells.

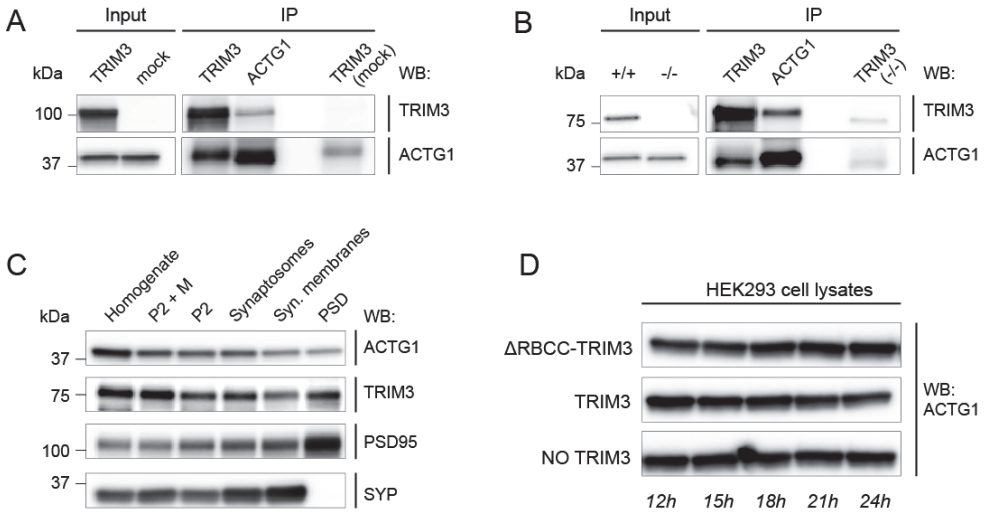

Figure 1 TRIM3 interacts and co-localizes with ACTG1 and decreases ACTG1 levels in HEK293 cells. (A) HEK293 cells were transfected with TRIM3 or mock transfected. Cells were lysed 48h after transfection. TRIM3 and ACTG1 were immunoprecipitated (IP) from the lysates, immunoblotted and stained for TRIM3 and ACTG1. TRIM3 can be observed in the ACTG1 IP, and ACTG1 in the TRIM3 IP. No or significantly less TRIM3 or ACTG1 protein was detected in TRIM3 IPs from mock-transfected cell lysate. **(B)** Hippocampal synapse-enriched fractions were prepared from wildtype and *Trim3*$^{-/-}$ mice. TRIM3 and ACTG1 were immunoprecipitated from the lysates, immunoblotted and stained for TRIM3 and ACTG1. TRIM3 can be observed in the ACTG1 IP, and ACTG1 in the TRIM3 IP. No or significantly less TRIM3 or ACTG1 protein was detected in the TRIM3 IP on the *Trim3*$^{-/-}$ tissue sample. **(C)** Biochemical fractionation of hippocampal tissue followed by Western blot analysis showed that ACTG1 and TRIM3 are both detected in synaptic fractions. Enrichment of synapses is evidenced by PSD95 and SYP staining. **(D)** TRIM3 regulates ACTG1 levels in HEK293 cells. HEK293 cells were transfected with TRIM3, ΔRBCC-TRIM3 or mock-transfected (NO TRIM3). After 12 h cells were lysed at three hour intervals for a time period of 12 h. Lysates were immunoblotted and stained for ACTG1. A decrease with time of ACTG1 could be observed in TRIM3 expressing cells, but not in cells expressing ΔRBCC-TRIM3 or mock-transfected cells.

In order to quantify the effect of TRIM3 on ACTG1 levels in HEK293 cells, we overexpressed TRIM3 and ΔRBCC-TRIM3 for 48 h and analyzed ACTG1 amounts in the lysates. Cells expressing TRIM3 showed a significant decrease of ACTG1 protein levels compared with ΔRBCC-TRIM3-expressing cells (ΔRBCC-TRIM3 1 ± 0.12, TRIM3 0.58 ± 0.05, n = 8, $^{**}p < 0.01$) (Figure 2A). We did however also observe a significant reduction in beta-actin (ACTB) levels (ΔRBCC-TRIM3 1 ± 0.08, TRIM3 0.67 ± 0.05, n = 8, $^{**}p < 0.01$) (Figure 2B), indicating that at least in HEK293 cells TRIM3 does not exclusively target ACTG1. In cultured hippocampal primary neurons a specific increase of ACTG1 levels was only observed in cells obtained from *Trim3*$^{-/-}$ mice compared with cells obtained from wildtype mice (TRIM3 1 ± 0.07, *Trim3*$^{-/-}$ 1.26 ± 0.10, n = 8, $^{*}p < 0.05$) (Figure 2C). ACTB levels (TRIM3 1 ± 0.16, *Trim3*$^{-/-}$ 1.06 ± 0.10), and tubulin beta-3 (TUBB3) (TRIM3 1 ± 0.21, *Trim3*$^{-/-}$ 0.85 ± 0.06) levels were not affected (Figure 2D - E). Taken together, these data show that ACTG1 protein levels are downregulated in the presence of TRIM3.

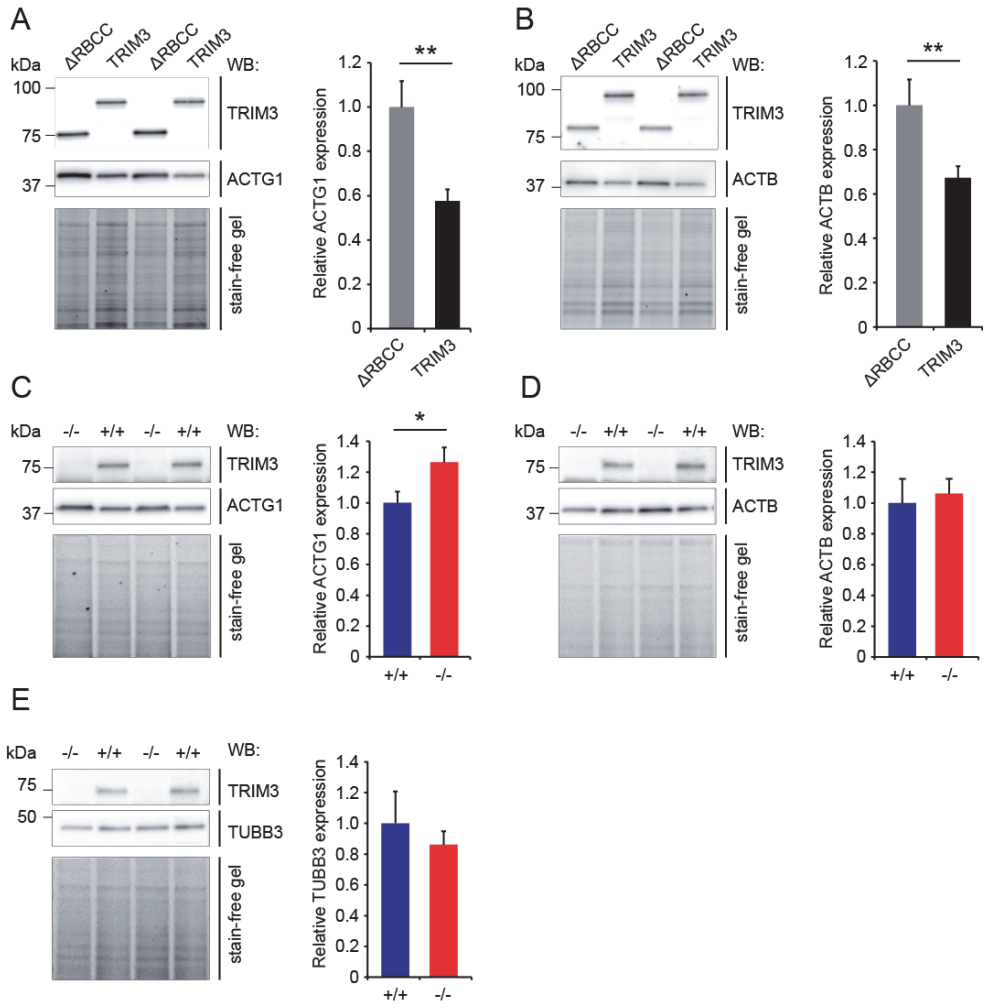

Figure 2 TRIM3 regulates gamma-actin. (A - B) HEK293 cells were transfected with TRIM3 or ΔRBCC-TRIM3. Cells were lysed 48 h after transfection, lysates immunoblotted and stained for TRIM3 and ACTG1 **(A)**, or TRIM3 and ACTB **(B)**. Both ACTG1 and ACTB protein levels were significantly reduced in TRIM3 expressing cells compared to cells expressing ΔRBCC-TRIM3 (means ± SEM, two-tailed t test, $^{**}p < 0.01$, n = 8 per condition). **(C - E)** Hippocampal neurons from wildtype and *Trim3*$^{-/-}$ mice were cultured *in vitro*. Cells were lysed after 14 days, lysates immunoblotted and stained for TRIM3 and ACTG1 **(C)**, TRIM3 and ACTB **(D)**, or TRIM3 and TUBB3 **(E)**. Normalized protein levels were calculated by dividing Western blot (WB) signal intensities by the total protein intensities (stain-free gel). ACTG1, but not ACTB or TUBB3, protein levels were significantly higher in neurons from *Trim3*$^{-/-}$ mice (means ± SEM, two-tailed t test, $^{*}p < 0.05$, n = 8 per genotype).

TRIM3 poly-ubiquitylates ACTG1

We then asked whether TRIM3 is indeed able to poly-ubiquitylate ACTG1. We expressed full length TRIM3 or ΔRBCC-TRIM3 in HEK293 cells for two days. Then proteasomal degradation was blocked by adding the proteasome inhibitor MG132 for four hours, cell lysates were harvested and ACTG1 was immunoprecipitated. The immunoprecipitates were subsequently immunoblotted for ubiquitin and for ACTG1. Unmodified ACTG1 was detected at the expected molecular weight of 42 kDa, but surprisingly we did not detect any increase in high-molecular weight ubiquitin staining (Figure 3A) or high-molecular weight ACTG1 species (Figure 3B) due to TRIM3 expression. Given that TRIM3 is part of mRNP particles and that many proteins in mRNP particles are involved in local translation (Kanai et al., 2004; Torvund-Jensen et al., 2014) we hypothesized that TRIM3 may exert its function during or shortly after translation. To test this hypothesis we repeated the overexpression experiments, but instead of only blocking the proteasome, we also stimulated the cells with tetradecanoylphorbol acetate (TPA) for a period of four hours prior to harvesting. Tetradecanoylphorbol acetate is a phorbol ester known to promote cell growth and protein synthesis that can be tolerated by cells for prolonged period of time (Herbert et al., 2000; Kazanietz et al., 2000). It acts by activating protein kinase C, the mTOR pathway and others (Carriere et al., 2011; Herbert et al., 2000; Kazanietz, 2000; Kazanietz et al., 2000). When we stimulated cells with TPA while blocking the proteasome, a strong increase in high-molecular weight ubiquitin staining following ACTG1 immunoprecipitation (Figure 3C) was observed, and ACTG1 staining confirmed the presence of 50 – 100 kDa modified ACTG1 species (Figure 3D) specifically in TRIM3 expressing cells, and not in ΔRBCC-TRIM3 or mock-transfected cells (mock 1 ± 0.14, ΔRBCC-TRIM3 0.91 ± 0.13, TRIM3 4.75 ± 0.77, $n = 3$, * $p < 0.05$) (Figure 3E). We observed a similar increase in 50 - 100 kDa modified ACTG1 species in cultured hippocampal neurons treated with TPA and MG132 for 4 h, specifically for wildtype neurons, and not in *Trim3*$^{-/-}$ neurons (Figure 3F). The discrete banding pattern of these high-molecular weight ACTG1 species is consistent with ubiquitin modifications consisting of one or more ubiquitin moieties.

TRIM3 protein and *Actg1* mRNA co-localize in mRNP particles

It was previously reported that poly-ubiquitylation of ACTG1 occurs co-translationally at Lys-18, which is buried in the protein core and inaccessible once the protein is fully

synthesized (Zhang et al., 2010). In that respect it is interesting to note that TRIM3 is found in mRNP particles (Chapter 3) as these might co-deliver TRIM3 and *Actg1* mRNA to synaptic sites, allowing TRIM3 to poly-ubiquitylate ACTG1 during local translation. In contrast to *Actb* mRNA however, *Actg1* mRNA was not previously reported to be present in mRNP particles. To test whether *Actg1* mRNA is available for local translation, we immunoprecipitated mRNP particles from hippocampal synapse-enriched fractions using antibodies against TRIM3 or PURA and quantified the levels of different mRNAs using quantitative real-time PCR. We found that *Actg1* and *Actb* mRNAs were both present in all immunoprecipitates and at similar levels, whereas a negative control transcript (*Slc1a3*) was detected at ~10 times lower levels (Figure 3G). The same results were obtained when mRNP particles were immunoprecipitated from *Trim3*$^{-/-}$ protein fractions using the PURA antibody, suggesting that TRIM3 itself is not required for the incorporation of *Actg1* mRNA into mRNP particles.

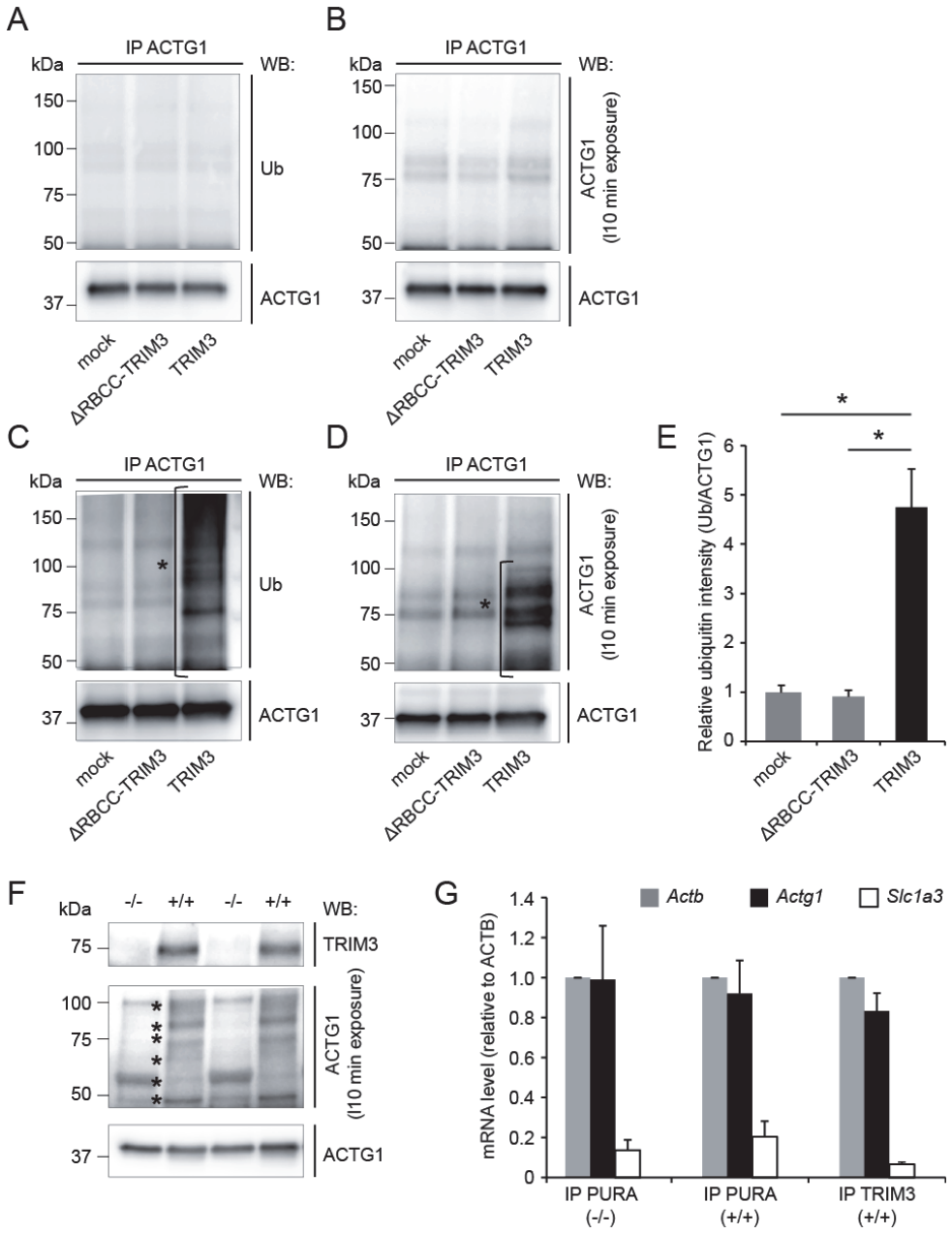

Figure 3 TRIM3 poly-ubiquitylates ACTG1. (A - B) HEK293 cells were transfected with TRIM3 or ΔRBCC-TRIM3. After 44 hours cells were incubated for four hours in the presence of MG132. Cells were then lysed and ACTG1 was immunoprecipitated from the lysates, resolved on SDS-PAGE and Western blotted. Blots were first stained for poly-ubiquitin **(A)**, and then stripped and re-stained for

ACTG1 **(B)**. Under basal conditions, only unmodified ACTG1 was detected, but no higher molecular weight poly-ubiquitylated forms of ACTG1. **(C-E)** HEK293 cells were transfected with TRIM3 or ΔRBCC-TRIM3. After 44 hours cells were incubated for four hours in the presence of MG132 and TPA. Cells were then lysed and ACTG1 was immunoprecipitated from the lysates, resolved on SDS-PAGE and Western blotted. Blots were first stained for poly-ubiquitin **(C)**, stripped and re-stained for ACTG1 **(D)**. TPA induced a significant increase in high-molecular weight poly-ubiquitylated forms of ACTG1 (indicated with *) specifically in TRIM3 transfected cells, and not in ΔRBCC-TRIM3 or mock transfected cells **(E)** (means ± SEM, two-tailed t test, $*p < 0.05$, n = 3 per condition). **(F)** Hippocampal neurons from wildtype and *Trim3*$^{-/-}$ mice were cultured for 14 days *in vitro*. Cells were then treated MG132 and TPA for 4h and lysed. Lysates were Western blotted and stained for ACTG1. TPA induced the appearance of multiple high-molecular weight (50 - 100 kDa) bands (indicated with *) consistent with poly-ubiquitylation and specifically in neurons from wildtype mice and not from *Trim3*$^{-/-}$ mice. **(G)** *Actg1* mRNA is present in TRIM3/PURA-containing mRNP granules. mRNP granules were immunoprecipitated with antibodies against TRIM3 or PURA from hippocampal lysates of wildtype and *Trim3*$^{-/-}$ mice. mRNA was isolated from immunoprecipitates, reverse-transcribed into cDNA and used for real-time qPCR. *Actg1* and *Actb* mRNA were detected at equal levels in all precipitates, whereas the negative control mRNA *Slc1a3* was ~10-fold lower detected.

Conditional *Actg1* knockout mice show enhanced fear memory

We finally wanted to establish whether and how a change in gamma-actin levels in neurons can affect hippocampus-dependent learning and memory. We therefore generated a forebrain specific *ACTG1* knockout mouse by crossing Actg1$^{lox/lox}$ mice (Perrin et al., 2010) with mice that express Cre-recombinase under the control of the CamKIIα (calcium/calmodulin-dependent protein kinase II alpha) promotor, which is activated in most forebrain neurons from the first postnatal week on (Mantamadiotis et al., 2002; Tsien et al., 1996). All conditional knockout animals were live born at expected Mendelian ratios and were indistinguishable from heterozygous and wildtype littermates. We used western blotting to (i) validate brain region specificity of our gamma-actin knockout mice and (ii) test the specificity of the used gamma-actin antibodies. While the specificity of ACTG1 antibody clone 2-4 was demonstrated earlier using muscle specific *ACTG1* knockout mice (Hanft et al., 2006), clone 2A3 has not been tested on knockout tissue. Both antibodies showed a significant reduction of gamma-actin in hippocampus, frontal cortex and olfactory bulb (ACTG1 clone 2A3: 32 ± 0.04 %, ACTG1 clone 2 - 4: 0.12 ± 0.04 %, $**p < 0.01$), at ratios expected for a conditional knockout targeting excitatory neurons (Figure 4A - B). Hindbrain (cerebellum, brain stem) SDS extracts showed normal gamma-actin levels for wildtype and knockout animals (Figure 4). Interestingly, we also observed a significant compensatory up-

regulation of beta-actin in the forebrain of gamma-actin deficient animals, which is in accordance with previously published literature (Belyantseva et al., 2009). TRIM3 on the other hand is not affected by loss of ACTG1 and is equally expressed in all tested brain regions regardless of the genotype (Figure 4). To assess hippocampus dependent memory performance, we tested *Actg1-cKO* mice and wildtype littermates in a contextual fear conditioning paradigm. We found that *Actg1-cKO* froze significantly more when re-exposed to the initial context 24 h after conditioning (WT: 35.7 ± 10.3 %, *Actg1-cKO*: 61.2 ± 2.9 %, $*p < 0.05$). When we re-exposed the same animals again to the context after 72 h, *Actg1-cKO* mice still froze significantly more (WT: 31.1 ± 9.0 %, *Actg1-cKO*: 60.1 ± 7.3%, $*p < 0.05$). Altogether, these data show that: (i) TRIM3 co-localizes and interacts with ACTG1 in hippocampal neurons, (ii) TRIM3 can poly-ubiquitylate ACTG1 at synaptic sites in an activity dependent manner, and (iii) ACTG1 is a crucial factor in hippocampus dependent learning and memory.

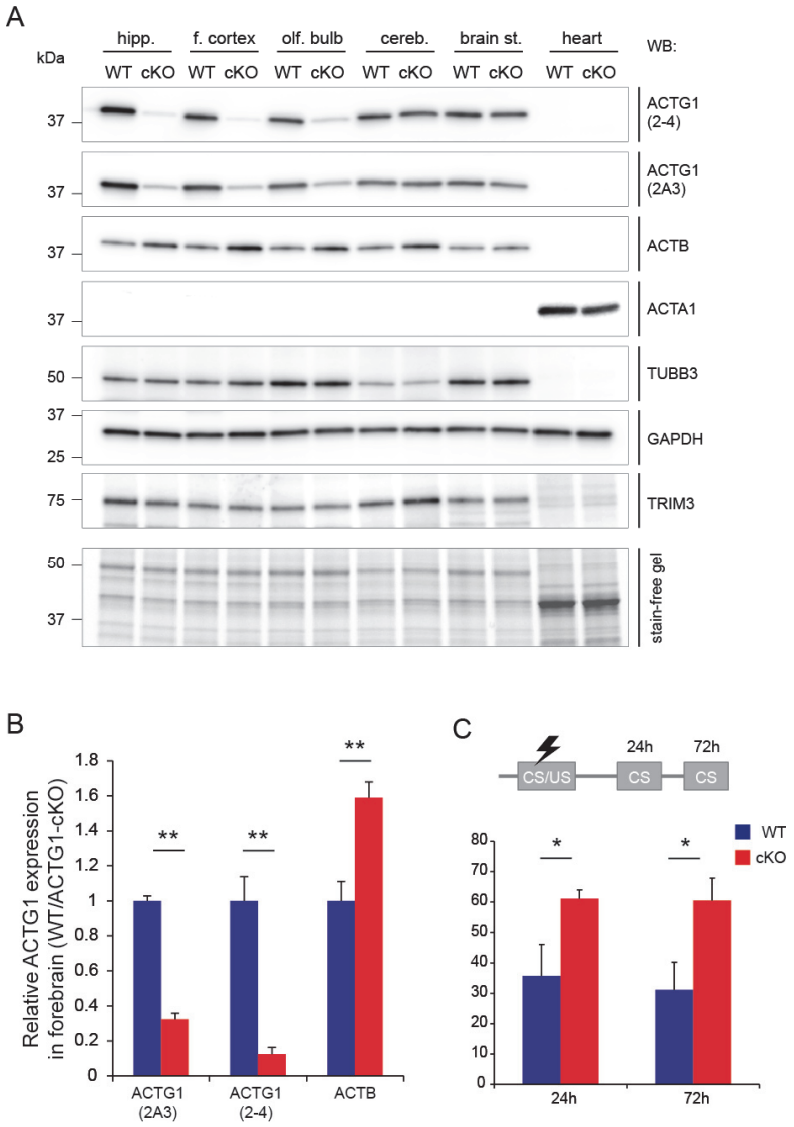

Figure 4 Forebrain-specific *Actg1* knockout mice show enhanced contextual fear memory. **(A - B)** Forebrain specific *ACTG1* knockout mice under the control of the CamKIIα promotor show a distinct and significant reduction of ACTG1 protein in hippocampus, frontal cortex and olfactory bulb **(B)**, but not in cerebellum and brain stem. Loss of ACTG1 protein is compensated by ACTB and not by ACTA1 up-regulation in the forebrain. TRIM3, TUBB3 and GAPDH are unaffected by loss of ACTG1 (means ± SEM, two-tailed t test, *$p < 0.01$, n = 3) **(C)** *Actg1-cKO* mice show significantly enhanced freezing 24 h after fear conditioning and still freeze more when re-exposed to the conditioning context after 72 h (means ± SEM, two-tailed t test, 24h *$p < 0.05$, n = 11; 72 h *$p < 0.05$, n = 6/5).

Discussion

In this chapter we demonstrated that TRIM3 and ACTG1 co-localize and interact in hippocampal synapses. TRIM3 is able to regulate ACTG1 amounts by poly-ubiquitylation and subsequent proteasomal degradation in a stimulus-dependent manner. We further showed that *Actg1* mRNA is present in PURA / TRIM3 containing mRNP granules, allowing the possibility that TRIM3 ubiquitylates ACTG1 co-translationally. We finally demonstrated the importance of ACTG1 in learning by showing that a forebrain-specific *Actg1* knockout mouse shows enhanced memory in a contextual fear memory paradigm.

TRIM3 interacts with ACTG1

Consistent with the finding from our substrate identification assay (Chapter 4) we were able validate ACTG1 as a TRIM3 interactor. By using immunoprecipitations of TRIM3 and ACTG1 we were able to show that TRIM3 interacts with ACTG1 and vice versa. We had earlier demonstrated that TRIM3 also interacts with PURA, but that this interaction is mediated by RNA, or by being part of the same mRNA transport granule (Chapter 3). To address the question of whether the interaction between ACTG1 and TRIM3 is direct, we treated synapse-enriched hippocampal fractions with RNase prior to immunoprecipitation. The interaction of ACTG1 and TRIM3 was still present after RNase treatment, indicating direct interaction. We further validated the interaction by overexpressing TRIM3 in HEK cells, followed by immunoprecipitation. TRIM3 is not endogenously expressed in HEK cells, making it unlikely that an observed interaction is RNA mediated, at least not by the same mechanism as in neurons. Indeed, we were able co-immunoprecipitate TRIM3 with ACTG1 and vice versa, leading us to conclude that the interaction is indeed direct. However, HEK cells share some properties with neurons and express numerous neuronal proteins (Lin et al., 2014; Shaw et al., 2002), allowing for the possibility that an unknown protein-protein mediator between ACTG1 and TRIM3 is involved. Immunoprecipitation of intact TRIM3 complexes from HEK cells followed by BN-PAGE could certainly shed light on this matter.

TRIM3 regulates ACTG1 by ubiquitylation

We observed that when we overexpress TRIM3 in HEK cells, ACTG1 levels were significantly decreased. In accordance we found significantly more ACTG1 in hippocampal

neurons from *TRIM3*$^{-/-}$ mice. Interestingly, in HEK cells we also observed a significant decrease of ACTB when we overexpressed TRIM3, indicating that with an excess of TRIM3, or a lack of suitable substrate, specificity of the ubiquitylation reaction decreases.

The detected changes in ACTG1 levels in neurons and HEK cells are likely caused by the presence or absence of TRIM3-mediated ubiquitylation. We found that TRIM3 was only able to ubiquitylate ACTG1 in HEK293 cells under conditions where protein synthesis was stimulated. A number of possible explanations may account for this finding. We had earlier hypothesized that TRIM3 ubiquitylates ACTG1 co-translationally at lysine 18 which is only accessible while in translation (Zhang et al., 2010). In our immunoprecipitation experiments for ACTG1 we transfected HEK293 cells at 60 - 80 % confluence and blocked the proteasome for four hours after 44 hours of transfection. At this moment in time cells were fully confluent and considering the relatively long half-life of actin of about 48 hours (Antecol et al., 1986) we may assume that there was little demand for new actin synthesis, and stimulation of protein synthesis would be required to reveal co-translational ubiquitylation. Indeed, we enriched for poly-ubiquitylated ACTG1 species when cells were stimulated with TPA while blocking the proteasome. TPA is a tumor promotor (Blumberg, 1988) and has effects on cell growth, gene transcription and proteins synthesis by activating among others protein kinase C (PKC) and the mTOR pathway (Carriere et al., 2011; Herbert et al., 2000; Kazanietz, 2000; Kazanietz et al., 2000). Only when blocking the proteasome and stimulating at the same time with TPA were we able to detect poly-ubiquitylated species of ACTG1, supporting our hypothesis that TRIM3 regulates ACTG1 co-translationally. However, due to the broad effect of TPA on cells, we cannot rule out other possibilities entirely. In some cases it is known that ubiquitylation is preceded by other post-translational modifications such as arginylation, acetylation and phosphorylation (Arnesen, 2011; Terman and Kashina, 2013). Since PKC phosphorylates actin (Carrascosa and Wieland, 1986; Walsh et al., 1981), the TPA-induction experiments might also indicate that only phosphorylated ACTG1 is targeted by TRIM3 for degradation. Similarly the Skp1-Cul1-F-box (SCF) ubiquitin ligase only ubiquitylates cyclin D1 when threonine 286 is phosphorylated (Lin et al., 2006). Also, TRIM3 itself has two known phosphorylation sites (Olsen et al., 2006) and it is possible that TPA-induced phosphorylation of TRIM3 enhances ubiquitylation of ACTG1.

Co-translational ubiquitylation of ACTG1 by TRIM3 is further supported by the fact that we were able to detect *Actg1* mRNA in TRIM3/PURA containing mRNA transport granules

from hippocampal neurons. Many mRNP granule proteins identified by Kanai et al. (2004), i.e. FMR1, DDX1, EF1A, EF2A and numerous hnRNP proteins, are involved in local translation (Chen et al., 2002; Lee et al., 2010; Nilsson and Nissen, 2005; Sidorov et al., 2013; Torvund-Jensen et al., 2014). Moreover, many locally translated mRNAs such as *Arc, Map2, CamKIIα* and *β-actin* are known components of mRNP granules (Hirokawa, 2006; Mikl et al., 2011). Although *Actg1* mRNA is often claimed not to be dendritically targeted, our findings are supported by a recent deep sequencing study showing that both *Actg1* and *Actb* transcripts are present in the hippocampal neuropil, and are among the 2,550 mRNAs that can be identified with high confidence as dendritic/axonal transcripts (Cajigas et al., 2012).

Actg1-cKO and the role of ACTG1 in learning

To test whether ACTG1 levels also affect learning we created a forebrain-specific *Actg1* knockout mouse. Recently generated global *Actg1* knockout mice were found to be born at only one-third of the expected Mendelian ratio (Belyantseva et al., 2009), indicating that ACTG1 is at least partially important for normal development. Furthermore these mice had significantly reduced body weights and showed a high rate of premature death (Belyantseva et al., 2009). To limit systemic and developmental effects of ACTG1 deficiency we generated a forebrain-specific *Actg1* knockout mouse (*Actg1-cKO*) employing CamKIIα promotor driven Cre expression. *Actg1-cKO* mice were viable and born at normal Mendelian ratios. We observed a significant reduction in ACTG1 protein levels in forebrain that was compensated by a significant upregulation of ACTB. We were not able to detect any alpha-actin expression in brain, regardless of the genotype. This was unexpected, since CNS-specific *Actb* knockout mice showed a strong up-regulation of both gamma-actin and of alpha-actin (Cheever et al., 2012), suggesting that in our case ACTB is either sufficient to compensate for loss of ACTG1, or that the sensitivity of our alpha-actin antibody was too low.

We tested *Actg1-cKO* mice in a contextual fear memory paradigm and observed that they show enhanced contextual fear memory. Interestingly, *Trim3*$^{-/-}$ mice, which have increased ACTG1 levels, showed a similar enhanced contextual fear memory phenotype. This suggests that normal expression of both ACTG1 and TRIM3 is required to constrain plasticity within physiological boundaries, and that an increase as well as the loss of ACTG1 contributes to

the manifestation of enhanced fear memory. An interpretation of these findings is currently difficult, for it is largely unknown how cytoskeletal rearrangements affect learning. Also, we do not yet know how LTP and spine densities, both of which are increased in *Trim3*$^{-/-}$ mice, are affected in *Actg1-cKO* mice. However, if we assume that changes in gamma-actin levels underlie both phenotypes, previously published data on the role of gamma-actin in determining the dynamic properties of the actin cytoskeleton are worth mentioning here. It is known that only two of the six known actin isoforms are expressed in neurons, β–actin and γ-actin (Rubenstein, 1990). Both isoforms readily co-polymerize to form filaments and it was recently demonstrated that the γ:β ratio dictates the stability of actin filaments. While high amounts of ACTG1 stabilize filaments, abundance of ACTB renders filaments more dynamic (Belyantseva et al., 2009; Bergeron et al., 2010). Our findings thus suggest that changing γ/β-actin ratio of actin filaments either way results in alterations in the dynamic properties of the actin cytoskeleton such that plasticity is enhanced. Determining actin polymerization and depolymerization rates in *Trim3*$^{-/-}$ mice and *Actg1-cKO* mice may help to better understand how these alterations correlate with structural and functional plasticity at the synapse.

CHAPTER 6

General Discussion

General Discussion

This study was aimed to elucidate the role of TRIM3 in hippocampal and cerebellar function by making use of a newly generated *Trim3* knockout mouse.

In the hippocampus, TRIM3 was found to be a synaptic ubiquitin ligase that targets ACTG1 for proteasomal degradation. As a consequence *Trim3*$^{-/-}$ mice have increased levels of ACTG1 at synaptic sites, higher spine densities, increased long-term potentiation (LTP) and enhanced contextual fear memory consolidation compared to wildtype controls. Interestingly, forebrain specific deletion of *Actg1* resulted in a similar enhancement of contextual fear memory, suggesting that normal expression of both ACTG1 and TRIM3 are required to constrain hippocampal plasticity within physiological boundaries. TRIM3 is also expressed in cerebellar granule cells (CGCs) and in neurons of the deep cerebellar nuclei, but not in Purkinje cells. The localization of TRIM3 in the molecular layer further supports a synaptic function in the cerebellum, in particular at parallel fiber to Purkinje cell synapses. Interestingly, we identified a different set of candidate TRIM3 synaptic substrates in the cerebellum compared with the hippocampus, suggesting different functions for TRIM3 in these brain regions. Determining the physiological and behavioral roles of TRIM3 and its substrates in the cerebellum will need further investigation.

Here, I will discuss potential similarities and dissimilarities between TRIM3 function in the hippocampus and the cerebellum. I will regularly refer to published data on two other RING-finger E3 ligases, TRIM2 and TRIM32, which are structurally closely related to TRIM3 and have partially overlapping expression patterns in the hippocampus and cerebellum. Studying potential functional complementarity and redundancy between these three proteins may thus help to understand some of the phenotypes that are associated with their deletion or overexpression.

TRIM3 and brain morphology

In adult mice TRIM3 is strongly expressed in hippocampus and cerebellum and cellular expression is highly localized to synaptic sites (El-Husseini, 1999; Hung et al., 2010) (Chapter 2). However, a direct effect of TRIM3 deletion in mice was not readily apparent,

and two independently generated *Trim3*$^{-/-}$ mouse lines were viable and of normal appearance (Cheung et al., 2010; Chapter 2). We performed detailed histological examination of brains of *Trim3*$^{-/-}$ mice and did not observe abnormalities. Overall hippocampal and cerebellar morphology and cytoarchitecture were unaffected after loss of TRIM3. It can therefore be concluded that TRIM3 is dispensable for normal brain development. Mice deficient for TRIM2, the closest relative of TRIM3, also presented with no apparent brain defects (Balastik et al., 2008). From the age of four months on, however, TRIM2 deficient mice developed seizures and showed strong progressive neurodegeneration of cerebellar Purkinje cells, neurons of the deep cerebellar nuclei, retinal ganglion cells and neurons in the spinal cord (Balastik et al., 2008). The same authors showed that TRIM2 targets neurofilament light chain for proteasomal degradation, and provided evidence that neurodegeneration in TRIM2 deficient mice is likely caused by neurofilament accumulations in axons and subsequent cell death (Balastik et al., 2008). To test for such an age-dependent accumulative effect in *Trim3*$^{-/-}$ mice we also examined brain morphology at 8 months of age. Aged *Trim3*$^{-/-}$ mice did not exhibit seizures, nor was there any sign of neurodegeneration, leading us to conclude that loss of TRIM3 does not result in age-dependent morphological alterations as was reported for TRIM2 deficient mice. In this respect it is interesting to note that in the cerebellum TRIM2 is uniquely expressed in Purkinje cells (Balastik et al., 2008) and TRIM3 in CGCs (Chapter 2), whereas in the hippocampus they are co-expressed in CA pyramidal neurons. Despite abundant TRIM2 expression in the hippocampus, TRIM2 deficient mice show no hippocampal degeneration, suggesting that TRIM3 might compensate for TRIM2 when both are expressed in the same cells. However, TRIM2 and TRIM3 are also co-expressed in neurons of the deep cerebellar nuclei, which do show age-dependent degeneration in TRIM2 deficient mice. Thus, functional redundancy between TRIM2 and TRIM3, if any, does seem to depend on the cell type in which they are expressed and possibly on subcellular localization and on the specific protein substrates that are targeted for proteasomal degradation. Additional research on double mutant mice and cell type-specific mutants should be able to resolve this issue.

At the synapse morphological level it was reported that TRIM3 overexpression in cultured rat hippocampal neurons leads to a decrease in spine head width, but did not have an effect on spine density or spine length (Hung et al., 2010). To assess potential synapse morphological abnormalities in *Trim3*$^{-/-}$ mice *in vivo*, we used fluorescent confocal

microscopy. Three spine parameters were investigated: (i) spine head size, (ii) spine length and (iii) spine density. In contrast to Hung et al. (2010) we observed a significant increase in spine density in *Trim3*$^{-/-}$ mice, while spine length and spine head size were not affected. These discrepancies may be explained in different ways. First Hung et al. (2010) overexpressed TRIM3 whereas we studied the consequences of TRIM3 deletion. Both studies confirm a role for TRIM3 in spine morphogenesis, but reducing or increasing TRIM3 levels may have different consequences for how this translates into spine morphology. Moreover, overexpression of TRIM3 was performed in cultured embryonic neurons, whereas we used slice preparations of adult mouse hippocampi for spine analysis. In addition to being of different developmental stages these preparation also have very different dynamics and network properties. This for instance might mean that a decreased spine head size after three days of TRIM3 overexpression in cultured neurons represents an early stage of spine pruning, while in slice preparations the long-term consequences of such spine pruning are observed as reduced spine densities. Whatever the explanation, both our data and that of Hung et al. (2010) strongly suggest that TRIM3 is important for maintaining normal hippocampal spine morphology.

TRIM3 and memory

Because of the strong expression of TRIM3 in the hippocampus and cerebellum, we specifically assessed hippocampus- and cerebellum-associated behaviors, i.e. motor coordination (rotarod) and contextual memory (contextual fear conditioning) in *Trim3*$^{-/-}$ mice. To rule out that observed behaviors stem from generally altered aspects of basal behavior, such as activity or anxiety, we also tested *Trim3*$^{-/-}$ mice using open field, light-dark box and elevated plus maze tasks. Our analysis showed that motor coordination is not affected by loss of TRIM3. Latencies of *Trim3*$^{-/-}$ mice to fall off the accelerating rotarod were not different from those of wildtype mice. Also, overall locomotor behavior was not affected by loss of TRIM3. *Trim3*$^{-/-}$ and wildtype mice were equally active on the elevated plus maze, in the open field and in the light-dark box. The lack of any defect in activity and motor parameters confirms at the behavioral level that there is no significant neuronal degeneration and cell loss in the cerebellum (Chapter 2), as was observed for TRIM2 deficient mice (Balastik et al., 2008).

When focusing on hippocampal learning and memory, we did identify one striking difference between *Trim3*$^{-/-}$ mice and wildtype controls. In a contextual fear memory task we observed enhanced memory acquisition, evidenced by higher freezing levels at two hours after conditioning. The levels of freezing were comparable to that of both *Trim3*$^{-/-}$ mice and wildtype mice at 24 h after conditioning, indicating that *Trim3*$^{-/-}$ mice have a specific enhancement of short-term memory. Having used a contextual fear conditioning paradigm without tone or light pairing, this behavioral abnormality is likely caused by the absence of TRIM3 in the hippocampus (Kim and Fanselow, 1992; Phillips and LeDoux, 1992), however, an involvement of the amygdala, where TRIM3 is normally also expressed, cannot be ruled out entirely. One might also question whether high freezing levels at two hours after conditioning are the result of increased fear memory consolidation or of higher anxiety levels. However, *Trim3*$^{-/-}$ mice and wildtype controls showed similar performance in the elevated plus maze, open field and light-dark box, indicating that basal anxiety levels did not differ. When inspecting closely the data obtained from the elevated plus maze, *Trim3*$^{-/-}$ mice tend to enter more often and spend more time in open arms, indicating slightly decreased anxiety. Interestingly *Trim3*$^{-/-}$ mice did spend significantly more time in the center area of the elevated plus maze. Although this is difficult to interpret, it is generally considered to be a measure of decision making (Carobrez and Bertoglio, 2005). Following this reasoning it appears that *Trim3*$^{-/-}$ mice took more time deciding, yet entered and explored open arms more often and longer, indicating decreased anxiety. In the light-dark box paradigm we observed a similar behavior. Although not significantly different, *Trim3*$^{-/-}$ mice showed a tendency to enter the light compartment more often, again arguing against increased anxiety as an explanation for the enhanced freezing levels of *Trim3*$^{-/-}$ mice at two hours after fear condition. Taken together it can be concluded that the enhanced fear memory consolidation of *Trim3*$^{-/-}$ mice is caused by the absence of TRIM3 in the hippocampus and not by higher activity and/or anxiety levels. This indicates that TRIM3 is a negative regulator of hippocampus dependent fear memory consolidation and that removing TRIM3 enhances learning and memory.

Based on the fear conditioning phenotype it is tempting to speculate that TRIM3 might also be involved in regulating motor learning in the cerebellum. Preliminary data (not included in this thesis) indicate that *Trim3*$^{-/-}$ mice show reduced motor learning using the Erasmus ladder, a device designed to measure conditioning of motor responses to an auditory stimulus (Van Der Giessen et al., 2008). *Trim3*$^{-/-}$ mice were less capable of pairing the tone

with a correct motor response, indicating decreased motor learning. Importantly, the number of missteps was not different between *Trim3*$^{-/-}$ mice and wildtype controls, indicating again that basal motor performance was not affected. Although preliminary in nature, these findings show that in contrast to enhanced hippocampal contextual fear conditioning, *Trim3*$^{-/-}$ mice show reduced cerebellar motor learning.

TRIM3 and synaptic plasticity

The fact that hippocampal learning is enhanced in *Trim3*$^{-/-}$ mice, whereas cerebellar motor learning appears to be decreased, puts to question the nature of the underlying synapse physiological and molecular mechanisms. We observed increased hippocampal long-term potentiation (LTP) in slice preparations from *Trim3*$^{-/-}$ mice (Chapter 2). Basal synaptic transmission parameters were unaffected, and spontaneous excitatory and inhibitory synaptic responses appeared normal in *Trim3*$^{-/-}$ mice. In a previous study, Cheung et al. (2010) reported that *Trim3*$^{-/-}$ mice have reduced spontaneous inhibitory synaptic transmission in the cortex, which correlates with reduced GABA-A receptor gamma-2 subunit surface expression. According to our data this is not the case in the hippocampus. The specific enhancement of LTP and not basal transmission may thus provide a good explanation for increased short-term fear memory consolidation. Cerebellar motor learning on the other hand depends, among others, on long-term depression (LTD) at parallel fiber-Purkinje cell synapses (De Zeeuw and Yeo, 2005; Hansel and Linden, 2000), which are probably the site of TRIM3 expression in the cerebellum (Chapter 2). It is thus tempting to speculate that TRIM3 is a regulator of meta-plasticity, and that TRIM3 deletion increases LTP while decreasing LTD, resulting in an enhancement of memory processes that depend on LTP and an impairment of memory processes that depend on LTD. However, there may be many other explanations for the differences observed in hippocampal versus cerebellar learning. For instance, as discussed above the subcellular localization of TRIM3 may be different, i.e., post- versus presynaptic respectively, and the substrates involved may also be different. The latter issue will be discussed in the following sections.

TRIM3 and the cytoskeleton

In chapter 4 we performed an open proteomics screen in order to identity TRIM3 ubiquitylation substrates in the hippocampus and in the cerebellum. By using a unique combination of poly-ubiquitin affinity purification and immunoprecipitation with multiple anti-TRIM3 antibodies, and employing *Trim3*$^{-/-}$ tissue as a negative control, we were able to identify potential substrate proteins with high confidence. We were initially surprised to find a ubiquitously expressed protein like ACTG1 as the most likely substrate in the hippocampus, but subsequent studies presented in chapter 5 demonstrated that TRIM3 indeed binds and negatively regulates ACTG1 via ubiquitylation, making ACTG1 the likely cause for the memory phenotype we observed in *Trim3*$^{-/-}$ mice. Behavioral analysis of hippocampus-specific *Actg1*$^{-/-}$ mice confirmed that ACTG1 indeed contributes to the formation of contextual fear memory, findings that will be discussed in more detail in the following sections.

The question of what the specific role of TRIM3 in the cerebellum is remains unanswered. From our findings we can, however, deduce that it likely differs from its role in the hippocampus. As aforementioned, TRIM3 is strongly expressed in the cerebellum (El-Husseini, 1999). Yet, whereas its expression in the hippocampus is primarily post-synaptic, in the cerebellum we observed predominantly pre-synaptic expression (Chapter 2). Moreover, our substrate identification strategy identified a different set of potential TRIM3 substrate proteins for cerebellum than for the hippocampus, including the intermediate filament protein vimentin (Chapter 4). It is thus interesting to speculate that all TRIM-NHL proteins (TRIM2, TRIM3 and TRIM32) target cytoskeletal proteins for proteasomal degradation, i.e., actin (TRIM32 in muscle cells), neurofilament (TRIM2 in cerebellum), gamma-actin (TRIM3 in hippocampus) and vimentin (TRIM3 in cerebellum). However, vimentin expression is generally thought to be limited to developmental stages and is not expressed in mature neurons (Yabe et al., 2003). This finding therefore needs to be considered with caution and requires further investigation. Finally, it would be interesting to see whether TRIM2 targets different cytoskeletal proteins in cerebellum and hippocampus explaining the lack of a neurodegenerative phenotype in the hippocampus as discussed above.

TRIM3 and mRNP granules

Identifying TRIM3 as an E3 ligase that targets ACTG1 for proteasomal degradation did not come as a complete surprise. A study in heterologous cells demonstrated that ACTG1 is poly-ubiquitylated co-translationally (Zhang et al., 2010). Non-coding sequences in *Actg1* mRNA cause ACTG1 to be synthesized at a much slower rate than ACTB, allowing a normally buried lysine residue at the N-terminus to be exposed long enough to be ubiquitylated. For TRIM3 to be responsible for co-translational ACTG1 ubiquitylation, TRIM3 protein and *Actg1* mRNA would need to be in close proximity. In this respect it is interesting to note that Kanai et al. (2004) found TRIM3 among a core set of 42 proteins that constitute a detergent-resistant, RNase-sensitive neuronal transport granule that associates with motor protein KIF5. These so-called messenger ribonucleoprotein (mRNP) granules transport mRNAs towards synapses (Buchan, 2014). We confirmed the presence of TRIM3 in mRNP granules by showing that TRIM3 co-immunoprecipitates with PURA (Chapter 3), one of the major components of mRNP granules (Elvira et al., 2006), in an RNase-sensitive manner. We also established that *Actg1* mRNA is present in mRNP granules that are immunoprecipitated with antibodies against either TRIM3 or PURA. *Actg1* mRNA lacks the zipcode sequence that is known to target *Actb* mRNA to dendrites (Eom et al., 2003; Poon et al., 2006). However, a recent deep sequencing study showed that both *Actg1* and *Actb* transcripts are present in the hippocampal neuropil, and are among the 2,550 mRNAs that can be identified with high confidence as dendritic/axonal transcripts (Cajigas et al., 2012). Our findings confirm that *Actg1* mRNA levels in TRIM3- or PURA-positive immunoprecipitates are comparable with those of *Actb*. Thus, TRIM3 and *Actg1* mRNA co-localize in mRNP granules that target mRNAs to dendritic spines for local translation, suggesting that TRIM3-mediated co-translational ubiquitylation of ACTG1 may occur at synaptic sites.

We furthermore found that TRIM3 is not essential for dendritic trafficking of PURA-positive mRNP granules (chapter 3). We did however detect a significant increase in the maximum velocity and maximum distance traveled of a small sub-population of long distance PURA-positive granules. These long distance clusters traveled more than 5 μm and accounted for 26 – 30 % of all detected clusters. In this respect we must consider that mRNP granules are diverse in composition (Buchan, 2014; Erickson and Lykke-Andersen, 2011) and that not all PURA-positive granules would necessarily contain TRIM3 and vice versa.

This suggests that the 26 – 30 % long distance granules may possibly reflect the entirety of mRNP granules containing TRIM3. Co-expression or co-labeling of both PURA and TRIM3 in neurons, followed by quantitative co-localization analysis would certainly shed light on that matter.

Wilhelm and Vale (Wilhelm and Vale, 1993) brought four essential aspects of mRNP granules forward that needed to be addressed in order to precisely understand their function: (i) how mRNP particles assemble, (ii) how they are localized and transported via cytoskeletal motors, (iii) how they are anchored to local sites, and (iv) how local translation is then facilitated. Although Wilhelm and Vale had already speculated that recognition of local sites and anchoring would have to involve cytoskeletal (actin) elements, this matter has largely been unaddressed since then. Taking our findings that (i) TRIM3 is part mRNP granules, that (ii) without TRIM3 these granules travel faster and further, and that (iii) TRIM3 strongly binds ACTG1, it is possible that TRIM3 not only regulates ACTG1 co-translationally at synaptic sites, but also functions as recognition or anchoring molecule of actin filament protrusions of synapses. Thus, mRNP granules lacking TRIM3 may have a reduced ability to recognize synaptic sites, which in return would explain the longer distances travelled and the higher velocity. It would be interesting to test that hypothesis in our recently generated *Actg1*-cKO mouse. If indeed the binding of TRIM3 to ACTG1 serves as a synapse identifier or synapse anchor for mRNP granules, then tracking mRNPs in ACTG1 deficient cells should yield a similar result as tracking them in TRIM3 deficient cells.

How do TRIM3 and gamma-actin affect spine morphology, synaptic plasticity and memory?

Consistent with our finding that TRIM3 protein and *Actg1* mRNA co-localize in mRNP granules trafficking to synaptic sites, our proteomic screen identified ACTG1 as high-confidence TRIM3-interactor as well as the most TRIM3-dependent poly-ubiquitylated protein in hippocampal synapse-enriched fractions. Moreover, TRIM3-dependent poly-ubiquitylated forms of ACTG1 can be detected in hippocampal neurons after stimulation with TPA, a PKC activator that induces protein synthesis and synaptic plasticity (Carriere et al., 2011; Herbert et al., 2000; Kim et al., 2013), and ACTG1 levels are significantly increased in *Trim3*$^{-/-}$ neurons. Together, these findings demonstrate that TRIM3

regulates synaptic ACTG1 levels in an activity-dependent manner, most likely via ubiquitin-dependent proteasomal degradation. Targeting a newly synthesized protein for degradation appears unintuitive at first glance. There are, however, a number of scenarios in which such an apparently wasteful procedure can be beneficial. First, TRIM3 may act as quality control of ACTG1. The incidence rate of misfolded protein is dependent on synthesis and folding rate (Dubitzky et al., 2011). Considering a sudden increase in ACTG1 translation after a stimulus, this would likely yield a larger amount of defective ACTG1, which can affect actin dynamics in any number of manners. Limiting the formation or promptly removing this pool of defective and/or non-functional ACTG1 may be highly beneficial. Examples of other quality control E3 ligases are Hel2, Ltn1 and Not4, all of which are known to be ribosome associated and to ubiquitylate proteins co-translationally (Panasenko, 2014). Second, it is possible that TRIM3 poly-ubiquitylates ACTG1 co-translationally and poly-ubiquitylated ACTG1 is then transiently incorporated into actin filaments. TRIM3 may possibly play an active role in this, as TRIM3 interacts with several actin-binding proteins, including myosin V (El-Husseini, 1999) and α-actinin-4 (El-Husseini et al., 2000), and is involved in actin-based transport (Yan et al., 2005). TRIM3 may thus facilitate incorporation of poly-ubiquitylated ACTG1 into F-actin. In the filament, poly-ubiquitylated ACTG1 may present another cross-linking opportunity for other synaptic proteins, allowing stabilization of postsynaptic proteins and thereby retaining a specific synaptic state (Kuriu et al., 2006; Renner et al., 2009). Upon de-polymerization of F-actin, prior incorporated poly-ubiquitylated ACTG1 would then be released, recognized by the ubiquitin proteasome system, degraded and thereby removed from the available actin pool. A transient increase in ACTG1 levels due to local translation and degradation might temporarily change the dynamic properties of the actin cytoskeleton and create a window of opportunity for ACTG1 to contribute to activity-induced synaptic plasticity. Interestingly, enhanced LTP in *Trim3*$^{-/-}$ mice is confined to the early phase of LTP (i.e., the first 30 min after induction), which was previously demonstrated to also depend on protein synthesis (Fonseca et al., 2006a; Fonseca et al., 2006b). After 30 min LTP levels are normal again, suggesting that ACTG1 turnover may not be completely abolished in the absence of TRIM3 or that compensatory mechanisms normalize plasticity at later time points.

What might be the specific contribution of ACTG1 to actin dynamics in dendritic spines in relation to synaptic plasticity? To date the role of ACTG1 in synaptic plasticity is unknown. Our findings show that increased synaptic ACTG1 protein levels correlate with alterations in spine density, LTP and contextual fear conditioning and to our knowledge provide the first link of ACTG1 to plasticity, learning and memory. Moreover, forebrain specific, postnatal deletion in hippocampal neurons of *Actg1* itself also causes fear memory deficits (Chapter 5). Although these findings do not provide definite proof that the plasticity and memory phenotypes in *Trim3*$^{-/-}$ mice are due to increased ACTG1 levels only, they do indicate that ACTG1 contributes to hippocampal plasticity and that TRIM3 is involved as an upstream regulator. In contrast to ACTB (Cheever et al., 2012), central nervous system specific deletion of ACTG1 does not result in detectable morphological or histological abnormalities (Cheever and Ervasti, 2013), indicating that ACTG1 has no major role in gross brain development. Several studies have hinted towards specific and unique roles for ACTG1 in adulthood. For instance, whereas ACTG1 and ACTB are each dispensable for the normal development of auditory hair cells in the cochlea (Perrin et al., 2010), ACTG1 deficient mice cannot properly maintain hair cell stereocilia actin cores and suffer from progressive age-dependent hearing loss (Belyantseva et al., 2009). The authors observed that ACTG1 accumulates at sites of stereocilia core disruptions, and conclude that ACTG1 is required for the reinforcement of long-term stability of actin filaments and the remodeling and repair of stereocilia cores following mechanical stress-induced damage. One possible explanation for these findings is that ACTG1-containing filaments have different biochemical and biophysical properties than filaments lacking ACTG1. Recent studies seem to confirm that ACTG1 may indeed contribute to more stable actin filaments (Bergeron et al., 2010). Although polymerization rates of ACTB and ACTG1 were indistinguishable in the Mg^{2+}-bound state, which is considered to be the physiologically most relevant state, turnover rates of ACTB in its Ca^{2+}-bound state were considerably faster than those of ACTG1, indicating that in the presence of Ca^{2+} ACTB is more dynamic, and ACTG1 is more stable. Moreover, since ACTB and ACTG1 readily copolymerized, it probably is the ACTB / ACTG1 ratio in actin filaments that determines their stability in the presence of Ca^{2+} (Bergeron et al., 2010). By regulating local ACTG1 levels TRIM3 may thus play a crucial role in controlling actin stability during synaptic plasticity. Changes in actin stability would directly affect spine morphogenesis (Sekino et al., 2007) and synaptic AMPA receptor

recycling (Osterweil et al., 2005; Zhou et al., 2001) and anchoring (Allison et al., 1998; Kuriu et al., 2006), thus explaining the hippocampal spine density, LTP and memory phenotypes observed in *Trim3*$^{-/-}$ mice.

Why at all have TRIM3 or ACTG1

If *Trim3*$^{-/-}$ and *Actg1*-cKO mice show an enhanced ability to remember a painful and potentially threatening situation, why would there still be ACTG1 and TRIM3?

In the case of ACTG1 this question can be addressed with a straightforward answer. The benefit of having ACTG1 largely outweighs the ability to remember better. Actins are structurally and functionally involved in nearly every aspect of cellular life (Perrin and Ervasti, 2010; Rubenstein, 1990; Rubenstein and Wen, 2014) and so it is not surprising that knocking actin isoforms out, has severe effects. A β-actin knockout in mice for example is embryonically lethal (Shawlot et al., 1998). γ-actin knockout mice on the other hand are viable, yet at a reduced rate (Belyantseva et al., 2009; Bunnell and Ervasti, 2010). In addition γ-actin knockout mice show delayed embryonic heart development, are smaller in size and develop skeletal muscle myopathy and progressive hearing loss (Belyantseva et al., 2009; Sonnemann et al., 2006). In addition to these published negative effects caused by the loss of ACTG1, it cannot be ruled out that the observed enhanced fear memory is not accompanied by other adverse effects, which can only be seen in different behavioral paradigms or at later phases in life of these mice. This finding, however, can be seen as a prolific foundation to base future hypotheses on.

In the case of TRIM3 the question of why it is there, is unarguably more complicated. Aside from its role in ACTG1 ubiquitylation TRIM3 may also target other proteins for degradation or serve other functions that we were unable to detect with our approach and are therefore unaware of. Given that we found *Trim3*$^{-/-}$ mice to be viable, healthy to an old age and in most aspects nearly indistinguishable from their wildtype littermates, we can assume that potential other functions are either of subtle nature or present in other physiological domains beyond the scope of this study. Our study revealed enhanced hippocampal LTP, increased hippocampal spine density and an enhanced fear memory consolidation in *Trim3*$^{-/-}$ mice. Reflecting theses points, it appears as if not having TRIM3 is solely beneficial and has no downsides. After all, a better memory is something that is

generally sought after. In regard to fear memory, however, better is probably only desirable to a certain degree. When a fear memory becomes disproportionate to the experienced event, it may be triggered by cues only faintly resembling the original setting. This inappropriate fear expression can interfere with daily life and may pose severe disadvantages when it comes to acquiring mating partners, food and other resources. In humans such misplaced expression of fear interfering with daily life would be placed within the group of anxiety disorders (Kandel et al., 2000; Michael et al., 2007; Reiss, 1991)**.**

In conclusion

We discovered the ubiquitin E3 ligase TRIM3 to be an important factor in modulating synaptic plasticity. We demonstrated its role at molecular, synaptic physiological, synaptic structural and behavioral levels. The study presented in this thesis clearly demonstrates the importance of E3-ligases in synaptic function underlying aspects of learning and memory. It also provides a methodological framework towards target identification of similar synaptic E3-ligases. We implicated ACTG1 as an important TRIM3 target. The way TRIM3 is activated during plasticity processes and how ACTG1 is involved in structural plasticity would deserve attention in future studies.

References

Albor, A., S. El-Hizawi, E.J. Horn, M. Laederich, P. Frosk, K. Wrogemann, and M. Kulesz-Martin. 2006. The interaction of Piasy with Trim32, an E3-ubiquitin ligase mutated in limb-girdle muscular dystrophy type 2H, promotes Piasy degradation and regulates UVB-induced keratinocyte apoptosis through NFkappaB. *J Biol Chem*. 281:25850-25866.

Allison, D.W., V.I. Gelfand, I. Spector, and A.M. Craig. 1998. Role of actin in anchoring postsynaptic receptors in cultured hippocampal neurons: differential attachment of NMDA versus AMPA receptors. *J Neurosci*. 18:2423-2436.

Anderson, J.P., D.E. Walker, J.M. Goldstein, R. de Laat, K. Banducci, R.J. Caccavello, R. Barbour, J. Huang, K. Kling, M. Lee, L. Diep, P.S. Keim, X. Shen, T. Chataway, M.G. Schlossmacher, P. Seubert, D. Schenk, S. Sinha, W.P. Gai, and T.J. Chilcote. 2006. Phosphorylation of Ser-129 is the dominant pathological modification of alpha-synuclein in familial and sporadic Lewy body disease. *J Biol Chem*. 281:29739-29752.

Anderson, P., and N. Kedersha. 2009. RNA granules: post-transcriptional and epigenetic modulators of gene expression. *Nat Rev Mol Cell Biol*. 10:430-436.

Antecol, M.H., A. Darveau, N. Sonenberg, and B.B. Mukherjee. 1986. Altered biochemical properties of actin in normal skin fibroblasts from individuals predisposed to dominantly inherited cancers. *Cancer Res*. 46:1867-1873.

Antequera, F., and A. Bird. 1993. Number of CpG islands and genes in human and mouse. *Proc Natl Acad Sci U S A*. 90:11995-11999.

Arabidopsis Genome, I. 2000. Analysis of the genome sequence of the flowering plant Arabidopsis thaliana. *Nature*. 408:796-815.

Arnesen, T. 2011. Towards a functional understanding of protein N-terminal acetylation. *PLoS Biol*. 9:e1001074.

Artola, A., and W. Singer. 1993. Long-term depression of excitatory synaptic transmission and its relationship to long-term potentiation. *Trends Neurosci*. 16:480-487.

Bagni, C., and W.T. Greenough. 2005. From mRNP trafficking to spine dysmorphogenesis: the roots of fragile X syndrome. *Nat Rev Neurosci*. 6:376-387.

Balastik, M., F. Ferraguti, A. Pires-da Silva, T.H. Lee, G. Alvarez-Bolado, K.P. Lu, and P. Gruss. 2008. Deficiency in ubiquitin ligase TRIM2 causes accumulation of neurofilament light chain and neurodegeneration. *Proc Natl Acad Sci U S A*. 105:12016-12021.

Barria, A., D. Muller, V. Derkach, L.C. Griffith, and T.R. Soderling. 1997. Regulatory phosphorylation of AMPA-type glutamate receptors by CaM-KII during long-term potentiation. *Science*. 276:2042-2045.

Beers, E.P., and J. Callis. 1993. Utility of polyhistidine-tagged ubiquitin in the purification of ubiquitin-protein conjugates and as an affinity ligand for the purification of ubiquitin-specific hydrolases. *The Journal of biological chemistry*. 268(29):21645-9.

Belyantseva, I.A., B.J. Perrin, K.J. Sonnemann, M. Zhu, R. Stepanyan, J. McGee, G.I. Frolenkov, E.J. Walsh, K.H. Friderici, T.B. Friedman, and J.M. Ervasti. 2009. Gamma-actin is required for cytoskeletal maintenance but not development. *Proc Natl Acad Sci U S A*. 106:9703-9708.

Bergeron, S.E., M. Zhu, S.M. Thiem, K.H. Friderici, and P.A. Rubenstein. 2010. Ion-dependent polymerization differences between mammalian beta- and gamma-nonmuscle actin isoforms. *J Biol Chem*. 285:16087-16095.

Berndsen, C.E., and C. Wolberger. 2014. New insights into ubiquitin E3 ligase mechanism. *Nat Struct Mol Biol*. 21:301-307.

Black, D.L. 2003. Mechanisms of alternative pre-messenger RNA splicing. *Annu Rev Biochem*. 72:291-336.

Bliss, T.V., and T. Lomo. 1973. Long-lasting potentiation of synaptic transmission in the dentate area of the anaesthetized rabbit following stimulation of the perforant path. *J Physiol*. 232:331-356.

Blumberg, P.M. 1988. Protein kinase C as the receptor for the phorbol ester tumor promoters: sixth Rhoads memorial award lecture. *Cancer research*. 48:1-8.

Bockers, T.M., M. Segger-Junius, P. Iglauer, J. Bockmann, E.D. Gundelfinger, M.R. Kreutz, D. Richter, S. Kindler, and H.J. Kreienkamp. 2004. Differential expression and dendritic transcript localization of Shank family members: identification of a dendritic targeting element in the 3' untranslated region of Shank1 mRNA. *Mol Cell Neurosci*. 26:182-190.

Boehm, J., M.G. Kang, R.C. Johnson, J. Esteban, R.L. Huganir, and R. Malinow. 2006. Synaptic incorporation of AMPA receptors during LTP is controlled by a PKC phosphorylation site on GluR1. *Neuron*. 51:213-225.

Boulay, J.L., U. Stiefel, E. Taylor, B. Dolder, A. Merlo, and F. Hirth. 2009. Loss of heterozygosity of TRIM3 in malignant gliomas. *BMC Cancer*. 9:71.

Bramham, C.R., and D.G. Wells. 2007. Dendritic mRNA: transport, translation and function. *Nat Rev Neurosci*. 8:776-789.

Bruinsma, C.F., S.M. Savelberg, M.J. Kool, M.A. Jolfaei, G.M. van Woerden, W.M. Baarends, and Y. Elgersma. 2015. An essential role for UBE2A/HR6A in learning and memory and mGLUR-dependent long-term depression. *Hum Mol Genet*. 25(1):1-8. doi: 10.1093/hmg/ddv436

Buchan, J.R. 2014. mRNP granules. Assembly, function, and connections with disease. *RNA Biol*. 11:1019-1030.

Bunnell, T.M., and J.M. Ervasti. 2010. Delayed embryonic development and impaired cell growth and survival in Actg1 null mice. *Cytoskeleton (Hoboken)*. 67:564-572.

Burgin, K.E., M.N. Waxham, S. Rickling, S.A. Westgate, W.C. Mobley, and P.T. Kelly. 1990. In situ hybridization histochemistry of Ca2+/calmodulin-dependent protein kinase in developing rat brain. *J Neurosci*. 10:1788-1798.

Buxbaum, A.R., B. Wu, and R.H. Singer. 2014. Single beta-actin mRNA detection in neurons reveals a mechanism for regulating its translatability. *Science*. 343:419-422.

Cahill, M.E., Z. Xie, M. Day, H. Photowala, M.V. Barbolina, C.A. Miller, C. Weiss, J. Radulovic, J.D. Sweatt, J.F. Disterhoft, D.J. Surmeier, and P. Penzes. 2009. Kalirin regulates cortical spine morphogenesis and disease-related behavioral phenotypes. *Proc Natl Acad Sci U S A*. 106:13058-13063.

Cajigas, I.J., G. Tushev, T.J. Will, S. tom Dieck, N. Fuerst, and E.M. Schuman. 2012. The local transcriptome in the synaptic neuropil revealed by deep sequencing and high-resolution imaging. *Neuron*. 74:453-466.

Carobrez, A.P., and L.J. Bertoglio. 2005. Ethological and temporal analyses of anxiety-like behavior: the elevated plus-maze model 20 years on. *Neurosci Biobehav Rev*. 29:1193-1205.

Caroni, P., F. Donato, and D. Muller. 2012. Structural plasticity upon learning: regulation and functions. *Nat Rev Neurosci*. 13:478-490.

Carrascosa, J.M., and O.H. Wieland. 1986. Evidence that (a) serine specific protein kinase(s) different from protein kinase C is responsible for the insulin-stimulated actin phosphorylation by placental membrane. *FEBS Letters*. 201:81-86.

Carriere, A., Y. Romeo, H.A. Acosta-Jaquez, J. Moreau, E. Bonneil, P. Thibault, D.C. Fingar, and P.P. Roux. 2011. ERK1/2 phosphorylate Raptor to promote Ras-dependent activation of mTOR complex 1 (mTORC1). *J Biol Chem*. 286:567-577.

Charrier, C., M.V. Ehrensperger, M. Dahan, S. Levi, and A. Triller. 2006. Cytoskeleton regulation of glycine receptor number at synapses and diffusion in the plasma membrane. *J Neurosci*. 26:8502-8511.

Cheever, T.R., and J.M. Ervasti. 2013. Actin isoforms in neuronal development and function. *International Review of Cell and Molecular Biology*. 301:157-213.

Cheever, T.R., B. Li, and J.M. Ervasti. 2012. Restricted morphological and behavioral abnormalities following ablation of beta-actin in the brain. *PLoS One*. 7:e32970.

Chen, H.C., W.C. Lin, Y.G. Tsay, S.C. Lee, and C.J. Chang. 2002. An RNA helicase, DDX1, interacting with poly(A) RNA and heterogeneous nuclear ribonucleoprotein K. *J Biol Chem*. 277:40403-40409.

Chen, N., R.C. Schors, and A.B. Smit. 2011a. A 1D-PAGE/LC-ESI Linear Ion Trap Orbitrap MS Approach for the Analysis of Synapse Proteomes and Synaptic Protein Complexes. Springer. 159-167 pp., DOI: 10.1007/978-1-61779-111-6_12;

Chen, N., R. van der Schors, and A.B. Smit. 2011b. A 1D-PAGE/LC-ESI linear ion trap orbitrap MS approach for the analysis of synapse proteomes and synaptic protein complexes. *In* Neuroproteomics. K.W. Li, editor. Humana Press, New York. 159-167.

Cheung, C.C., C. Yang, T. Berger, K. Zaugg, P. Reilly, A.J. Elia, A. Wakeham, A. You-Ten, N. Chang, L. Li, Q. Wan, and T.W. Mak. 2010. Identification of BERP (brain-expressed RING finger protein) as a p53 target gene that modulates seizure susceptibility through interacting with GABA(A) receptors. *Proc Natl Acad Sci U S A*. 107:11883-11888.

Chiang, A.P., J.S. Beck, H.J. Yen, M.K. Tayeh, T.E. Scheetz, R.E. Swiderski, D.Y. Nishimura, T.A. Braun, K.Y. Kim, J. Huang, K. Elbedour, R. Carmi, D.C. Slusarski, T.L. Casavant, E.M. Stone, and V.C. Sheffield. 2006. Homozygosity mapping with SNP arrays identifies TRIM32, an E3 ubiquitin ligase, as a Bardet-Biedl syndrome gene (BBS11). *Proc Natl Acad Sci U S A*. 103:6287-6292.

Choi, J.K., and L.A.J. Howe. 2009. Histone acetylation: truth of consequences? This paper is one of a selection of papers published in this Special Issue, entitled CSBMCB's 51st Annual Meeting- &. *Histone acetylation: truth of consequences? This paper is one of a selection of papers published in this Special Issue, entitled CSBMCB's 51st Annual Meeting- &*. Biochem Cell Biol. 2009 Feb;87(1):139-50. doi: 10.1139/O08-112.

Choquet, D., and A. Triller. 2003. The role of receptor diffusion in the organization of the postsynaptic membrane. *Nat Rev Neurosci*. 4:251-265.

Clayton-Smith, J., and L. Laan. 2003. Angelman syndrome: a review of the clinical and genetic aspects. *J Med Genet*. 40:87-95.

Colledge, M., E.M. Snyder, R.A. Crozier, J.A. Soderling, Y. Jin, L.K. Langeberg, H. Lu, M.F. Bear, and J.D. Scott. 2003. Ubiquitination regulates PSD-95 degradation and AMPA receptor surface expression. *Neuron*. 40:595-607.

Correia, S.S., S. Bassani, T.C. Brown, M.F. Lise, D.S. Backos, A. El-Husseini, M. Passafaro, and J.A. Esteban. 2008. Motor protein-dependent transport of AMPA receptors into spines during long-term potentiation. *Nat Neurosci*. 11:457-466.

Cossee, M., C. Lagier-Tourenne, C. Seguela, M. Mohr, F. Leturcq, H. Gundesli, J. Chelly, C. Tranchant, M. Koenig, and J.L. Mandel. 2009. Use of SNP array analysis to identify a novel TRIM32 mutation in limb-girdle muscular dystrophy type 2H. *Neuromuscul Disord*. 19:255-260.

Coux, O., K. Tanaka, and A.L. Goldberg. 1996. Structure and functions of the 20S and 26S proteasomes. *Annu Rev Biochem*. 65:801-847.

Dantuma, N.P., and L.C. Bott. 2014. The ubiquitin-proteasome system in neurodegenerative diseases: precipitating factor, yet part of the solution. *Front Mol Neurosci*. 7:70.

Dawitz, J., T. Kroon, J.J. Hjorth, and R.M. Meredith. 2011. Functional calcium imaging in developing cortical networks. *J Vis Exp*. 2011 Oct 22;(56). pii: 3550. doi: 10.3791/3550.

Dawson, T.M., and V.L. Dawson. 2003. Molecular pathways of neurodegeneration in Parkinson's disease. *Science*. 302:819-822.

De Zeeuw, C.I., and C.H. Yeo. 2005. Time and tide in cerebellar memory formation. *Curr Opin Neurobiol*. 15:667-674.

Derkach, V., A. Barria, and T.R. Soderling. 1999. Ca2+/calmodulin-kinase II enhances channel conductance of alpha-amino-3-hydroxy-5-methyl-4-isoxazolepropionate type glutamate receptors. *Proc Natl Acad Sci U S A*. 96:3269-3274.

Derkach, V.A., M.C. Oh, E.S. Guire, and T.R. Soderling. 2007. Regulatory mechanisms of AMPA receptors in synaptic plasticity. *Nat Rev Neurosci*. 8:101-113.

Deshaies, R.J., and C.A. Joazeiro. 2009. RING domain E3 ubiquitin ligases. *Annu Rev Biochem*. 78:399-434.

Di Liegro, C.M., G. Schiera, and I. Di Liegro. 2014. Regulation of mRNA transport, localization and translation in the nervous system of mammals (Review). *Int J Mol Med*. 33:747-762.

Dorval, V., M. Mazzella, P. Mathews, R. Hay, and P. Fraser. 2007. Modulation of Abeta generation by small ubiquitin-like modifiers does not require conjugation to target proteins. *Biochem. J.* 404:309-316.

Drury, L.S., G. Perkins, and J.F. Diffley. 1997. The Cdc4/34/53 pathway targets Cdc6p for proteolysis in budding yeast. *EMBO J.* 16:5966-5976.

Dubitzky, W., J. Southgate, and H. Fuss. 2011. Understanding the dynamics of biological systems: lessons learned from integrative systems biology. Springer Science & Business Media. ISBN-10: 1441979638

Dudek, S.M., and M.F. Bear. 1992. Homosynaptic long-term depression in area CA1 of hippocampus and effects of N-methyl-D-aspartate receptor blockade. *Proc Natl Acad Sci U S A*. 89:4363-4367.

Duttler, S., S. Pechmann, and J. Frydman. 2013. Principles of cotranslational ubiquitination and quality control at the ribosome. *Mol Cell*. 50:379-393.

Ehlers, M.D. 2003. Activity level controls postsynaptic composition and signaling via the ubiquitin-proteasome system. *Nat Neurosci*. 6:231-242.

El-Husseini, A.E., D. Kwasnicka, T. Yamada, S. Hirohashi, and S.R. Vincent. 2000. BERP, a novel ring finger protein, binds to alpha-actinin-4. *Biochem Biophys Res Commun*. 267:906-911.

El-Husseini, A.E.d. 1999. Cloning and Characterization of a Novel RING Finger Protein That Interacts with Class V Myosins. *Journal of Biological Chemistry*. 274:19771-19777.

Elvira, G., S. Wasiak, V. Blandford, X.K. Tong, A. Serrano, X. Fan, M. del Rayo Sanchez-Carbente, F. Servant, A.W. Bell, D. Boismenu, J.C. Lacaille, P.S. McPherson, L. DesGroseillers, and W.S. Sossin. 2006. Characterization of an RNA granule from developing brain. *Mol Cell Proteomics*. 5:635-651.

Engert, F., and T. Bonhoeffer. 1999. Dendritic spine changes associated with hippocampal long-term synaptic plasticity. *Nature*. 399:66-70.

Eom, T., L.N. Antar, R.H. Singer, and G.J. Bassell. 2003. Localization of a beta-actin messenger ribonucleoprotein complex with zipcode-binding protein modulates the density of dendritic filopodia and filopodial synapses. *J Neurosci*. 23:10433-10444.

Erickson, S.L., and J. Lykke-Andersen. 2011. Cytoplasmic mRNP granules at a glance. *J Cell Sci*. 124:293-297.

Farley, A.R., and A.J. Link. 2009. Identification and quantification of protein posttranslational modifications. *Methods Enzymol*. 463:725-763.

Fields, C., M.D. Adams, O. White, and J.C. Venter. 1994. How many genes in the human genome? *Nat Genet*. 7:345-346.

Fifkova, E., and C.L. Anderson. 1981. Stimulation-induced changes in dimensions of stalks of dendritic spines in the dentate molecular layer. *Exp Neurol*. 74:621-627.

Fonseca, R., U.V. Nagerl, and T. Bonhoeffer. 2006a. Neuronal activity determines the protein synthesis dependence of long-term potentiation. *Nat Neurosci*. 9:478-480.

Fonseca, R., R.M. Vabulas, F.U. Hartl, T. Bonhoeffer, and U.V. Nagerl. 2006b. A balance of protein synthesis and proteasome-dependent degradation determines the maintenance of LTP. *Neuron*. 52:239-245.

Frey, U., M. Krug, K.G. Reymann, and H. Matthies. 1988. Anisomycin, an inhibitor of protein synthesis, blocks late phases of LTP phenomena in the hippocampal CA1 region in vitro. *Brain Res*. 452:57-65.

Fujii, R., S. Okabe, T. Urushido, K. Inoue, and A. Yoshimura. 2005. The RNA binding protein TLS is translocated to dendritic spines by mGluR5 activation and regulates spine morphology. *Curr Biol*. 15:587-593.

Fujii, S., K. Saito, H. Miyakawa, K. Ito, and H. Kato. 1991. Reversal of long-term potentiation (depotentiation) induced by tetanus stimulation of the input to CA1 neurons of guinea pig hippocampal slices. *Brain Res*. 555:112-122.

Fukazawa, Y., Y. Saitoh, F. Ozawa, Y. Ohta, K. Mizuno, and K. Inokuchi. 2003. Hippocampal LTP Is Accompanied by Enhanced F-Actin Content within the Dendritic Spine that Is Essential for Late LTP Maintenance In Vivo. *Neuron*. 38:447-460.

Garner, C.C., R.P. Tucker, and A. Matus. 1988. Selective localization of messenger RNA for cytoskeletal protein MAP2 in dendrites. *Nature*. 336:674-677.

Geiss-Friedlander, R., and F. Melchior. 2007. Concepts in sumoylation: a decade on. *Nat Rev Mol Cell Biol*. 8:947-956.

Glickman, M.H., and A. Ciechanover. 2002. The ubiquitin-proteasome proteolytic pathway: destruction for the sake of construction. *Physiol Rev*. 82:373-428.

Goetze, B., F. Tuebing, Y. Xie, M.M. Dorostkar, S. Thomas, U. Pehl, S. Boehm, P. Macchi, and M.A. Kiebler. 2006. The brain-specific double-stranded RNA-binding protein Staufen2 is required for dendritic spine morphogenesis. *J Cell Biol*. 172:221-231.

Goldstein, G., M. Scheid, U. Hammerling, D.H. Schlesinger, H.D. Niall, and E.A. Boyse. 1975. Isolation of a polypeptide that has lymphocyte-differentiating properties and is probably represented universally in living cells. *Proceedings of the National Academy of Sciences*. 72:11-15.

Graveley, B.R. 2001. Alternative splicing: increasing diversity in the proteomic world. *Trends Genet*. 17:100-107.

Greer, P.L., R. Hanayama, B.L. Bloodgood, A.R. Mardinly, D.M. Lipton, S.W. Flavell, T.K. Kim, E.C. Griffith, Z. Waldon, R. Maehr, H.L. Ploegh, S. Chowdhury, P.F. Worley, J. Steen, and M.E. Greenberg. 2010. The Angelman Syndrome protein Ube3A regulates synapse development by ubiquitinating arc. *Cell*. 140:704-716.

Griffin, N.M., J. Yu, F. Long, P. Oh, S. Shore, Y. Li, J.A. Koziol, and J.E. Schnitzer. 2010. Label-free, normalized quantification of complex mass spectrometry data for proteomic analysis. *Nat Biotechnol*. 28:83-89.

Haglund, K., and I. Dikic. 2012. The role of ubiquitylation in receptor endocytosis and endosomal sorting. *J Cell Sci*. 125:265-275.

Hammell, C.M., I. Lubin, P.R. Boag, T.K. Blackwell, and V. Ambros. 2009. nhl-2 Modulates microRNA activity in Caenorhabditis elegans. *Cell*. 136:926-938.

Hammond, C. 2001. Cellular and Molecular Neurobiology, Second Edition. Academic Press; 2 edition (May 31, 2001). 493 pp.

Han, K.K., and A. Martinage. 1992a. Possible relationship between coding recognition amino acid sequence motif or residue(s) and post-translational chemical modification of proteins. *Int J Biochem*. 24:1349-1363.

Han, K.K., and A. Martinage. 1992b. Post-translational chemical modification(s) of proteins. *Int J Biochem*. 24:19-28.

Han, K.K., and A. Martinage. 1993. Post-translational chemical modifications of proteins--III. Current developments in analytical procedures of identification and quantitation of post-translational chemically modified amino acid(s) and its derivatives. *Int J Biochem*. 25:957-970.

Han, X., H. Du, and M.A. Massiah. 2011. Detection and characterization of the in vitro e3 ligase activity of the human MID1 protein. *J Mol Biol*. 407:505-520.

Hanft, L.M., I.N. Rybakova, J.R. Patel, J.A. Rafael-Fortney, and J.M. Ervasti. 2006. Cytoplasmic gamma-actin contributes to a compensatory remodeling response in dystrophin-deficient muscle. *Proc Natl Acad Sci U S A*. 103:5385-5390.

Hansel, C., and D.J. Linden. 2000. Long-term depression of the cerebellar climbing fiber--Purkinje neuron synapse. *Neuron*. 26:473-482.

Harris, K.M., J.C. Fiala, and L. Ostroff. 2003. Structural changes at dendritic spine synapses during long-term potentiation. *Philos Trans R Soc Lond B Biol Sci*. 358:745-748.

Hebb, D.O. 1949. The Organization of Behavior: A Neuropsychological Theory. Psychology Press; New Ed edition (May 1, 2002). 335 pp.

Hegde, A.N. 2010. The ubiquitin-proteasome pathway and synaptic plasticity. *Learn Mem*. 17:314-327.

Herbert, T.P., G.R. Kilhams, I.H. Batty, and C.G. Proud. 2000. Distinct signalling pathways mediate insulin and phorbol ester-stimulated eukaryotic initiation factor 4F assembly and protein synthesis in HEK 293 cells. *J Biol Chem*. 275:11249-11256.

Herculano-Houzel, S. 2009. The human brain in numbers: a linearly scaled-up primate brain. *Front Hum Neurosci*. 3:31. doi: 10.3389/neuro.09.031.2009

Hershko, A. 1983. Ubiquitin: roles in protein modification and breakdown. *Cell*. 34:11-12.

Hershko, A. 2005. The ubiquitin system for protein degradation and some of its roles in the control of the cell division cycle. *Cell Death Differ*. 12:1191-1197.

Hershko, A., and A. Ciechanover. 1998. The ubiquitin system. *Annu Rev Biochem*. 67:425-479.

Hershko, A., A. Ciechanover, and A. Varshavsky. 2000. Basic Medical Research Award. The ubiquitin system. *Nat Med*. 6:1073-1081.

Hirokawa, N. 2006. mRNA transport in dendrites: RNA granules, motors, and tracks. *J Neurosci*. 26:7139-7142.

Hjerpe, R., F. Aillet, F. Lopitz-Otsoa, V. Lang, P. England, and M.S. Rodriguez. 2009. Efficient protection and isolation of ubiquitylated proteins using tandem ubiquitin-binding entities. *EMBO Rep*. 10:1250-1258.

Hochstrasser, M. 2009. Origin and function of ubiquitin-like proteins. *Nature*. 458:422-429.

Holtmaat, A., and K. Svoboda. 2009. Experience-dependent structural synaptic plasticity in the mammalian brain. *Nat Rev Neurosci*. 10:647-658.

Horn, E.J., A. Albor, Y. Liu, S. El-Hizawi, G.E. Vanderbeek, M. Babcock, G.T. Bowden, H. Hennings, G. Lozano, W.C. Weinberg, and M. Kulesz-Martin. 2004. RING protein Trim32 associated with skin carcinogenesis has anti-apoptotic and E3-ubiquitin ligase properties. *Carcinogenesis*. 25:157-167.

Hotulainen, P., and C.C. Hoogenraad. 2010. Actin in dendritic spines: connecting dynamics to function. *J Cell Biol*. 189:619-629.

Huang, Y.Y., P.V. Nguyen, T. Abel, and E.R. Kandel. 1996. Long-lasting forms of synaptic potentiation in the mammalian hippocampus. *Learn Mem*. 3:74-85.

Hung, A.Y., C.C. Sung, I.L. Brito, and M. Sheng. 2010. Degradation of postsynaptic scaffold GKAP and regulation of dendritic spine morphology by the TRIM3 ubiquitin ligase in rat hippocampal neurons. *PLoS One*. 5:e9842.

Hunter, T. 1995. Protein kinases and phosphatases: the yin and yang of protein phosphorylation and signaling. *Cell*. 80:225-236.

Huttelmaier, S., D. Zenklusen, M. Lederer, J. Dictenberg, M. Lorenz, X. Meng, G.J. Bassell, J. Condeelis, and R.H. Singer. 2005. Spatial regulation of beta-actin translation by Src-dependent phosphorylation of ZBP1. *Nature*. 438:512-515.

International Human Genome Sequencing, C. 2004. Finishing the euchromatic sequence of the human genome. *Nature*. 431:931-945.

Jaafari, N., F.A. Konopacki, T.F. Owen, S. Kantamneni, P. Rubin, T.J. Craig, K.A. Wilkinson, and J.M. Henley. 2013. SUMOylation is required for glycine-induced increases in AMPA receptor surface expression (ChemLTP) in hippocampal neurons. *PLoS One*. 8:e52345.

Jensen, O.N. 2004. Modification-specific proteomics: characterization of post-translational modifications by mass spectrometry. *Curr Opin Chem Biol*. 8:33-41.

Jiang, Y.H., D. Armstrong, U. Albrecht, C.M. Atkins, J.L. Noebels, G. Eichele, J.D. Sweatt, and A.L. Beaudet. 1998. Mutation of the Angelman ubiquitin ligase in mice causes increased cytoplasmic p53 and deficits of contextual learning and long-term potentiation. *Neuron*. 21:799-811.

Joazeiro, C.A., and A.M. Weissman. 2000. RING finger proteins: mediators of ubiquitin ligase activity. *Cell*. 102:549-552.

Kafkafi, N., and G.I. Elmer. 2005. Texture of locomotor path: a replicable characterization of a complex behavioral phenotype. *Genes Brain Behav*. 4:431-443.

Kanai, Y., N. Dohmae, and N. Hirokawa. 2004. Kinesin transports RNA: isolation and characterization of an RNA-transporting granule. *Neuron*. 43:513-525.

Kandel, E., J. Schwartz, and T. Jessel. 2000. Principles of Neural Science. McGraw-Hill Medical; 4 edition (January 5, 2000). 1414 pp.

Kato, A., N. Rouach, R.A. Nicoll, and D.S. Bredt. 2005. Activity-dependent NMDA receptor degradation mediated by retrotranslocation and ubiquitination. *Proc Natl Acad Sci U S A*. 102:5600-5605.

Kazanietz, M.G. 2000. Eyes wide shut: Protein kinase C isozymes are not the only receptors for the phorbol ester tumor promoters. *Molecular Carcinogenesis*. 28:5-11.

Kazanietz, M.G., M.J. Caloca, P. Eroles, T. Fujii, M.L. Garcia-Bermejo, M. Reilly, and H. Wang. 2000. Pharmacology of the receptors for the phorbol ester tumor promoters: multiple receptors with different biochemical properties. *Biochem Pharmacol*. 60:1417-1424.

Khalili, K., L. Del Valle, V. Muralidharan, W.J. Gault, N. Darbinian, J. Otte, E. Meier, E.M. Johnson, D.C. Daniel, Y. Kinoshita, S. Amini, and J. Gordon. 2003. Pur Is Essential for Postnatal Brain Development and Developmentally Coupled Cellular Proliferation As Revealed by Genetic Inactivation in the Mouse. *Molecular and Cellular Biology*. 23:6857-6875.

Khoury, G.A., R.C. Baliban, and C.A. Floudas. 2011. Proteome-wide post-translational modification statistics: frequency analysis and curation of the swiss-prot database. *Sci Rep*. 1. Article number: 90 (2011) doi:10.1038/srep00090

Kiebler, M.A., and G.J. Bassell. 2006. Neuronal RNA granules: movers and makers. *Neuron*. 51:685-690.

Kiebler, M.A., and L. DesGroseillers. 2000. Molecular insights into mRNA transport and local translation in the mammalian nervous system. *Neuron*. 25:19-28.

Kim, J.J., and M.S. Fanselow. 1992. Modality-specific retrograde amnesia of fear. *Science*. 256:675-677.

Kim, T.K., J.Y. Sul, H. Helmfors, U. Langel, J. Kim, and J. Eberwine. 2013. Dendritic glutamate receptor mRNAs show contingent local hotspot-dependent translational dynamics. *Cell Rep*. 5:114-125.

Kim, W., E.J. Bennett, E.L. Huttlin, A. Guo, J. Li, A. Possemato, M.E. Sowa, R. Rad, J. Rush, M.J. Comb, J.W. Harper, and S.P. Gygi. 2011. Systematic and quantitative assessment of the ubiquitin-modified proteome. *Mol Cell*. 44:325-340.

Kishino, T., M. Lalande, and J. Wagstaff. 1997. UBE3A/E6-AP mutations cause Angelman syndrome. *Nat Genet*. 15:70-73.

Klemmer, P., A.B. Smit, and K.W. Li. 2009. Proteomics analysis of immuno-precipitated synaptic protein complexes. *J Proteomics*. 72:82-90.

Knafo, S., G. Ariav, E. Barkai, and F. Libersat. 2004. Olfactory learning-induced increase in spine density along the apical dendrites of CA1 hippocampal neurons. *Hippocampus*. 14:819-825.

Knowles, R.B., J.H. Sabry, M.E. Martone, T.J. Deerinck, M.H. Ellisman, G.J. Bassell, and K.S. Kosik. 1996. Translocation of RNA granules in living neurons. *J Neurosci*. 16:7812-7820.

Kohrmann, M., M. Luo, C. Kaether, L. DesGroseillers, C.G. Dotti, and M.A. Kiebler. 1999. Microtubule-dependent Recruitment of Staufen-Green Fluorescent Protein into Large RNA-containing Granules and Subsequent Dendritic Transport in Living Hippocampal Neurons. *Molecular Biology of the Cell*. 10:2945-2953.

Komander, D., M.J. Clague, and S. Urbe. 2009. Breaking the chains: structure and function of the deubiquitinases. *Nat Rev Mol Cell Biol*. 10:550-563.

Komander, D., and M. Rape. 2012. The ubiquitin code. *Annu Rev Biochem*. 81:203-229.

Krucker, T., G.R. Siggins, and S. Halpain. 2000. Dynamic actin filaments are required for stable long-term potentiation (LTP) in area CA1 of the hippocampus. *Proc Natl Acad Sci U S A*. 97:6856-6861.

Kudryashova, E., D. Kudryashov, I. Kramerova, and M.J. Spencer. 2005. Trim32 is a ubiquitin ligase mutated in limb girdle muscular dystrophy type 2H that binds to skeletal muscle myosin and ubiquitinates actin. *J Mol Biol*. 354:413-424.

Kudryashova, E., J. Wu, L.A. Havton, and M.J. Spencer. 2009. Deficiency of the E3 ubiquitin ligase TRIM32 in mice leads to a myopathy with a neurogenic component. *Hum Mol Genet*. 18:1353-1367.

Kuriu, T., A. Inoue, H. Bito, K. Sobue, and S. Okabe. 2006. Differential control of postsynaptic density scaffolds via actin-dependent and -independent mechanisms. *J Neurosci*. 26:7693-7706.

Kwon, S.C., H. Yi, K. Eichelbaum, S. Fohr, B. Fischer, K.T. You, A. Castello, J. Krijgsveld, M.W. Hentze, and V.N. Kim. 2013. The RNA-binding protein repertoire of embryonic stem cells. *Nat Struct Mol Biol*. 20:1122-1130.

Labonte, D., E. Thies, Y. Pechmann, A.J. Groffen, M. Verhage, A.B. Smit, R.E. van Kesteren, and M. Kneussel. 2013. TRIM3 regulates the motility of the kinesin motor protein KIF21B. *PLoS One*. 8:e75603.

Lecuyer, E., H. Yoshida, N. Parthasarathy, C. Alm, T. Babak, T. Cerovina, T.R. Hughes, P. Tomancak, and H.M. Krause. 2007. Global analysis of mRNA localization reveals a prominent role in organizing cellular architecture and function. *Cell*. 131:174-187.

Lee, E.K., H.H. Kim, Y. Kuwano, K. Abdelmohsen, S. Srikantan, S.S. Subaran, M. Gleichmann, M.R. Mughal, J.L. Martindale, X. Yang, P.F. Worley, M.P. Mattson, and M. Gorospe. 2010. hnRNP C promotes APP translation by competing with FMRP for APP mRNA recruitment to P bodies. *Nat Struct Mol Biol*. 17:732-739.

Lee, H.K. 2006. Synaptic plasticity and phosphorylation. *Pharmacol Ther*. 112:810-832.

Lee, K.A., L.P. Hammerle, P.S. Andrews, M.P. Stokes, T. Mustelin, J.C. Silva, R.A. Black, and J.R. Doedens. 2011. Ubiquitin ligase substrate identification through quantitative proteomics at both the protein and peptide levels. *J Biol Chem*. 286:41530-41538.

Lee, L., E. Dale, A. Staniszewski, H. Zhang, F. Saeed, M. Sakurai, M. Fa, I. Orozco, F. Michelassi, N. Akpan, H. Lehrer, and O. Arancio. 2014. Regulation of synaptic plasticity and cognition by SUMO in normal physiology and Alzheimer's disease. *Sci Rep*. 4:7190. doi: 10.1038/srep07190

Leuner, B., and E. Gould. 2010. Structural plasticity and hippocampal function. *Annu Rev Psychol*. 61:111-140, C111-113.

Leung, K.M., F.P. van Horck, A.C. Lin, R. Allison, N. Standart, and C.E. Holt. 2006. Asymmetrical beta-actin mRNA translation in growth cones mediates attractive turning to netrin-1. *Nat Neurosci*. 9:1247-1256.

Li, W., M.H. Bengtson, A. Ulbrich, A. Matsuda, V.A. Reddy, A. Orth, S.K. Chanda, S. Batalov, and C.A. Joazeiro. 2008. Genome-wide and functional annotation of human E3 ubiquitin ligases identifies MULAN, a mitochondrial E3 that regulates the organelle's dynamics and signaling. *PLoS One*. 3:e1487.

Li, Y., H. Wang, S. Wang, D. Quon, Y.W. Liu, and B. Cordell. 2003. Positive and negative regulation of APP amyloidogenesis by sumoylation. *Proc Natl Acad Sci U S A*. 100:259-264.

Lin, A., Q. Hou, L. Jarzylo, S. Amato, J. Gilbert, F. Shang, and H.Y. Man. 2011. Nedd4-mediated AMPA receptor ubiquitination regulates receptor turnover and trafficking. *J Neurochem*. 119:27-39.

Lin, A.W., and H.Y. Man. 2013. Ubiquitination of neurotransmitter receptors and postsynaptic scaffolding proteins. *Neural Plast*. 2013:432057.

Lin, D.I., O. Barbash, K.G.S. Kumar, J.D. Weber, and J.W. Harper. 2006. Phosphorylation-dependent ubiquitination of cyclin D1 by the SCF (FBX4-αB crystallin) complex. *Mol Cell*. 24:355-366.

Lin, Y.C., M. Boone, L. Meuris, I. Lemmens, N. Van Roy, A. Soete, J. Reumers, M. Moisse, S. Plaisance, R. Drmanac, J. Chen, F. Speleman, D. Lambrechts, Y. Van de Peer, J. Tavernier, and N. Callewaert. 2014. Genome dynamics of the human embryonic kidney 293 lineage in response to cell biology manipulations. *Nat Commun*. 5:4767.

Liu-Yesucevitz, L., G.J. Bassell, A.D. Gitler, A.C. Hart, E. Klann, J.D. Richter, S.T. Warren, and B. Wolozin. 2011. Local RNA translation at the synapse and in disease. *J Neurosci*. 31:16086-16093.

Loch, C.M., M.J. Eddins, and J.E. Strickler. 2011. Protein microarrays for the identification of praja1 e3 ubiquitin ligase substrates. *Cell Biochem Biophys*. 60:127-135.
Loedige, I., D. Gaidatzis, R. Sack, G. Meister, and W. Filipowicz. 2013. The mammalian TRIM-NHL protein TRIM71/LIN-41 is a repressor of mRNA function. *Nucleic Acids Res*. 41:518-532.
Loedige, I., M. Stotz, S. Qamar, K. Kramer, J. Hennig, T. Schubert, P. Loffler, G. Langst, R. Merkl, H. Urlaub, and G. Meister. 2014. The NHL domain of BRAT is an RNA-binding domain that directly contacts the hunchback mRNA for regulation. *Genes Dev*. 28:749-764.
Lopitz-Otsoa, F., E. Rodriguez-Suarez, F. Aillet, J. Casado-Vela, V. Lang, R. Matthiesen, F. Elortza, and M.S. Rodriguez. 2012. Integrative analysis of the ubiquitin proteome isolated using Tandem Ubiquitin Binding Entities (TUBEs). *J Proteomics*. 75:2998-3014.
Luo, J., E. Ashikaga, P.P. Rubin, M.J. Heimann, K.L. Hildick, P. Bishop, F. Girach, F. Josa-Prado, L.T. Tang, R.E. Carmichael, J.M. Henley, and K.A. Wilkinson. 2013. Receptor trafficking and the regulation of synaptic plasticity by SUMO. *Neuromolecular Med*. 15:692-706.
Luscher, C., and R.C. Malenka. 2012. NMDA receptor-dependent long-term potentiation and long-term depression (LTP/LTD). *Cold Spring Harb Perspect Biol*. 4. pii: a005710. doi: 10.1101/cshperspect.a005710.
Lynch, G., and M. Baudry. 1984. The biochemistry of memory: a new and specific hypothesis. *Science*. 224:1057-1063.
Ma, X.M., J. Huang, Y. Wang, and B.A. Eipper. 2003. Kalirin, a multifunctional Rho guanine nucleotide exchange factor, is necessary for maintenance of hippocampal pyramidal neuron dendrites and dendritic spines. *J Neurosci*. 23:10593-10603.
Maas, C., D. Belgardt, H.K. Lee, F.F. Heisler, C. Lappe-Siefke, M.M. Magiera, J. van Dijk, T.J. Hausrat, C. Janke, and M. Kneussel. 2009. Synaptic activation modifies microtubules underlying transport of postsynaptic cargo. *Proc Natl Acad Sci U S A*. 106:8731-8736.
Mabb, A.M., and M.D. Ehlers. 2010. Ubiquitination in postsynaptic function and plasticity. *Annu Rev Cell Dev Biol*. 26:179-210.
Mabb, A.M., H.S. Je, M.J. Wall, C.G. Robinson, R.S. Larsen, Y. Qiang, S.A. Correa, and M.D. Ehlers. 2014. Triad3A regulates synaptic strength by ubiquitination of Arc. *Neuron*. 82:1299-1316.
Mahajan, R., C. Delphin, T. Guan, L. Gerace, and F. Melchior. 1997. A small ubiquitin-related polypeptide involved in targeting RanGAP1 to nuclear pore complex protein RanBP2. *Cell*. 88:97-107.
Malenka, R.C. 1994. Synaptic plasticity in the hippocampus: LTP and LTD. *Cell*. 78:535-538.
Malinow, R., and R.C. Malenka. 2002. AMPA receptor trafficking and synaptic plasticity. *Annu Rev Neurosci*. 25:103-126.
Maniatis, T., and B. Tasic. 2002. Alternative pre-mRNA splicing and proteome expansion in metazoans. *Nature*. 418:236-243.
Mansuy, I.M. 2003. Calcineurin in memory and bidirectional plasticity. *Biochem Biophys Res Commun*. 311:1195-1208.
Mantamadiotis, T., T. Lemberger, S.C. Bleckmann, H. Kern, O. Kretz, A. Martin Villalba, F. Tronche, C. Kellendonk, D. Gau, J. Kapfhammer, C. Otto, W. Schmid, and G. Schutz. 2002. Disruption of CREB function in brain leads to neurodegeneration. *Nat Genet*. 31:47-54.
Martin, S., K.A. Wilkinson, A. Nishimune, and J.M. Henley. 2007. Emerging extranuclear roles of protein SUMOylation in neuronal function and dysfunction. *Nat Rev Neurosci*. 8:948-959.
Matsuzaki, M., N. Honkura, G.C. Ellis-Davies, and H. Kasai. 2004. Structural basis of long-term potentiation in single dendritic spines. *Nature*. 429:761-766.
Matunis, M.J. 1996. A novel ubiquitin-like modification modulates the partitioning of the Ran-GTPase-activating protein RanGAP1 between the cytosol and the nuclear pore complex. *The Journal of Cell Biology*. 135:1457-1470.
May, V., M.R. Schiller, B.A. Eipper, and R.E. Mains. 2002. Kalirin Dbl-homology guanine nucleotide exchange factor 1 domain initiates new axon outgrowths via RhoG-mediated mechanisms. *J Neurosci*. 22:6980-6990.

Meroni, G., and G. Diez-Roux. 2005. TRIM/RBCC, a novel class of 'single protein RING finger' E3 ubiquitin ligases. *Bioessays*. 27:1147-1157.

Meyer-Arendt, K., W.M. Old, S. Houel, K. Renganathan, B. Eichelberger, K.A. Resing, and N.G. Ahn. 2011. IsoformResolver: A peptide-centric algorithm for protein inference. *J Proteome Res*. 10:3060-3075.

Michael, T., U. Zetsche, and J. Margraf. 2007. Epidemiology of anxiety disorders. *Psychiatry*. 6:136-142.

Mikl, M., G. Vendra, and M.A. Kiebler. 2011. Independent localization of MAP2, CaMKIIalpha and beta-actin RNAs in low copy numbers. *EMBO Rep*. 12:1077-1084.

Miller, S., M. Yasuda, J.K. Coats, Y. Jones, M.E. Martone, and M. Mayford. 2002. Disruption of Dendritic Translation of CaMKIIα Impairs Stabilization of Synaptic Plasticity and Memory Consolidation. *Neuron*. 36:507-519.

Misane, I., P. Tovote, M. Meyer, J. Spiess, S.O. Ogren, and O. Stiedl. 2005. Time-dependent involvement of the dorsal hippocampus in trace fear conditioning in mice. *Hippocampus*. 15:418-426.

Moser, M.B., M. Trommald, and P. Andersen. 1994. An increase in dendritic spine density on hippocampal CA1 pyramidal cells following spatial learning in adult rats suggests the formation of new synapses. *Proc Natl Acad Sci U S A*. 91:12673-12675.

Mosesson, Y., D. Chetrit, L. Schley, J. Berghoff, T. Ziv, S. Carvalho, F. Milanezi, A. Admon, F. Schmitt, M. Ehrlich, and Y. Yarden. 2009. Monoubiquitinylation regulates endosomal localization of Lst2, a negative regulator of EGF receptor signaling. *Dev Cell*. 16:687-698.

Mouse Genome Sequencing, C., R.H. Waterston, K. Lindblad-Toh, E. Birney, J. Rogers, J.F. Abril, P. Agarwal, R. Agarwala, R. Ainscough, M. Alexandersson, P. An, S.E. Antonarakis, J. Attwood, R. Baertsch, J. Bailey, K. Barlow, S. Beck, E. Berry, B. Birren, T. Bloom, P. Bork, M. Botcherby, N. Bray, M.R. Brent, D.G. Brown, S.D. Brown, C. Bult, J. Burton, J. Butler, R.D. Campbell, P. Carninci, S. Cawley, F. Chiaromonte, A.T. Chinwalla, D.M. Church, M. Clamp, C. Clee, F.S. Collins, L.L. Cook, R.R. Copley, A. Coulson, O. Couronne, J. Cuff, V. Curwen, T. Cutts, M. Daly, R. David, J. Davies, K.D. Delehaunty, J. Deri, E.T. Dermitzakis, C. Dewey, N.J. Dickens, M. Diekhans, S. Dodge, I. Dubchak, D.M. Dunn, S.R. Eddy, L. Elnitski, R.D. Emes, P. Eswara, E. Eyras, A. Felsenfeld, G.A. Fewell, P. Flicek, K. Foley, W.N. Frankel, L.A. Fulton, R.S. Fulton, T.S. Furey, D. Gage, R.A. Gibbs, G. Glusman, S. Gnerre, N. Goldman, L. Goodstadt, D. Grafham, T.A. Graves, E.D. Green, S. Gregory, R. Guigo, M. Guyer, R.C. Hardison, D. Haussler, Y. Hayashizaki, L.W. Hillier, A. Hinrichs, W. Hlavina, T. Holzer, F. Hsu, A. Hua, T. Hubbard, A. Hunt, I. Jackson, D.B. Jaffe, L.S. Johnson, M. Jones, T.A. Jones, A. Joy, M. Kamal, et al. 2002. Initial sequencing and comparative analysis of the mouse genome. *Nature*. 420:520-562.

Na, C.H., D.R. Jones, Y. Yang, X. Wang, Y. Xu, and J. Peng. 2012. Synaptic protein ubiquitination in rat brain revealed by antibody-based ubiquitome analysis. *J Proteome Res*. 11:4722-4732.

Nabavi, S., H.W. Kessels, S. Alfonso, J. Aow, R. Fox, and R. Malinow. 2013. Metabotropic NMDA receptor function is required for NMDA receptor-dependent long-term depression. *Proc Natl Acad Sci U S A*. 110:4027-4032.

Nagerl, U.V., N. Eberhorn, S.B. Cambridge, and T. Bonhoeffer. 2004. Bidirectional activity-dependent morphological plasticity in hippocampal neurons. *Neuron*. 44:759-767.

Nayak, A., D.J. Zastrow, R. Lickteig, N.R. Zahniser, and M.D. Browning. 1998. Maintenance of late-phase LTP is accompanied by PKA-dependent increase in AMPA receptor synthesis. *Nature*. 394:680-683.

Nilsson, J., and P. Nissen. 2005. Elongation factors on the ribosome. *Curr Opin Struct Biol*. 15:349-354.

O'Malley, A., C. O'Connell, and C.M. Regan. 1998. Ultrastructural analysis reveals avoidance conditioning to induce a transient increase in hippocampal dentate spine density in the 6 hour post-training period of consolidation. *Neuroscience*. 87:607-613.

Ohashi, S., S. Kobayashi, A. Omori, S. Ohara, A. Omae, T. Muramatsu, Y. Li, and K. Anzai. 2002. The Single-Stranded DNA- and RNA-Binding Proteins Pur α and Pur β Link BC1 RNA to Microtubules Through Binding to the Dendrite-Targeting RNA Motifs. *Journal of Neurochemistry*. 75:1781-1790.

Ohkawa, N., K. Kokura, T. Matsu-Ura, T. Obinata, Y. Konishi, and T.A. Tamura. 2001. Molecular cloning and characterization of neural activity-related RING finger protein (NARF): a new member of the RBCC family is a candidate for the partner of myosin V. *J Neurochem*. 78:75-87.

Okamoto, K., T. Nagai, A. Miyawaki, and Y. Hayashi. 2004. Rapid and persistent modulation of actin dynamics regulates postsynaptic reorganization underlying bidirectional plasticity. *Nat Neurosci*. 7:1104-1112.

Olsen, J.V., B. Blagoev, F. Gnad, B. Macek, C. Kumar, P. Mortensen, and M. Mann. 2006. Global, in vivo, and site-specific phosphorylation dynamics in signaling networks. *Cell*. 127:635-648.

Osterweil, E., D.G. Wells, and M.S. Mooseker. 2005. A role for myosin VI in postsynaptic structure and glutamate receptor endocytosis. *J Cell Biol*. 168:329-338.

Ozato, K., D.M. Shin, T.H. Chang, and H.C. Morse, 3rd. 2008. TRIM family proteins and their emerging roles in innate immunity. *Nat Rev Immunol*. 8:849-860.

Panasenko, O.O. 2014. The role of the E3 ligase Not4 in cotranslational quality control. *Front Genet*. 5:141.

Peng, J., D. Schwartz, J.E. Elias, C.C. Thoreen, D. Cheng, G. Marsischky, J. Roelofs, D. Finley, and S.P. Gygi. 2003. A proteomics approach to understanding protein ubiquitination. *Nat Biotechnol*. 21:921-926.

Penzes, P., R.C. Johnson, V. Kambampati, R.E. Mains, and B.A. Eipper. 2001. Distinct roles for the two Rho GDP/GTP exchange factor domains of kalirin in regulation of neurite growth and neuronal morphology. *J Neurosci*. 21:8426-8434.

Perrin, B.J., and J.M. Ervasti. 2010. The actin gene family: function follows isoform. *Cytoskeleton (Hoboken)*. 67:630-634.

Perrin, B.J., K.J. Sonnemann, and J.M. Ervasti. 2010. beta-actin and gamma-actin are each dispensable for auditory hair cell development but required for Stereocilia maintenance. *PLoS Genet*. 6:e1001158.

Pertel, T., S. Hausmann, D. Morger, S. Zuger, J. Guerra, J. Lascano, C. Reinhard, F.A. Santoni, P.D. Uchil, L. Chatel, A. Bisiaux, M.L. Albert, C. Strambio-De-Castillia, W. Mothes, M. Pizzato, M.G. Grutter, and J. Luban. 2011. TRIM5 is an innate immune sensor for the retrovirus capsid lattice. *Nature*. 472:361-365.

Phillips, R.G., and J.E. LeDoux. 1992. Differential contribution of amygdala and hippocampus to cued and contextual fear conditioning. *Behav Neurosci*. 106:274-285.

Pickart, C.M. 2004. Back to the future with ubiquitin. *Cell*. 116:181-190.

Pickart, C.M., and M.J. Eddins. 2004. Ubiquitin: structures, functions, mechanisms. *Biochim Biophys Acta*. 1695:55-72.

Polo, S. 2012. Signaling-mediated control of ubiquitin ligases in endocytosis. *BMC Biol*. 10:25.

Poon, M.M., S.H. Choi, C.A. Jamieson, D.H. Geschwind, and K.C. Martin. 2006. Identification of process-localized mRNAs from cultured rodent hippocampal neurons. *J Neurosci*. 26:13390-13399.

Popovic, D., D. Vucic, and I. Dikic. 2014. Ubiquitination in disease pathogenesis and treatment. *Nat Med*. 20:1242-1253.

Raheja, R., Y. Liu, E. Hukkelhoven, N. Yeh, and A. Koff. 2014. The ability of TRIM3 to induce growth arrest depends on RING-dependent E3 ligase activity. *Biochem J*. 458:537-545.

Rajsbaum, R., A. Garcia-Sastre, and G.A. Versteeg. 2014. TRIMmunity: the roles of the TRIM E3-ubiquitin ligase family in innate antiviral immunity. *J Mol Biol*. 426:1265-1284.

Reck-Peterson, S.L., D.W. Provance, Jr., M.S. Mooseker, and J.A. Mercer. 2000. Class V myosins. *Biochim Biophys Acta*. 1496:36-51.

Reiss, S. 1991. Expectancy model of fear, anxiety, and panic. *Clinical Psychology Review*. 11:141 141 153.

Reiter, L., M. Claassen, S.P. Schrimpf, M. Jovanovic, A. Schmidt, J.M. Buhmann, M.O. Hengartner, and R. Aebersold. 2009. Protein identification false discovery rates for very large proteomics data sets generated by tandem mass spectrometry. *Mol Cell Proteomics*. 8:2405-2417.

Renner, M., D. Choquet, and A. Triller. 2009. Control of the postsynaptic membrane viscosity. *J Neurosci*. 29:2926-2937.

Reyes-Turcu, F.E., K.H. Ventii, and K.D. Wilkinson. 2009. Regulation and cellular roles of ubiquitin-specific deubiquitinating enzymes. *Annu Rev Biochem*. 78:363-397.

Reymond, A., G. Meroni, A. Fantozzi, G. Merla, S. Cairo, L. Luzi, D. Riganelli, E. Zanaria, S. Messali, S. Cainarca, A. Guffanti, S. Minucci, P.G. Pelicci, and A. Ballabio. 2001. The tripartite motif family identifies cell compartments. *EMBO J*. 20:2140-2151.

Rodriguez, A., D.B. Ehlenberger, D.L. Dickstein, P.R. Hof, and S.L. Wearne. 2008. Automated three-dimensional detection and shape classification of dendritic spines from fluorescence microscopy images. *PLoS One*. 3:e1997.

Rubenstein, P.A. 1990. The functional importance of multiple actin isoforms. *Bioessays*. 12:309-315.

Rubenstein, P.A., and K.K. Wen. 2014. Insights into the effects of disease-causing mutations in human actins. *Cytoskeleton (Hoboken)*. 71:211-229.

Rybak, A., H. Fuchs, K. Hadian, L. Smirnova, E.A. Wulczyn, G. Michel, R. Nitsch, D. Krappmann, and F.G. Wulczyn. 2009. The let-7 target gene mouse lin-41 is a stem cell specific E3 ubiquitin ligase for the miRNA pathway protein Ago2. *Nat Cell Biol*. 11:1411-1420.

Ryu, Y.S., Y. Lee, K.W. Lee, C.Y. Hwang, J.S. Maeng, J.H. Kim, Y.S. Seo, K.H. You, B. Song, and K.S. Kwon. 2011. TRIM32 protein sensitizes cells to tumor necrosis factor (TNFalpha)-induced apoptosis via its RING domain-dependent E3 ligase activity against X-linked inhibitor of apoptosis (XIAP). *J Biol Chem*. 286:25729-25738.

Saccone, V., M. Palmieri, L. Passamano, G. Piluso, G. Meroni, L. Politano, and V. Nigro. 2008. Mutations that impair interaction properties of TRIM32 associated with limb-girdle muscular dystrophy 2H. *Hum Mutat*. 29:240-247.

Sandebring, A., and A. Cedazo-Mínguez. 2012. Parkin-An E3 Ubiquitin Ligase with Multiple Substrates. *J Alzheimers Dis Parkinsonism S*. 10:2161-2460.

Schnell, E., M. Sizemore, S. Karimzadegan, L. Chen, D.S. Bredt, and R.A. Nicoll. 2002. Direct interactions between PSD-95 and stargazin control synaptic AMPA receptor number. *Proc Natl Acad Sci U S A*. 99:13902-13907.

Schrenk, F., O. Kullmer, and T. Bromage. 2007. The Earliest Putative Homo Fossils. Springer Berlin Heidelberg. 2145 - 2165 pp.

Schulz, T.W., T. Nakagawa, P. Licznerski, V. Pawlak, A. Kolleker, A. Rozov, J. Kim, T. Dittgen, G. Kohr, M. Sheng, P.H. Seeburg, and P. Osten. 2004. Actin/alpha-actinin-dependent transport of AMPA receptors in dendritic spines: role of the PDZ-LIM protein RIL. *J Neurosci*. 24:8584-8594.

Schwamborn, J.C., E. Berezikov, and J.A. Knoblich. 2009. The TRIM-NHL protein TRIM32 activates microRNAs and prevents self-renewal in mouse neural progenitors. *Cell*. 136:913-925.

Schwarz, L.A., B.J. Hall, and G.N. Patrick. 2010. Activity-dependent ubiquitination of GluA1 mediates a distinct AMPA receptor endocytosis and sorting pathway. *J Neurosci*. 30:16718-16729.

Sekino, Y., N. Kojima, and T. Shirao. 2007. Role of actin cytoskeleton in dendritic spine morphogenesis. *Neurochem Int*. 51:92-104.

Semon, R. 1904. Die Mneme - Als erhaltenes Prinzip im Wechsel des organischen Geschehens. Adamant Media Corporation, Leipzig.

Seo, J., and K.J. Lee. 2004. Post-translational modifications and their biological functions: proteomic analysis and systematic approaches. *J Biochem Mol Biol. 2004 Jan 31;37(1):35-44.*.

Sharma, S.K. 2010. Protein acetylation in synaptic plasticity and memory. *Neurosci Biobehav Rev*. 34:1234-1240.

Shaw, G., S. Morse, M. Ararat, and F.L. Graham. 2002. Preferential transformation of human neuronal cells by human adenoviruses and the origin of HEK 293 cells. *FASEB J*. 16:869-871.
Shawlot, W., J.M. Deng, L.E. Fohn, and R.R. Behringer. 1998. Restricted beta-galactosidase expression of a hygromycin-lacZ gene targeted to the beta-actin locus and embryonic lethality of beta-actin mutant mice. *Transgenic Res*. 7:95-103.
Shepherd, J.D., and R.L. Huganir. 2007. The cell biology of synaptic plasticity: AMPA receptor trafficking. *Annu Rev Cell Dev Biol*. 23:613-643.
Shilov, I.V., S.L. Seymour, A.A. Patel, A. Loboda, W.H. Tang, S.P. Keating, C.L. Hunter, L.M. Nuwaysir, and D.A. Schaeffer. 2007. The Paragon Algorithm, a next generation search engine that uses sequence temperature values and feature probabilities to identify peptides from tandem mass spectra. *Mol Cell Proteomics*. 6:1638-1655.
Shimono, K., M. Baudry, L. Ho, M. Taketani, and G. Lynch. 2002. Long-term recording of LTP in cultured hippocampal slices. *Neural Plast*. 9:249-254.
Shin, S.M., N. Zhang, J. Hansen, N.Z. Gerges, D.T. Pak, M. Sheng, and S.H. Lee. 2012. GKAP orchestrates activity-dependent postsynaptic protein remodeling and homeostatic scaling. *Nat Neurosci*. 15:1655-1666.
Short, K.M., and T.C. Cox. 2006. Subclassification of the RBCC/TRIM superfamily reveals a novel motif necessary for microtubule binding. *J Biol Chem*. 281:8970-8980.
Sidorov, M.S., B.D. Auerbach, and M.F. Bear. 2013. Fragile X mental retardation protein and synaptic plasticity. *Mol Brain*. 6:15.
Silva-Santos, S., G.M. van Woerden, C.F. Bruinsma, E. Mientjes, M.A. Jolfaei, B. Distel, S.A. Kushner, and Y. Elgersma. 2015. Ube3a reinstatement identifies distinct developmental windows in a murine Angelman syndrome model. *J Clin Invest*. 125:2069-2076.
Slack, F.J., and G. Ruvkun. 1998. A novel repeat domain that is often associated with RING finger and B-box motifs. *Trends in Biochemical Sciences*. 23:474-475.
Sonnemann, K.J., D.P. Fitzsimons, J.R. Patel, Y. Liu, M.F. Schneider, R.L. Moss, and J.M. Ervasti. 2006. Cytoplasmic gamma-actin is not required for skeletal muscle development but its absence leads to a progressive myopathy. *Dev Cell*. 11:387-397.
Steward, O., and W.B. Levy. 1982. Preferential localization of polyribosomes under the base of dendritic spines in granule cells of the dentate gyrus. *J Neurosci*. 2:284-291.
Stiedl, O., I. Misane, J. Spiess, and S.O. Ogren. 2000. Involvement of the 5-HT1A receptors in classical fear conditioning in C57BL/6J mice. *J Neurosci*. 20:8515-8527.
Streich, F.C., Jr., V.P. Ronchi, J.P. Connick, and A.L. Haas. 2013. Tripartite motif ligases catalyze polyubiquitin chain formation through a cooperative allosteric mechanism. *J Biol Chem*. 288:8209-8221.
Strieter, E.R., and D.A. Korasick. 2012. Unraveling the complexity of ubiquitin signaling. *ACS Chem Biol*. 7:52-63.
Sutton, M.A., and E.M. Schuman. 2006. Dendritic protein synthesis, synaptic plasticity, and memory. *Cell*. 127:49-58.
Takagi, H., M. Setou, S. Ito, and I. Yao. 2012. SCRAPPER regulates the thresholds of long-term potentiation/depression, the bidirectional synaptic plasticity in hippocampal CA3-CA1 synapses. *Neural Plast*. 2012:352829.
Takahashi, H., E. Ohama, S. Suzuki, Y. Horikawa, A. Ishikawa, T. Morita, S. Tsuji, and F. Ikuta. 1994. Familial juvenile parkinsonism: clinical and pathologic study in a family. *Neurology*. 44:437-441.
Tanaka, J., Y. Horiike, M. Matsuzaki, T. Miyazaki, G.C. Ellis-Davies, and H. Kasai. 2008. Protein synthesis and neurotrophin-dependent structural plasticity of single dendritic spines. *Science*. 319:1683-1687.
Tang, Z., O. El Far, H. Betz, and A. Scheschonka. 2005. Pias1 interaction and sumoylation of metabotropic glutamate receptor 8. *J Biol Chem*. 280:38153-38159.
Terman, J.R., and A. Kashina. 2013. Post-translational modification and regulation of actin. *Curr Opin Cell Biol*. 25:30-38.

Thomas, D., L. Kuras, R. Barbey, H. Cherest, P.L. Blaiseau, and Y. Surdin-Kerjan. 1995. Met30p, a yeast transcriptional inhibitor that responds to S-adenosylmethionine, is an essential protein with WD40 repeats. *Mol Biol Cell*. 15:6526-6534.

Toni, N., P.A. Buchs, I. Nikonenko, C.R. Bron, and D. Muller. 1999. LTP promotes formation of multiple spine synapses between a single axon terminal and a dendrite. *Nature*. 402:421-425.

Torvund-Jensen, J., J. Steengaard, L. Reimer, L.B. Fihl, and L.S. Laursen. 2014. Transport and translation of MBP mRNA is regulated differently by distinct hnRNP proteins. *J Cell Sci*. 127:1550-1564.

Tsien, J.Z., D.F. Chen, D. Gerber, C. Tom, E.H. Mercer, D.J. Anderson, M. Mayford, E.R. Kandel, and S. Tonegawa. 1996. Subregion- and cell type-restricted gene knockout in mouse brain. *Cell*. 87:1317-1326.

Uchil, P.D., A. Hinz, S. Siegel, A. Coenen-Stass, T. Pertel, J. Luban, and W. Mothes. 2013. TRIM protein-mediated regulation of inflammatory and innate immune signaling and its association with antiretroviral activity. *J Virol*. 87:257-272.

Udeshi, N.D., D.R. Mani, T. Eisenhaure, P. Mertins, J.D. Jaffe, K.R. Clauser, N. Hacohen, and S.A. Carr. 2012. Methods for quantification of in vivo changes in protein ubiquitination following proteasome and deubiquitinase inhibition. *Mol Cell Proteomics*. 11:148-159.

Van Der Giessen, R., S. Koekkoek, S. van Dorp, J. De Gruijl, A. Cupido, S. Khosrovani, B. Dortland, K. Wellershaus, J. Degen, and J. Deuchars. 2008. Role of olivary electrical coupling in cerebellar motor learning. *Neuron*. 58:599-612.

van Hagen, J.M., J.N. van der Geest, R.S. van der Giessen, G.C. Lagers-van Haselen, H.J. Eussen, J.J. Gille, L.C. Govaerts, C.H. Wouters, I.F. de Coo, C.C. Hoogenraad, S.K. Koekkoek, M.A. Frens, N. van Camp, A. van der Linden, M.C. Jansweijer, S.S. Thorgeirsson, and C.I. De Zeeuw. 2007. Contribution of CYLN2 and GTF2IRD1 to neurological and cognitive symptoms in Williams Syndrome. *Neurobiol Dis*. 26:112-124.

Vandekerckhove, J., and K. Weber. 1978. At least six different actins are expressed in a higher mammal: an analysis based on the amino acid sequence of the amino-terminal tryptic peptide. *Elsevier*. 126. J Mol Biol. 1978 Dec 25;126(4):783-802.

Wagner, S.A., P. Beli, B.T. Weinert, M.L. Nielsen, J. Cox, M. Mann, and C. Choudhary. 2011. A proteome-wide, quantitative survey of in vivo ubiquitylation sites reveals widespread regulatory roles. *Mol Cell Proteomics*. 10:M111 013284.

Walden, H., and R.J. Martinez-Torres. 2012. Regulation of Parkin E3 ubiquitin ligase activity. *Cell Mol Life Sci*. 69:3053-3067.

Walsh, C. 2006. Posttranslational modification of proteins: expanding nature's inventory. Roberts and Company Publishers; 1st Edition edition (October 3, 2005). ISBN-10: 0974707732, 576pp

Walsh, C.T., S. Garneau-Tsodikova, and G.J. Gatto, Jr. 2005. Protein posttranslational modifications: the chemistry of proteome diversifications. *Angew Chem Int Ed Engl*. 44:7342-7372.

Walsh, M.P., S. Hinkins, and D.J. Hartshorne. 1981. Phosphorylation of smooth muscle actin by the catalytic subunit of the cAMP-dependent protein kinase. *Biochem Biophys Res Commun*. 102:149-157.

Wang, C., L. Tian, V.M. Popov, and R.G. Pestell. 2011. Acetylation and nuclear receptor action. *J Steroid Biochem Mol Biol*. 123:91-100.

Wang, Z., J.G. Edwards, N. Riley, D.W. Provance, Jr., R. Karcher, X.D. Li, I.G. Davison, M. Ikebe, J.A. Mercer, J.A. Kauer, and M.D. Ehlers. 2008. Myosin Vb mobilizes recycling endosomes and AMPA receptors for postsynaptic plasticity. *Cell*. 135:535-548.

West, A.E., E.C. Griffith, and M.E. Greenberg. 2002. Regulation of transcription factors by neuronal activity. *Nat Rev Neurosci*. 3:921-931.

Whalley, K. 2012. Synaptic plasticity: Ubiquitin activates synaptic plasticity. *Nat Rev Neurosci*. 13:73.

Wilhelm, J.E., and R.D. Vale. 1993. RNA on the move: the mRNA localization pathway. *J Cell Biol*. 123:269-274.

Wilkinson, K.A., A. Nishimune, and J.M. Henley. 2008. Analysis of SUMO-1 modification of neuronal proteins containing consensus SUMOylation motifs. *Neurosci Lett*. 436:239-244.

Wilkinson, K.D. 2000. Ubiquitination and deubiquitination: targeting of proteins for degradation by the proteasome. *Semin Cell Dev Biol*. 11:141-148.
Winder, D.G., and J.D. Sweatt. 2001. Roles of serine/threonine phosphatases in hippocampal synaptic plasticity. *Nat Rev Neurosci*. 2:461-474.
Winer, J., C.K. Jung, I. Shackel, and P.M. Williams. 1999. Development and validation of real-time quantitative reverse transcriptase-polymerase chain reaction for monitoring gene expression in cardiac myocytes in vitro. *Anal Biochem*. 270:41-49.
Xu, G., J.S. Paige, and S.R. Jaffrey. 2010. Global analysis of lysine ubiquitination by ubiquitin remnant immunoaffinity profiling. *Nat Biotechnol*. 28:868-873.
Yabe, J.T., W.K. Chan, F.S. Wang, A. Pimenta, D.D. Ortiz, and T.B. Shea. 2003. Regulation of the transition from vimentin to neurofilaments during neuronal differentiation. *Cell Motil Cytoskeleton*. 56:193-205.
Yan, Q., W. Sun, P. Kujala, Y. Lotfi, T.A. Vida, and A.J. Bean. 2005. CART: an Hrs/actinin-4/BERP/myosin V protein complex required for efficient receptor recycling. *Mol Biol Cell*. 16:2470-2482.
Yang, Y., X.B. Wang, M. Frerking, and Q. Zhou. 2008. Spine expansion and stabilization associated with long-term potentiation. *J Neurosci*. 28:5740-5751.
Yao, I., H. Takagi, H. Ageta, T. Kahyo, S. Sato, K. Hatanaka, Y. Fukuda, T. Chiba, N. Morone, S. Yuasa, K. Inokuchi, T. Ohtsuka, G.R. Macgregor, K. Tanaka, and M. Setou. 2007. SCRAPPER-dependent ubiquitination of active zone protein RIM1 regulates synaptic vesicle release. *Cell*. 130:943-957.
Yao, I., K. Takao, T. Miyakawa, S. Ito, and M. Setou. 2011. Synaptic E3 ligase SCRAPPER in contextual fear conditioning: extensive behavioral phenotyping of Scrapper heterozygote and overexpressing mutant mice. *PLoS One*. 6:e17317.
Yaron, A., A. Hatzubai, M. Davis, I. Lavon, S. Amit, A.M. Manning, J.S. Andersen, M. Mann, F. Mercurio, and Y. Ben-Neriah. 1998. Identification of the receptor component of the IkappaBalpha-ubiquitin ligase. *Nature*. 396:590-594.
Ylikallio, E., R. Poyhonen, M. Zimon, E. De Vriendt, T. Hilander, A. Paetau, A. Jordanova, T. Lonnqvist, and H. Tyynismaa. 2013. Deficiency of the E3 ubiquitin ligase TRIM2 in early-onset axonal neuropathy. *Hum Mol Genet*. 22:2975-2983.
Zalfa, F., T. Achsel, and C. Bagni. 2006. mRNPs, polysomes or granules: FMRP in neuronal protein synthesis. *Curr Opin Neurobiol*. 16:265-269.
Zalfa, F., M. Giorgi, B. Primerano, A. Moro, and D.A. Penta. 2003. The fragile X syndrome protein FMRP associates with BC1 RNA and regulates the translation of specific mRNAs at synapses. *Cell.*112(3):317-27.
Zhang, F., S. Saha, S.A. Shabalina, and A. Kashina. 2010. Differential arginylation of actin isoforms is regulated by coding sequence-dependent degradation. *Science*. 329:1534-1537.
Zhang, H.L., T. Eom, Y. Oleynikov, S.M. Shenoy, D.A. Liebelt, J.B. Dictenberg, R.H. Singer, and G.J. Bassell. 2001. Neurotrophin-induced transport of a beta-actin mRNP complex increases beta-actin levels and stimulates growth cone motility. *Neuron*. 31:261-275.
Zhao, Y., and O.N. Jensen. 2009. Modification-specific proteomics: strategies for characterization of post-translational modifications using enrichment techniques. *Proteomics*. 9:4632-4641.
Zhong, J., T. Zhang, and L.M. Bloch. 2006. Dendritic mRNAs encode diversified functionalities in hippocampal pyramidal neurons. *BMC Neurosci*. 7:17.
Zhou, Q., M. Xiao, and R.A. Nicoll. 2001. Contribution of cytoskeleton to the internalization of AMPA receptors. *Proc Natl Acad Sci U S A*. 98:1261-1266.
Zivraj, K.H., Y.C. Tung, M. Piper, L. Gumy, J.W. Fawcett, G.S. Yeo, and C.E. Holt. 2010. Subcellular profiling reveals distinct and developmentally regulated repertoire of growth cone mRNAs. *J Neurosci*. 30:15464-15478.

SUMMARY

Summary

Animals and their behavior have been shaped by evolution to succeed in their respective natural environments. The ability to learn, memorize and retrieve information has proven to be an invaluable property in the success of most species living on earth today. The brain, be it as small as 20,000 neurons in honeybees or as large as 257 billion neurons in African elephants, is generally considered to be the organ that enables animals to learn about and interact with their environments. One brain region in particular, the mammalian hippocampus, is indispensable for many types of learning and has drawn the attention of thousands of researches over the last decades. As with all other brain regions, the primary functional building blocks of the hippocampus are neurons, which communicate via synapses. Synaptic transmission can vary in efficacy depending on various factors. This variation in transmission efficacy, often called synaptic plasticity, is accompanied by structural and compositional synaptic changes facilitated by an increase, decrease, displacement and rearrangement of numerous synaptic proteins. Synaptic plasticity is generally considered the basis of learning and memory.

TRIM3, the subject of this thesis, is one such synaptic protein. It is a RING E3 ubiquitin ligase that is expressed at synapses in the hippocampus and the cerebellum and was supposed to regulate ubiquitin-proteasome-mediated degradation of particular synaptic protein substrates. However, at the start of the research described in this thesis, its precise role and function in neurons and especially at synaptic sites had remained elusive. In order to understand the role of TRIM3 in hippocampal and cerebellar function, we made use of a newly generated *Trim3* knockout mouse and investigated it in a multidisciplinary manner.

Chapter 2 focuses on the descriptive characterization of TRIM3 and on the effect of its loss on brain morphology, learning behavior and synaptic function. We used immunohistochemistry, immunocytochemistry, sub-cellular fractionation and overexpression experiments to show that TRIM3 protein is highly expressed at synaptic sites of the hippocampus and cerebellum and that it is indeed an ubiquitin ligase. We found that knocking out *Trim3* has no overall effect on gross brain morphology and cytoarchitecture, and that basal locomotor and anxiety-related behaviors are unaffected. Hippocampus-dependent fear memory, however, was significantly enhanced in *Trim3*$^{-/-}$ mice, in particular short-term memory measured at two hours after conditioning. By using an

electrophysiological approach we showed that hippocampal LTP is enhanced in *Trim3*$^{-/-}$ mice, but that spontaneous activity of hippocampal pyramidal cells is indistinguishable from that of wildtype neurons. Finally, we showed that loss of TRIM3 causes an increase in spine density in hippocampal pyramidal cells. Together these findings support a role for TRIM3 in structural and functional hippocampal synaptic plasticity.

Chapter 3 explores the possibility that the behavioral, electrophysiological and structural abnormalities of *Trim3*$^{-/-}$ mice described in chapter 2 are caused by deficits in the trafficking properties of messenger ribonucleoprotein (mRNP) particles. We used biochemistry to demonstrate that TRIM3 is part of PURA-containing mRNP granules in hippocampus. By co-immunoprecipitation and overexpression experiments we showed that TRIM3 interacts with PURA, one of the main protein constituents of mRNPs, but that the interaction is mediated by RNA and not by direct contact of TRIM3 and PURA. We further demonstrated that PURA abundance is unaffected by the presence or absence of TRIM3, making PURA an unlikely ubiquitylation substrate. We furthermore used time lapse imaging to analyze mRNP trafficking and mobility in cultured neurons, to find that TRIM3 is not essential for mRNP trafficking, but that the loss of TRIM3 does result in a small but significant increase in travelled distance and velocity of a small subpopulation of mRNP particles.

Chapter 4 describes a novel strategy to identify TRIM3 ubiquitylation substrates. We applied Tandem Ubiquitin Binding Entities (TUBEs) affinity purification and immunoprecipitation with three different TRIM3 antibodies in parallel to *Trim3*$^{-/-}$ mice and wildtype controls. Using this universally applicable, two-pillared quantitative mass spectrometry based strategy we identified synaptic TRIM3 interactors on the one side and differentially ubiquitylated synaptic proteins on the other. We demonstrate the suitability and reproducibility of our approach and present γ-actin (ACTG1) as the most likely ubiquitylation substrate of TRIM3 in hippocampal synapses.

Chapter 5 focuses on the validation of ACTG1 as a TRIM3 substrate in the hippocampus. By co-immunoprecipitating ACTG1 with TRIM3 and TRIM3 with ACTG1 from hippocampal synaptic fractions and from HEK293 cells after TRIM3 overexpression, we were able to show that TRIM3 and ACTG1 interact directly. We further demonstrate that loss of TRIM3 leads to an increase in ACTG1 in hippocampal neurons, and that overexpressing TRIM3 in heterologous cells causes a decrease in endogenous ACTG1 levels.

This decrease is caused by ubiquitylation and subsequent proteasomal degradation mediated by TRIM3. Finally, the importance of ACTG1 in learning and memory is evidenced for the first time by generating a forebrain specific *Actg1* knockout mouse. These mice are viable, and show similar memory deficits in a contextual fear conditioning paradigm as *Trim3*$^{-/-}$ mice. However, whereas *Trim3*$^{-/-}$ mice showed increased short-term memory at two hours after conditioning, conditional *Actg1* mice do so at 24 - 72 hours after conditioning. Taken together our findings suggest that temporal control of ACTG1 levels by TRIM3 is required to regulate the timing of hippocampal plasticity.

Chapter 6 summarizes and discusses obtained data, placing TRIM3 and ACTG1 into a working model in which TRIM3, by fine tuning the expression, degradation and potentially polymerization of ACTG1, keeps the acquisition, consolidation and later expression of a fear memory within physiological boundaries, allowing individuals to function and properly react to their environment.

Acknowledgements

Four years compressed in a book.

Thanks to…

The people behind the scenes - Guus, Ronald and Chris! I am glad and honored to have you as promotors.

Guus for giving me the chance to be a part of the MCN group and Sylics, his guidance, motivation and understanding.

Ronald for being such a patient, calm and trusting supervisor. Without his support there wouldn't be a thesis.

Chris for meeting me without an appointment, for introducing me to Guus and Ronald and for understanding my fascination with the cerebellum.

Sylics and all colleagues for their scientific and moral support. (and for the birthday flowers)

Cerebnet and all its members for the scientific training and feedback, and the delightful meetings.

Prof. Dr. Matthias Kneussel, Prof. Dr. Jens Schwamborn, Prof. Dr. Casper Hogenraad, Dr. Ruud Toonen and Dr. Ka Wan Li for taking the time to read my thesis and for being part of the thesis committee.

Marlene for introducing me to the lab and the TRIM3 project.

Pim for his number crunching expertise, for not getting tired of it and always adding the right musical flavor.

Tim for his confocal magic. There is a reason why one of the images is part of the cover.

Julia and Jaap for their electrophysiological recordings and the many explanations.

Marion for all her help with primary cultures.

Rolinka for her precise and quick dissection skills that she applied so many times. Also for her patience with my snail-like skills.

Ka Wan (again) for always asking questions, never getting tired of questions, his *open door* policy and his can-do way of thinking.

Iryna for making sure that there is some TRIM3 time on the MALDI, for her troubleshooting skills, for her attitude and for understanding what sleep deprivation really is.

Roel for his vast experience and his willingness to take the time to share it.

Sabine for the positive vibes she always brought to the lab and for letting me help with so many practical lab courses.

Nikhil for the countless conversations about science, world politics, tech, sports, religion and much more. Also for being the only one tough enough to share an office with me for four years.

Frank for being like-minded. There aren't very many.

Anya and Remco for being great friends and colleagues, and the most meticulous scientists in a wet lab. I learned much more from the two of you than could be said in a few sentences. I wish you two only the best.

Loek for letting me break his nose and not holding a grudge.

The ladies from the "kletskamers" - Celine, Danai, Esther, Anne-Lieke, Karen, Mariette, Sigrid, Andrea and Leanne - for never kicking me out and for always being willing to help with whatever request I came. Celine and Leanne especially for their help with terrifying mice.

Jasper for being a piece of the homeland and my fellow Cerebnet fellow. I am grateful for every break, walk, travel and training together.

All other MCN colleagues, Yvonne, Brigitte, Mark, Jochem, Ruud, Andrea, Rene, Priyanka, Michel, Lody, Bart, Ning, Patricia, Natasha, Sophie, Maija, Miguel, Demirhan, Brigitte and Mariana for the great work atmosphere, the scientific expertise and discussions, and not to forget, the lively lab outings.

Jan and Konstantin for being an inspiration in terms of determination, drive and professionalism. I am proud to call you friends.

My Family.

Lars, my brother, for being brother. I couldn't wish for a better one.

My parents, Sibylle and Karl-Heinz, for their unlimited and unconditional love and support.

My wonderful daughters Lilia and Klara for having changed everything, for being wild horses and for being my motivation and daily sunshine.

Jadwiga (aka Miss Rabbit), my loving wife, for bringing us to the Netherlands, for the constant support, for the many discussions, for keeping me grounded, for being with me despite my directness and for always believing in me.